EFFECTS OF ELECTROSTATIC FORCES ON DROP COLLISION AND COALESCENCE IN AIR

by
HUBERT RUSSEL PLUMLEE

25 September 1964

AMC-63-G2
NSF GP-2528

Supported by
ADVANCED RESEARCH PROJECTS AGENCY
and
NATIONAL SCIENCE FOUNDATION

CHARGED PARTICLE RESEARCH LABORATORY
REPORT NO. CPRL-8-64
DEPARTMENT OF ELECTRICAL ENGINEERING
ENGINEERING EXPERIMENT STATION
UNIVERSITY OF ILLINOIS
AND
ILLINOIS STATE WATER SURVEY
URBANA, ILLINOIS

EFFECTS OF ELECTROSTATIC FORCES ON DROP COLLISION AND COALESCENCE IN AIR

BY

Hubert Russel Plumlee

25 September 1964

AMC-63-G2

NSF GP-2528

Supported by

ADVANCED RESEARCH PROJECTS AGENCY

and

NATIONAL SCIENCE FOUNDATION

Charged Particle Research Laboratory

Report No. CPRL-8-64

Department of Electrical Engineering

Engineering Experiment Station

University of Illinois

and

Illinois State Water Survey

Urbana, Illinois

ACKNOWLEDGEMENT

I wish to express my sincere thanks to my major professor, Dr. Charles D. Hendricks, Jr., and to the co-director of the Charged Particle Research Laboratory, Mr. Richard G. Semonin for their assistance and encouragement during the preparation of this thesis. I am also indebted to Miss Rebecca Bryar for her able assistance in the handling of the data and in the preparation of the graphs used in this paper. And finally, I wish to thank Miss Ruth Pembroke, who typed the manuscript, and the entire staff of the Charged Particle Research Laboratory for their many helpful discussions.

This work was supported by an Advanced Research Projects Agency Grant AMC 63-G2 and a National Science Foundation Grant GP-2528.

TABLE OF CONTENTS

LIST OF ILLUSTRATIONS

LIST OF SYMBOLS

a radius

a_ℓ radius of large sphere (drop)

a_s radius of small sphere (droplet)

A constant in the bispherical coordinate system

A_n coefficient of the electric potential expansion

B_n coefficient of the electric potential expansion

c $\cos\theta$

c_ℓ constant in the bispherical coordinate system

c_s constant in the bispherical coordinate system

$C_{\ell\ell}$ coefficient of self capacitance

$C_{\ell s}$ coefficient of mutual capacitance

$C_{s\ell}$ coefficient of mutual capacitance

C_{ss} coefficient of self capacitance

D_s drag coefficient

D_r^2 differential operator (Stokes)

D_ρ^2 differential operator (Oseen)

E electric field

E_c collision efficiency

f_n terms of the outer-flow expansion

F_e electrostatic force on droplet

F_g gravitational force on droplet

F_h hydrodynamic force on droplet

F_o constant force

F_{xe} x-component of electrostatic force

F_{ze} z-component of electrostatic force

g acceleration of gravity

G Green's function

G_n coefficient of the electric potential expansion

h distance from $z = 0$ to flat surface

h_n term of the inner flow expansion

h_o constant h

h_1 constant h

h_μ	scale factor
h_η	scale factor
h_λ	scale factor
H_n	coefficient of the electric potential expansion
J	current density
k	constant
K	constant ($8\pi\epsilon A^2$)
m_s	mass of droplet
p	pressure of fluid
p_n	term in the expansion of pressure
p_∞	free stream pressure
P_o	constant pressure
P_n	Legendre polynomial
P_n^1	Legendre polynomial
$P_{\ell\ell}$	coefficient of self induction
$P_{\ell s}$	coefficient of mutual induction
$P_{s\ell}$	coefficient of mutual induction
P_{ss}	coefficient of self induction
q_ℓ	net charge on drop
q_s	net charge on droplet
Q_ℓ	induced charge on drop
Q_s	induced charge on droplet
r	radial coordinate
r_n	term of the expansion of pressure
R_e	Reynolds number
S_n	term of the expansion of the electrostatic force
t	time
t_1	constant t
T_n	term of the expansion of the electrostatic force
u	velocity of the fluid
u'	perturbation of the fluid velocity
u_r	r-component of the fluid velocity

u_θ	θ-component of the fluid velocity
u_∞	free stream fluid velocity
U	velocity of the fluid
v_c	collision velocity
v_s	velocity of droplet
v_{xs}	x-component of velocity of droplet
v_{ys}	y-component of velocity of droplet
V	velocity of surface
W_n	coefficient of the expansion of surface charge
x	Cartesian coordinate
x_s	x-coordinate of droplet
X_n	coefficient of the expansion of surface charge
y	Cartesian coordinate
y_k	initial horizontal separation
y_s	y-coordinate of droplet
Y_c	initial horizontal separation of the grazing trajectory
Y_n	coefficient of the expansion of surface charge
z	Cartesian coordinate
Z_n	coefficient of the expansion of surface charge
β	angle of electric field with x-axis
ϵ	permittivity
ϵ_n	coefficient of the expansion of fluid velocity
η	bispherical coordinate
θ	angular coordinate
λ	angular coordinate
μ	bispherical coordinate
μ_ℓ	constant μ
μ_o	$\mu_\ell + \mu_s$
μ_s	constant μ
ν	viscosity of the fluid
ξ	distance from $z = 0$ to surface
π	constant

ρ	Oseen's variable
ρ_A	mass density of the fluid
ρ_W	charge density of water
σ	electrical conductivity
σ_L	surface charge density of drop
σ_s	surface charge density of droplet
ϕ	electric potential
ϕ_L	electric potential of drop
ϕ_s	electric potential of droplet
ϕ_o	constant electric potential
$\$$	Oseen's expansion
$\$_n$	term of Oseen's expansion
Ψ	Stokes stream function
$\Psi(r)$	a function of r
Ψ	Stokes expansion
Ψ_n	term of Stokes expansion
ω	angle of electric field with the line of centers

ABSTRACT

The collision and coalescence of drops are studied with emphasis on the effects of electrostatic forces. A historical review is used to point out some of the earlier research in this field of study.

A mathematical model describing the effects of forces acting on two spherical drops immersed in a viscous medium is described. The model includes the interaction of the drops with an externally applied electric field and with any charge present. The collision efficiencies between pairs of drops ranging in size from 5 to 70 microns in radius are given as a result of computing the grazing trajectories of the smaller droplets relative to the larger drops. For a fixed droplet size, the collision efficiency is found to increase as the drop size is increased. However, applied electric fields produce increases in the collision efficiency for a given pair of drops. For example a horizontal electric field of 3600 volts per centimeter increases the collision efficiency of a 30 and 5 microns drop pair by a factor of 34.5. Also for a given pair of drops with charges of the same sign, the collision efficiency decreases to zero as the charges increase in a field-free region but increases in value when a vertically applied field is present. When the charges on a given drop pair are of opposite sign, the collision efficiency increases to values greater than unity as the charges are increased in a field-free region but may decrease in value when a vertically applied field is present.

The coalescence of a pair of drops 2 millimeters in radius immersed in air is investigated by first considering a mathematical model which includes the hydrodynamic flow of the air from between the two approaching surfaces, the effect of the flattening of the adjacent surfaces, and the effect of an

electric potential between the drops. With this model the time required for the surfaces to move a given distance is determined as a function of the viscosity of the air, and the potential difference. High speed photographs of the profile view of two colliding drops are used in support of this model. The time interval between the initial deformation of the approaching drops and their coalescence, the rate of growth of the flatten deformation of the adjacent surfaces, and the collision velocity of the drops are measured. It is found that the time for coalescence is independent of moderate charges in the air pressure, varies inversely with the potential difference, and decreases for an increase in the collision velocity. Also the time interval during which charge flows between the drops before they actually coalesce is investigated.

CHAPTER I

INTRODUCTION

The collision of small particles with a collector is an important problem in several areas of interest. For example, this is the fundamental mechanism by which dust and smoke are removed in many types of air cleaning equipment; it is the method by which water drops are collected on aircraft wings and turbine blades resulting in icing; it produces wash-out from the air of particulate matter from industrial pollution and atomic explosion residues and it plays a role in the formation of clouds and in the development of rain.

A particular problem which is of great interest is the growth in the size of liquid drops by the collision and coalescence of two particles borne in a fluid medium. Viscous forces arise from the fluid flow around the particles. These viscous forces affect the trajectories of the particles, and, therefore, the conditions under which the two particles collide. Coalescence itself is a second stage of the process, since it is by no means certain that two liquid drops will coalesce if they collide.

This aggregate process is of great interest to cloud physicists to help explain the rapid growth of small cloud droplets into rain-size drops which occurs in non-freezing clouds. Initially, water droplets are formed by the condensation of moisture on small nuclei. The droplets grow to about an average radius of 6 microns and have approximately a Gaussian size distribution (Weickmann and aufm Kampe, 1953). However, warm clouds have an average drop radius of 30 microns and Best (1951) showed that the condensation process was too slow to produce these larger drops. Also,

since the lower limit of raindrop radius is about 100 microns, the coalesce process is necessary to explain the rapid production of rain size drops from these warm clouds. Findeisen (1939) was the first to calculate the growth by the coalescence process of a drop falling through a given cloud thickness. However, he did not accept his own calculations thinking they were unsubstantiated by observations. Other investigators such as Moore and Vonnegut (1960) have indicated that only by having high collection efficiency of cloud droplets can the rapid change in the droplet size spectrum of warm clouds by explained.

Although it is recognized that the aggregation of water drops involves the two independent stages of collision and coalescence, very few experiments are able to separate the two processes. The collision process which is of initial importance in bringing the drops together has been approached both from the theoretical and experimental point of view. However, very little is known about the coalescence process and only a few experimental observations are available.

The investigation reported in the following pages has been separated into two parts, i.e., the conditions leading to the collision of two water drops and the parameters governing the coalescence of two water surfaces immersed in air. It was of primary interest to determine the influence of electrostatic forces due to either an externally applied electric field or the presence of a net charge on either or both drops. For convenience, all measurements of drop sizes in the rest of this report have been given as the radius of the drops and the smaller of two drops has been referred to as the "droplet". The collisions between drops and

droplets were determined from the computation of the trajectories of the droplets while subjected to gravitational, hydrodynamic, and electrostatic forces. Collision efficiencies were determined from collisions in air for water droplets ranging from 5 microns to 50 microns with a wide range of net charges and applied electric fields.

The coalescence of two water surfaces was studied by taking high speed photographs of two colliding drops suspended from two hypodermic needles. From the profile view of the collision, measurements of the time interval that the surfaces were in contact before coalescence occurred were taken and the rate of growth of the resulting drop was determined. The effects of an electric potential difference between the drops, the collision velocity of the approaching drops, and the air pressure of the environment on the coalescence process were investigated. Also, investigated was the time interval before coalescence, during which charge flowed between the approaching drops.

Rationalized mks units are used throughout the following chapters.

CHAPTER II

HISTORICAL REVIEW

Setting up a well controlled experiment or postulating a working model of the collision and coalescence of liquid drops immersed in a viscous medium has proved to be very difficult. Stokes as early as 1845 was interested in the motion of objects in a viscous medium. But even up to the present time no completely general description has been determined for two drops in proximity. However, a limited amount of both theoretical and experimental work has been reported and most of the important work is outlined in this chapter.

2.1 Theoretical Aspects of Computing Collision Efficiencies

The first step in attempting a mathematical analysis of the problem of possible collision between particles is to identify and to state the process or processes of greatest importance and the physical laws on which these depend. A complex assemblage of particles can be reduced to only two particles immersed in a fluid. This obviously ignores the perturbing influence of all the other particles but is generally accepted for most applications. Further physical simplifying assumptions are that one particle is much larger than the other and that both particles are spherical in shape. This particle is the collector and will be referred to as the 'drop'. The smaller particle is the collected drop and will be referred to as the 'droplet'. If care is exercised, large deformed drops and irregular solid particles can be taken into account and the same approach can still be used.

When one particle is much larger than the other, the fluid flow pattern is assumed to be characterized by the flow around the larger Most workers have assumed that the droplet does not affect this flow pattern; therefore, the determination of the flow pattern around the drop is of great importance.

2.1a Hydrodynamics

The Navier-Stokes equation which describes the flow for a viscous fluid is non-linear and a general solution for the steady flow past a fixed sphere has not been determined. It is assumed that the fluid has no slip on the surface of the sphere and a uniform flow at infinity. Stokes (1851) was the first to consider this problem and obtained a solution by ignoring the inertia force in the differential equation. However, at a distance from the sphere where the uniform stream has been reached, the inertia force and the viscous force become comparable in magnitude and Stokes' solution is no longer valid. Whitehead (1889) attempted to improve this solution by obtaining higher order approximations of the flow. He used Stokes' solution to calculate the neglected inertia terms by developing an iterative procedure. However, the method failed because it was not possible to match the resulting velocity with the uniform stream at infinity.

Oseen (1910) assumed that the sphere caused a small perturbation in the uniform parallel flow and neglected the second order perturbation terms which took into account the inertia terms. The Oseen's equation which resulted is a linear approximation of the Navier-Stokes equation. But since the perturbation close to the sphere becomes large, Oseen's

solution is only valid away from the sphere. Goldstein (1929) worked out the exact analytical solution of Oseen's linearized equation for the case of steady flow of an incompressible viscous fluid past a sphere. Tomotika and Aoi (1950) and Pearcey and McHugh (1955) used Goldstein's solution to determine the flow pattern around a sphere for various Reynolds numbers but did not improve the range of validity of the solution.

By assuming a special form for the solution of the flow pattern which satisfied an integrated form of the Navier-Stokes equation, Kawaguti (1948) was able to obtain a solution for the first and second order terms of the equation. Although Kawaguti (1950) made numerical corrections to his previous work, nothing new was developed.

A new approach was used by Lagerstrom and Cole (1955) and Kaplun and Lagerstrom (1957) which expanded the stream function into two expansions in terms of the Reynolds number. One expansion was good in the region close to the sphere and the other expansion was good for the outer flow. These expansions were substituted into the Navier-Stokes equation to yield the separate coefficients of the expansion since only one set of physical boundary conditions was applicable to each expansion. A unique solution was derived by employing a procedure which yielded a higher order approximation of the flow. Therefore, the linearized Stokes analysis near the surface of the sphere was combined with the Oseen analysis far from the sphere for small Reynolds numbers. Later Proudman and Pearson (1957) extended Kaplun's method to obtain additional terms for the stream function expansion.

By employing a digital computer and using a relaxation method, Jenson (1959) numerically determined the stream function about a fixed sphere for Reynolds numbers of 5, 10, 20, and 40. This method gave satisfactory results but was inconvenient to use since a large table of values had to be generated.

Hocking (1956) determined the drag forces when there were two spheres of comparable size present. Since he used the Stokes linearization of the Navier-Stokes equation, his results were limited to Reynolds numbers less than one. His calculations were based on the superposition of two solutions, one when the relative motion of the two spheres was along their line of centers and one when it was at right angles to this line of centers. Since the solution for Stokes' case is linear, the superposition of these two solutions did give the drag forces for any relative motion between the two spheres for which the Stokes approximations apply. After the fluid flow was determined around the drop, the viscous drag on a droplet was taken to be directly proportional to the relative velocity of the droplet in this fluid. Stokes derived a simple law for calculating the drag for small spheres which was used for larger spheres after being corrected by the use of a drag coefficient determined experimentally as reported by Davies (1945)

2.1b Electrostatics

It is necessary to determine the electrostatic force on the two drops if this force is to be considered. The easiest case to handle is that in which the drops can be considered as conducting spheres. The electrostatic force can be approximated when a uniform electric field is

applied by determining the interaction between induced dipoles of spheres as calculated by Smythe (1950). Smythe also derived a more accurate expression for the force along the line of centers of the two conducting spheres in a uniform field. For the case of charged spheres with no applied field, the method of images can be used to compute the mutual force action between the spheres. A more thorough treatment of the electrostatic problem of two spheres was given by Buchholz (1957); however, the most thorough treatment to date was reported by Davis (1962). Davis determined the forces on two conducting spheres, charged or uncharged, in an applied uniform electric field with any orientation.

2.1c. Equations of Motion

The equations of motion of the droplet can be written including the various forces which are assumed to be acting on it such as gravitation, viscous force caused by the fluid, and electrostatic force due to both charge and an applied electric field. These equations are non-linear and must be solved numerically. Therefore, the numerical technique invariably uses a step-by-step solution of the individual trajectories of the small droplet. The trajectory is usually determined for given initial conditions where the droplet is a great distance from the drop and is a distance y from the line through the center of the drop and parallel to the relative fluid flow. Each trajectory either hits or misses the larger sphere and the value y_c, which corresponds to a grazing trajectory with the drop is found by a trial-and-error. The collision cross-section or the collision efficiency E_c is then determined as $y_c^2/(a_l + a_s)^2$, where a_l is the radius of the drop and a_s is the radius of the droplet. The main objective of this type of computation is to evaluate F_c under various conditions

2.1d Collision Efficiencies

Many investigators have attempted to determine the collision efficiency between two drops and each have made different assumptions in order to obtain a solution. Sell (1931) assumed ideal fluid flow around the drop but apparently neglected any gravitational or electrostatic forces. He did not give any details about the calculation; therefore, his work is mainly of historical interest.

Langmuir and Blodgett (1944-1945) evaluated the collision efficiency of two falling drops by assuming only a drag force on the droplet caused by an ideal fluid flow around the drop which is only valid for a very large collector drop. The droplet was taken as a point mass and a differential analyzer was used to calculate the trajectories. Later Langmuir (1948) evaluated a similar efficiency for smaller collector drops by assuming a Stokes flow pattern around the drop. From these two solutions, Langmuir made a guess as to the collision efficiency for intermediate sizes of drops. His work has been shown to be in fair agreement with experimental results. Das (1950) computed the droplet trajectories using the approximation of an ideal fluid flow but, unlike Langmuir, took into account the size of the droplet. No details were given about his method of computing the trajectories and the results were given only graphically. Ludlam (1951) made rough corrections to Langmuir's calculated collision efficiencies by assuming that the path of the center of a droplet of finite radius a_s would be that calculated by Langmuir, but displaced by a distance a_s. An electrostatic force was added to this model by Kanz (1959) who included the interaction of the induced dipole of each drop in the presence of a uniform electric field.

Pearcey and Hill (1957) have given a treatment using Oseen's approximation for the flow around the drop and taking into account the effect of the droplet motion on the larger sphere by superposing the individual flow patterns. This is obviously not satisfactory when the two drops are in proximity since the system is non-linear. The equations of motion were solved by a digital computer and were extended up to a Reynolds number of 40. Within the framework of the assumptions, the results were accurate and there was no interpolation between the extreme cases as in the case of Langmuir's results.

Hocking employed the drag force he had determined for two spheres of comparable size and in the Stokes range. He evaluated the collision efficiency for drops of about 30 microns to which the Stokes linearization was applicable. The most important point which emerged from this calculation was the fact that when the drop had a radius of 18 microns or less its collision efficiency was zero for all smaller droplets. This radius was much greater than the cut-off value of about 6 microns found by Pearcey and Hill.

Sartor (1960) indicated that he used Hocking's drag forces and an expression for the induced electrostatic force between the drops resulting from an applied uniform electric field. No details were given as to how he actually set up his equations of motion, but a digital computer was used to determine a limited number of collision efficiencies for normally non-colliding droplets when a uniform field was present.

Lindblad and Semonin (1963) computed collision efficiencies using Proudman and Pearson's (1956) results for the fluid flow pattern around the drop with both an electrostatic force due to the induced dipole

caused by an applied electric field, and a force due to gravity. They used a digital computer to determine the collision efficiency of drops in the range of 30 to 50 microns and for fields up to 3600 volts per centimeter. Calculations show that collision efficiencies may be increased as much as 2400 per cent in horizontal fields of 3600 volts per centimeter when only the dipole interaction was included.

Shafrir and Neiburger (1963) used a modification of the relaxation method, first used by Jenson, to determine the fluid flow pattern around each isolated drop. The interaction between the flow patterns was approximated by superimposing the two separate flow patterns around each drop even though the flow patterns were solutions of a non-linear differential equation. The force due to gravity was also included and the collision efficiencies of drops up to 136 microns were determined by the use of a digital computer. Hocking's work was used as a standard and Shafrir and Neiberger's work proved to compare favorably in the over-laping range. No consideration was given to the effects of any electrostatic force.

2.2 Experimental Collision Efficiencies

Experiments to investigate the collision-coalescence process are of two types. The first type of experiments are performed on actual cloud droplets and the results are immediately applicable to natural clouds. Because of the very small size of cloud droplets and the rather high terminal velocity of larger drops, these experiments are difficult to perform. The second type of experiment is designed to overcome these difficulties by using a modeling technique whereby cloud droplets are simulated by drops of macroscopic size moving through a liquid. But these results are only a qualitative interest since the modeling of

matching Reynolds numbers of drops falling through a liquid, to those of cloud droplets falling in air, holds only for uniform, unaccelerated motion. This failure of the modeling technique is a result of the fact that in air most of the kinetic energy of motion is associated with the droplet, while in a liquid environment, because of its greater density, much of the kinetic energy is carried by the medium surrounding the drops.

2.2a Cloud Size Droplets

Findeisen (1932) observed that the drop size of a fog in an enclosed space increased and he interpreted this as evidence of the collision and coalescence of the droplets. But this observation could have also resulted from an evaporation-condensation process. Observations of small fog droplets using a microscope were reported by Dady (1947) and Swinbank (1947) who observed many collisions without coalescences between droplets of radius 2 microns.

Gunn and Hitschfeld (1951) investigated the collection efficiency of 1.5 millimeter drops falling through a cloud of smaller droplets of 6-100 microns. They weighed the drops before and after passage through a 3 meter column of uniform cloud droplets. The experimental results were in agreement with those computed by using the theory of Langmuir and indicated that the assumption that coalescence always occurs for each collision was valid. No effect was found when the collector drop was charged to $\pm$ .67 x 10^{-10} coulombs and it was concluded that charging was therefore unimportant as far as the later stages of growth of raindrops was concerned.

A study of the coalescence of water droplets of approximately equal size was made by Telford, Thorndike, and Bowen (1955). A uniform cloud

of droplets approximately 75 microns in radius was produced by a spinning disk. These droplets were injected into a vertical wind tunnel where the speed of the air was adjusted such that all droplets moved slowly upward through the field of view. Any larger drops formed by coalescence of two cloud droplets then moved down through the field of view and were recorded photographically by using a film moving at right angles to the direction of travel of the droplets. The experiment indicated an unexpectedly high collision efficiency, $E_c = 12.6 \pm 3.4$, and was explained qualitatively on the basis of capture of the upper droplet by the wake of the lower. Pearcey and Hill (1957) gave a value of $E_c = 12.6$ for droplets of radius 80 microns which is in agreement with the experimental results. The agreement also indicates that the assumption of a coalescence for every collision is substantially valid. The experiment was also arranged such that all drops were charged and the droplets could either all be charged with the same sign or an equal number having an opposite charge. It was found that unlike charges of the order of 2×10^{-13} coulombs per 65 micron drops increased the coagulation rate by a factor from 2 to 20 depending upon the droplet concentration. However when all droplets were charged with the same charge, coalescence appeared to be completely inhibited. It seems very likely that most of these effects were caused by the changes in the collision efficiency but it was possible that the coalescence process also could have been altered.

By tracing the growth of single drops as they fell through a dense fog, Kinzer and Cobb (1958) obtained the collision efficiencies for a wide range of collector drop sizes. A dense uniform fog with

droplets of 5.5 to 8 microns was formed in a vertical wind-tunnel and the growth of a single drop was observed by means of a microscope. The drop was kept stationary by adjusting the air speed through the wind-tunnel. The collection efficiency of this growing drop was found to decrease steadily to less than 0.2 for drops between 20 and 40 microns. The collection efficiency then rose to nearly unity for 200 micron drops and fell again to small values for drops greater than 1000 microns. The collection efficiency for drops greater than 20 microns was roughly in agreement with the calculations of Langmuir. For drops less than 20 microns the experimental procedure was difficult, and humidity and temperature were carefully controlled to avoid size change due to evaporation-condensation. The case in which both the collector drop and the cloud droplets were charged was investigated. It was concluded that little effect on the collision efficiency was found for drops greater than 8 microns in radius, although there were some indications that drops did coalesce spontaneously when they came within 2 or 3 microns of each other.

2.2b Scaled Model Droplets

The basic faults of the model experiments have already been pointed out. However, Sartor (1954) constructed a model consisting of water drops a few millimeters in diameter falling through mineral oil. Many of the effects discussed in this chapter were observed, such as the pushing aside of small droplets and the effect of drop wake, but no coalescence was observed despite many collisions. This failure to observe coalescence seems to indicate the difference in structure of the oil-water interface and illustrates a fault of this modeling technique when compared to water

droplets in air. However, when an electric field was applied vertically in the tank, coalescences occurred. There was negligible effect on the droplet trajectories if the fields were less than 200 volts per centimeter, but the coalescence efficiency on collision rose from zero to 100 percent as the applied field was varied from zero to about 240 volts per centimeter, the variation being approximately linear. No calculation of the relationship of the field strengths in this model to those in a cloud situation was given.

A model using steel balls falling through a concentrated sugar solution was employed by Schotland and Kaplun (1956). After Schotland (1957) made some corrections in the results, the collision efficiencies were found to follow the pattern calculated by Pearcey and Hill with the exception that the overall values were higher and there was apparently no cut-off for small drops.

2.3 Coalescence Experiments

Rayleigh (1845) was one of the first investigators to report the significance of the coalescence of liquid drops. He explained the dispersion of drops from a jet of liquid shooting up into the air as the result of drops bouncing from each other. When the drops were charged properly, the jet was made to collapse back on itself with very little dispersion. This observation was explained by the increase in the coalescence of the colliding drops with charge. Since that time many investigators have been interested in learning more about the process which leads to the coalescence of two liquid surfaces.

Observations of water drops bouncing across the surface of pure water were reported by Reynolds (1881). However, he also observed that

if the surface of the water was dirty any drops falling on the surface would coalesce immediately. He concluded that any scum on the water reduced the surface tension and enhanced the coalescence. It is generally accepted that the definition of the stability of a liquid drop is the time the drop is in proximity of a second liquid surface before coalescence occurs.

Hazelhurst and Neville (1937) found that drops of certain liquids, falling from a limited height onto a liquid surface, do not immediately coalesce with the body of the liquid, but may roll or remain at rest upon the surface for a short time. However, non-polar or molecular structures which have a low moment of inertia have a short rotation time and are less strongly oriented resulting in a short time for coalescence. Examples in this category are water, electrolytes, formic acid, formaldihydes and ethylene glycol. Hazelhurst and Neville concluded that the character and stability of the oriented surface film was the determining factor for coalescence.

By using interference patterns, Derjaguin and Kussakov (1939) measured the distance between a flat plane and an approaching bubble and discovered that not only did the bubble flatten at a finite distance from the plane but that a dimple formed in the middle of this deformation. Their findings also supported the theory that hydrodynamics of the air film trapped between the surfaces determined the coalescence properties of the system. Elton (1948) included the effect of an electrostatic force on the viscosity of the trapped air film in attempting to improve the theory of this system.

The rates of coalescence of oil drops in water and water drops in oil have been measured in the presence of various chemical agents by Cockbain

and McRoberts (1953). It was concluded that the main factor determining stability in all the systems examined was the resistance to wetting of segments of the absorbed film by the discontinuous phase.

Gillespie and Ridial (1955) also studied the stability of drops at an oil-water interface. An analysis of their results indicated that a film was formed between the drop and the interface which drained unevenly. Rupture of the film leading to coalescence was found to be a statistical process and very dependent on any temperature gradient in the system.

The thickness of the air gap separating the colliding surfaces was again measured by the use of light interference patterns by Prokhorov (1954). He varied the humidity of the air around the liquid surfaces and found that for volatile liquids, if the humidity approached zero per cent, the liquid surfaces would remain separated without coalescence for long periods of time. However, for 100 per cent humidity the surfaces would coalesce very rapidly. He concluded that the outflow of the vapor from the liquid surfaces created a hydrostatic pressure which kept the surfaces from moving together. He also verified that a dimple does form at the center of the deformed surfaces.

Liquid drops floating on a surface of the same liquid were studied by Linton and Sutherland (1956). They found that the time for coalescence of the drops with the bulk liquid was proportional to the diameter of the drop and the time for coalescence of the drops with other drops was proportional to the cube of the diameter of the smaller drop. It was also concluded that drops larger than 0.05 centimeters would bounce while drops less than 0.025 centimeters would coalesce.

The coalescence of water resting on an oil-water interface was studied by Elton and Picknett (1957) where the temperature and contamination was carefully controlled. Their results supported the theory that the drainage of the liquid trapped between the drop and the interface controls the time for coalescence. However, they concluded that an electrical double layer force was important in forcing the trapped liquid out between the approaching surfaces.

The rate of coalescence of oil globules in water was studed by Van den Tempel (1957). He found that the thickness of the water film between the oil surfaces at the moment before coalescence decreased with an increase in electrolyte concentration. He postulated that an additional repulsive force was present in the system other than electrostatic repulsion and van der Waals-London attraction.

Nielsen, Wall, and Adams (1958) found from oil-water interfaces that water drops are more stable if an oil soluble agent was added and oil drops were more stable if a water soluble agent was added. Both types of drops were less stable with an increase in temperature and it was concluded that any factor which disturbed the oil-water interface on a molecular scale decreased the stability of the drops.

By studying drop coalescence with a flat surface of the same liquid, Charles and Mason (1960) also found that the stability of the drops increased with a decrease in the temperature. However, the stability was found to decrease with an applied electrostatic field. They also studied the formation of small drops when large drops fell on a surface of the liquid. It was concluded that a column of liquid was projected up into the air and was split into small secondary droplets. This phenomena was called partial coalescence.

The stability of drops which were influenced by a concentration of a solute was studied by Groothuis and Zuiderwig (1960). After the solute was added to the drops, the surface tension was decreased when the solute was diffused to the continuous phase. But when the solute was added to the continuous medium, the solute diffused to the drops, increased the surface tension, and decreased the coalescence.

The coalescence of two water drops in air was studied by Freir (1960). He formed a stream of uniform drops which interacted with each other to cause collisions and a few coalescences. The greatest increase in coalescence resulted when an applied electric field was oriented in the direction of motion of the colliding drops.

Berg, Fernish, and Gaukler (1963) photographed two liquid drops presred together. The time for coalescence was found to decrease with an increase in an electric potential applied between the drops. They concluded that the coalescence was effected by the formation of bonds across the interface between the drops.

CHAPTER III

THEORETICAL MODEL FOR DETERMINING COLLISION EFFICIENCIES

3.1 Definition of Collision Efficiency

The collision efficiency is a measure of the cross-sectional area relative to the collector drop of radius a_ℓ such that if a collected droplet of radius a_s passes through this area the two drops will collide. Conversely, if the droplet does not pass through this area, then the two drops will not collide. In order to determine this cross-sectional area, the trajectory of the droplet must be determined such that it just grazes the collector drop. If the two drops are initially traveling in the vertical direction and if the initial horizontal separation of the grazing trajectory is called Y_c on one side and $-Y'_c$ on the other side, the most useful definition of the collision efficiency E_c is

$$E_c = \frac{\pi(Y_c + Y'_c)^2}{4\pi(a_\ell + a_s)^2} \tag{3-1}$$

Although other authors have used different definitions for E_c, this definition is consistant with other areas of physics and it also takes into account any non-symmetrical cases as shown in Figure 3-1.

If the origin of the coordinate system is selected at the center of the collector drop, then the equation of motion for the droplet can be written as

$$m_s \frac{d\bar{v}_s}{dt} = \bar{F}_g + \bar{F}_h + \bar{F}_e \tag{3-2}$$

where m_s is the mass of the droplet, $\bar{v}_s$ is the velocity of the droplet, $\bar{F}_h$ is the hydrodynamic force on the droplet caused by the viscous medium,

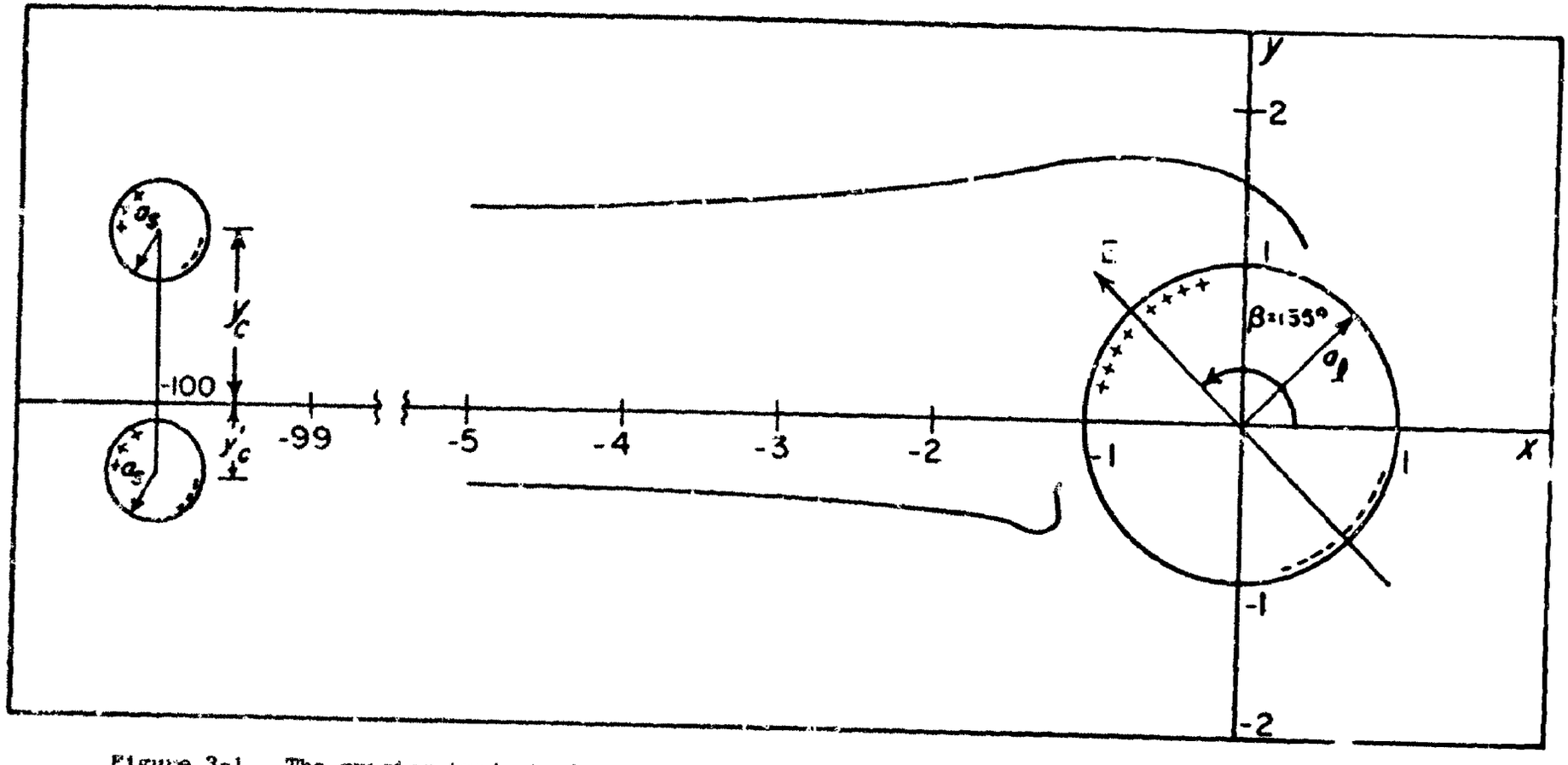

Figure 3-1 The grazing trajectories in the half-planes ($y > 0$ and $y < 0$) for a 30 micron drop and a 5 micron droplet in an electric field oriented at $\beta = 135^{o}$.

$\bar{F}_e$ is electrostatic force on the droplet caused by any electric charge or field present, and $\bar{F}_g$ is the gravitational force. By solving the equation of motion the trajectory of the droplet can be determined.

For this investigation, seven trajectories were obtained for a pair of drops to determine the collision efficiency. These trajectories were selected in the following manner. For the first trajectory the horizontal separation was always $y_1 = a_\ell$. Then, if the first trajectory resulted in a collision with the collector drop the computer selected $y_2 = y_1 + 1/2\ a_\ell$, and for a miss $y_2 = y_1 - 1/2\ a_\ell$, so in general we have $y_{k+1} = y_k \pm (1/2)^k a_\ell$. The grazing trajectory was then defined as $Y_c = y_7 \pm (1/2)^7\ a_\ell$.

The next step was to determine the three forces which acted on the droplet. Care had to be exercised in formulating both the hydrodynamic and electrostatic problems since these would limit the results.

3.2 Hydrodynamics

The problem of two spheres was simplified by assuming that the fluid containing the droplet was flowing around a stationary drop. Also, if the ratio of the droplet radius to the drop radius was small, the mutual interaction of the flow patterns set up by the two spheres could be neglected. Hocking (1959) estimated that the ratio should be approximately one-tenth. However, by comparing the collision efficiencies of the present work with Hocking's and with Shafrir and Neiburger's (1963) as in Figure 3-2, it was indicated that the ratio of one-tenth was more conservative than necessary. Lindblad and Semonin (1963b) also discussed the limitation of the ratio of the drop radius and came to the same conclusion.

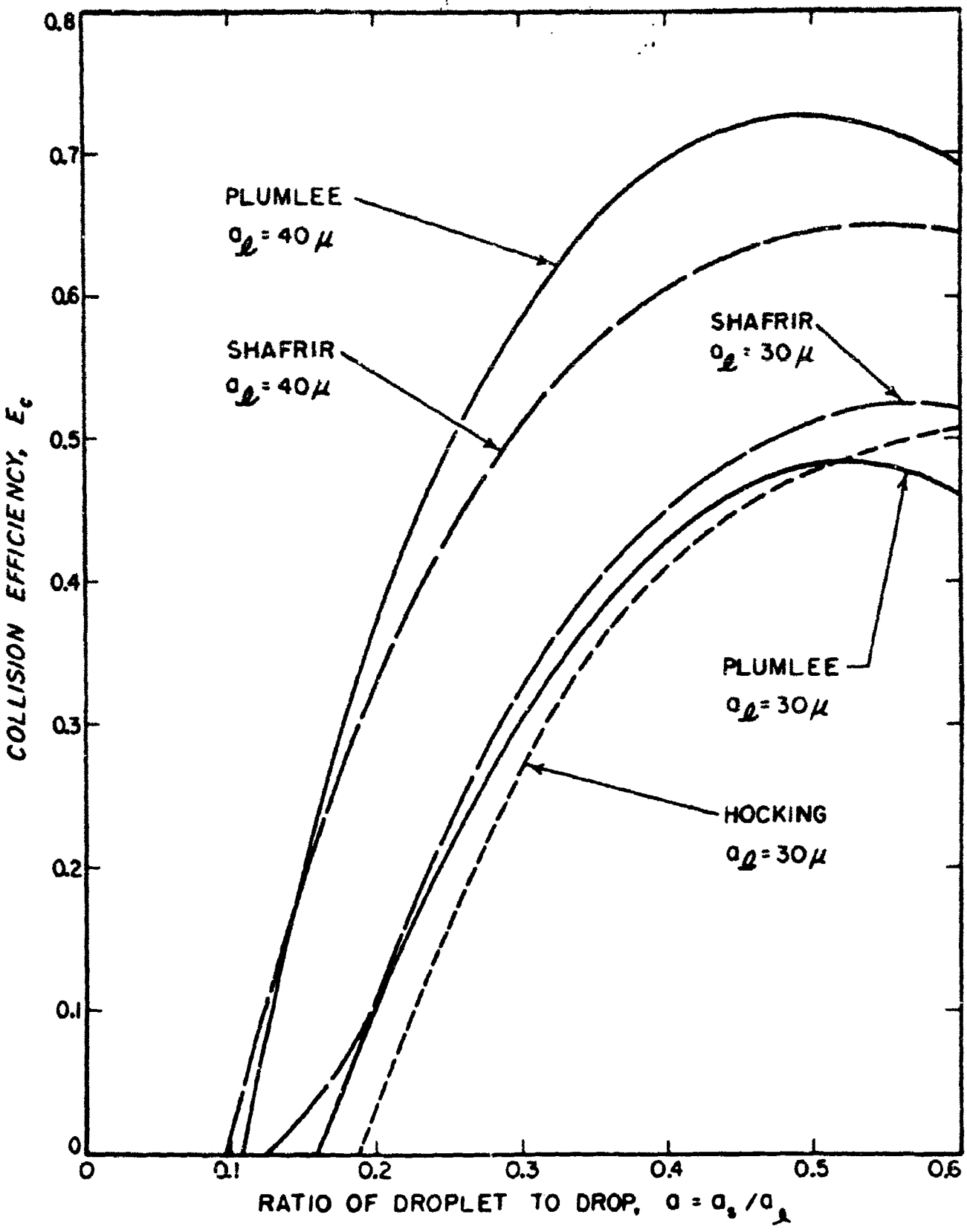

Figure 3-2 Comparison of collision efficiency as calculated by various authors.

The flow of a fluid around a single sphere was determined by solving the Navier-Stokes equations which may be written in vector form

$$\nabla \cdot \bar{u} = 0$$

$$\rho_A \left[\frac{\partial \bar{u}}{\partial t} + \nabla\left(\frac{1}{2}\bar{u}^2\right) - \bar{u} \times \nabla \times \bar{u} \right] = -\nabla p - \nu(\nabla \times \nabla \times \bar{u} - \nabla^2 \bar{u}) \qquad (3\text{-}3)$$

where $\bar{u}$ is the velocity of the fluid, ρ_A is the density of the fluid and ν is the viscosity of the fluid. If the viscous force which is proportional to the first power of the velocity is considerably greater than the inertia force which is proportional to the second power of the velocity, then the inertia term can be omitted from the equations of motion of the fluid. The resulting equations are good for Reynolds numbers, R_e, < 1 and written as

$$\nabla \cdot \bar{u} = 0$$

$$\rho_A \frac{\partial \bar{u}}{\partial t} = -\nabla p + \nu \nabla^2 \bar{u} \qquad (3\text{-}4)$$

The equations (3-4) are referred to as Stokes' equations. For slow streaming past a fixed obstacle, the error involved in this approximation is greatest in the distant parts of the flow field where the inertia force is comparable to the viscous force.

An improvement of Stokes' solution was given by Oseen (1910), who took the inertia term in the Navier-Stokes equations partly into account. He assumed the velocity components could be represented as the sum of a constant and a perturbation term. Thus

$$\bar{u} = \bar{u}_\infty + \bar{u}' \qquad (3\text{-}5)$$

where $\bar{u}'$ represented the perturbation terms, and as such, was small with respect to the free stream velocity, $\bar{u}_\infty$, which was a constant. The Navier-Stokes equations for $R_e < 1$ can now be reduced to the approximate form

$$\nabla \cdot \bar{u}' = 0$$

$$\rho_A \left[\frac{\partial \bar{u}'}{\partial t} + \bar{u}_\infty \cdot (\nabla \cdot \bar{u}') \right] = -\nabla p + \nu \nabla^2 u' \qquad (3\text{-}6)$$

which give a second order approximation to the outer flow and are called Oseen's equations. For slow streaming past a fixed obstacle the error involved in this approximation is greatest in the near parts of the flow field where the variations from the uniform flow field are greatest.

For steady state flow $\frac{\partial \bar{u}}{\partial t} = 0$, which eliminates this term from the equation. When the obstacle is a sphere, the spherical polar coordinates, r, θ, λ, are the most convenient coordinates to use with the axis $\theta = 0$ chosen to lie in the direction of the free stream velocity $\bar{u}_\infty$. If there is no fluid rotation about the $\theta = 0$ axis which is normally the case, then the velocity function for this fluid is independent of λ. Now the velocity vector can be transformed into a Stokes stream function, ψ, where the velocity components are given in terms of ψ as

$$u_r = \frac{+1}{r^2} \frac{\partial \psi}{\partial c}, \quad u_\theta = \frac{-1}{r(1 - c^2)^{1/2}} \frac{\partial \psi}{\partial r} \qquad (3\text{-}7)$$

where $c = \cos\theta$. For the case of a fixed sphere, ψ must be such that the velocity is zero on the surface of the sphere $r = a$, and the velocity is $\bar{u}_\infty$ at infinity.

Stokes' equations now can be reduced to

$$D_r^4 \psi = 0 \tag{3-8}$$

$$\nabla^2 p = 0 \tag{3-9}$$

where

$$D_r^2 = \frac{\partial^2}{\partial r^2} + \frac{(1 - c^2)}{r^2} \frac{\partial^2}{\partial c^2}$$

Equation (3-8) yields a solution

$$\psi = \frac{u_\infty a^2 \sin^2\theta}{2} \left(\frac{r^2}{a^2} - \frac{3r}{2a} + \frac{a}{2r}\right) \tag{3-10}$$

and equation (3-9) yields a solution

$$p = p_\infty - \frac{3\nu u_\infty a}{2r^2} \cos\theta \tag{3-11}$$

By using the stream function, Oseen's equation (3-6) reduces to

$$\frac{1 - c^2}{\rho} \frac{\partial D_\rho^2 \psi}{\partial c} + \frac{c}{2} \frac{\partial D_\rho^4 \psi}{\partial \rho} = D_\rho^4 \psi \tag{3-12}$$

where

$$D_\rho^2 = \frac{\partial^2}{\partial \rho^2} + \frac{1 - c^2}{\rho^2} \frac{\partial^2}{\partial c^2}$$

and gives a solution

$$\psi = \frac{u_\infty a^2}{2} \left\langle (1-c^2)\left(\frac{r}{a}\right)^2 - \frac{6}{R_e}\left(1 + \frac{3R_e}{16}\right)(1+c) \left\{1 - \exp\left[\frac{-R_e}{4}\left(\frac{r}{a}\right)(1-c)\right]\right\}\right\rangle \tag{3-13}$$

However, both solutions are good only in separate regions of the flow field and only when the Reynolds number is small.

Kaplun and his associates (Lagerstrom and Cole, 1955; Kaplun and Lagerstrom, 1957; Kaplun, 1957: and Proudman and Pearson 1957) used a clever approach to determine the viscous flow around a sphere for a small Reynolds number. They distinguished between the inner flow in the region near the sphere, where the normalized Stokes variable, $\bar{r}$ $(= \bar{r}/a)$, is O(1), and the outer flow when the Oseen variable, $\bar{\rho}$ $(= R_e \bar{r})$, is O(1). If the radius, a, of the sphere is used as the representative length, the Stokes variable, $\bar{r}$, is equal to $\bar{r}/a$ and the Reynolds number is equal to $2 \rho_A a u/\nu$ where ν is the viscosity of the medium. The outer flow is represented by expressions for the velocity and pressure in the forms

$$\frac{\bar{u}}{u_\infty} = \sum_{n=0}^{\infty} \epsilon_n \bar{f}_n(\bar{\rho})$$

$$\frac{p - p_\infty}{\rho_A u_\infty^2} = \sum_{n=0}^{\infty} \epsilon_n p_n(\bar{\rho}) \qquad (3\text{-}14)$$

where the ϵ_n are functions of R_e such that $\epsilon_o = 1$ and $\epsilon_{n+1}/\epsilon_n \to 0$ as $R_e \to 0$. The inner flow is similarly represented by

$$\frac{\bar{u}}{u_\infty} = \sum_{n=0}^{\infty} \epsilon_n \bar{h}_n(\bar{r})$$

$$\frac{R_e(p - p_\infty)}{\rho_A u_\infty^2} = \sum_{n=0}^{\infty} \epsilon_n r_n(\bar{r}) \qquad (3\text{-}15)$$

The equations satisfied by $\bar{f}_n$, p_n and $\bar{h}_n$, r_n are obtained by inserting the expansions (3-14) and (3-15) into the Navier-Stokes equations, written in terms of the Oseen and Stokes variables respectively, and solving for the values of the coefficients. The velocity functions must satisfy the boundary conditions $\bar{f}_n \to 0$ $(n \geq 1)$ as $\bar{r} \to \infty$, and $\bar{h}_n = 0$ on the body, but the inner conditions on $\bar{f}_n$ and the outer one on $\bar{h}_n$ are still to be determined. This is done by matching the inner and outer expressions. The Stokes stream function, ψ, may be expressed as an Oseen expansion

$$\frac{\psi R_e^2}{u_\infty a^2} = \Phi = \sum_{n=0}^{\infty} \epsilon_n \Phi_n(\bar{\rho}) \tag{3-16}$$

in the outer flow, and by a Stokes expansion

$$\frac{\psi}{u_\infty a^2} = \Psi = \sum_{n=0}^{\infty} \epsilon_n \Psi_n(\bar{r}) \tag{3-17}$$

in the inner flow.

Since $\epsilon_o = 1$, it follows that

$$\Phi_o = \frac{1}{2} \rho^2 (1-c^2) \tag{3-18}$$

because the leading term must represent the undisturbed stream. The matching condition requires that

$$\Psi \to \frac{1}{2} r^2 (1-c^2) \quad \text{as } r \to \infty \tag{3-19}$$

and has no-slip at $r = 1$. However, the Stokes solution does satisfy these conditions and is

$$\Psi_o = \frac{1}{4}(2r^2 - 3r + \frac{1}{r})(1-c^2) \tag{3-20}$$

By substituting the expansion for ψ into the Navier-Stokes equation written in terms of the Oseen variable, $\bar{\rho} = R_e \bar{r}$, the term involving ϵ_1 shows that Φ_1 satisfies Oseen's equation

$$(D_\rho^2 - \frac{c}{2}\frac{\partial}{\partial \rho} - \frac{1-c^2}{2\rho}\frac{\partial}{\partial c})D_\rho^2 \Phi_1 = 0 \qquad (3\text{-}21)$$

This equation is solved by substituting

$$D_\rho^2 \Phi = \exp(\frac{\rho c}{4})\ f(\rho)\ g(c) \qquad (3\text{-}22)$$

The solution that gives a vanishing velocity as $\rho \to \infty$ and will match the Stokes expansion is

$$\Phi_1 = -3(1+c)\left\{1 - \exp\left[-\frac{\rho(1-c)}{4}\right]\right\} \qquad (3\text{-}23)$$

By substituting the Stokes expansion into the Navier-Stokes equation the second term, $\epsilon_1 \Psi_1$, in the expansion will satisfy the inhomogeneous Stokes equation.

$$D_r^4 \Psi_1 = \frac{-9}{8}(\frac{2}{r^2} - \frac{3}{r^3} + \frac{1}{r^5})\ c(1-c^2) \qquad (3\text{-}24)$$

In order for Ψ_1 to satisfy the no-slip condition on the sphere and match the Oseen's expansion as $r \to \infty$,

$$\epsilon_1 = R_e$$

$$\Psi_1 = \frac{3(r-1)^2(1-c^2)}{64}\left[(2 + \frac{1}{r}) - c(2 + \frac{1}{r} + \frac{1}{r^2})\right] \qquad (3\text{-}25)$$

The third term, $\epsilon_2 \Psi_2$, can be found as follows. If $\epsilon_2 = R_e^2 \ell n(R_e)$, it is found that Ψ_2 must satisfy

$$D_r^4 \Psi_2 = 0 \tag{3-26}$$

and has the form $k\Psi_o$. The value of k is found to be 9/40; therefore,

$$\Psi_2 = \frac{9}{160}(2r^2 - 3r' + \frac{1}{r})(1 - c^2) \tag{3-27}$$

But it is found that there is no term of $R_e^2 \ell n(R_e)$ in the Oseen expansion and Ψ_2 is a valid representation of the third term of the Stokes expansion.

The first two terms of the Stokes expansion as given by Proudman and Pearson (1957) may be written in the unnormalized system as

$$\psi = u_\infty a^2 \Psi = \frac{u_\infty a^2}{4}(\frac{r}{a} - 1)^2(1 - c^2)\left[(1 + \frac{3R_e}{16})(2 + \frac{a}{r}) - \frac{3R_e}{16}(2 + \frac{a}{r} + \frac{a^2}{r^2})c\right] \tag{3-28}$$

for sufficiently small values of R_e. Now the two velocity terms can be written as

$$u_r = \frac{u_\infty}{4}(1 - \frac{a}{r})\left[2 - \frac{3R_e}{16}(3\cos^2\theta - 1)(2 + \frac{a}{r} + \frac{a^2}{r^2}) - 2\cos\theta(1 + \frac{3R_e}{16})(2 + \frac{a}{r})\right] \tag{3-29}$$

$$u_\theta = \frac{u_\infty \sin\theta}{4}(1 - \frac{a}{r})\left[(1 + \frac{3R_e}{16})(4 + \frac{a}{r} + \frac{a^2}{r^2}) - \frac{3R_e\cos\theta}{16}(4 + \frac{a}{r} + \frac{a^2}{r^2} + \frac{2a^3}{r^3})\right] \tag{3-30}$$

These equations describe an approximation for the fluid flow around a single sphere in a uniform fluid flow when $R_e < 4$.

3.3 Electrostatics

If water drops are considered to be conducting spheres the derivation of the electrostatic forces acting on them will be simplified. Since the

drops to be considered are small and travel at moderate velocities, the assumption of the drops being spheres wi introduce only a small error in the results. From the equation of continuity of charge, $\nabla \cdot \bar{J} + \frac{\partial \rho_w}{\partial t} = 0$, where $\bar{J}$ is the current density and ρ_w is the charge density in the water, the relaxation time of the charge distribution in water can be derived in the following manner. Since $\bar{J} = \sigma \bar{E}$ where σ is the conducti of water, then the continuity equation reduces to $\sigma \nabla \cdot \bar{E} + \frac{\partial \rho_w}{\partial t} = 0$.

But $\nabla \cdot E = \rho_w / \epsilon$ where permittivity of water, therefore $\sigma \rho_w / \epsilon + \partial \rho_w / \partial t = 0$. The charge density is proportional to $\exp(-\sigma t / \epsilon)$ where the time constant, ϵ / σ, is the relaxation time of the material. For distilled water, the relaxation time is of the order of one micro-second. The charge density, thus the electric field intensity within the drop, decreases rapidly to zero with increasing time. This expresses the well known fact that the field within a conductor is zero and justifies the assumption that water can be considered as a conducting material.

The electrostatic force acting on two spheres is determined by solving for the charge distributions σ_ℓ and σ_s on surfaces of the two spheres of radius a_ℓ and a_s. Given these two charge distributions, the force is found by integrating the electrical stresses, $\sigma_\ell^2 / 2\epsilon$ nd $\sigma_s^2 / 2\epsilon$, over the surfaces of the separate spheres. Smythe (1950) gives an expression for the force along the line of centers between two equal uncharged spheres in a uniform field. However, Davis (1962) solved the more general problem required for the present application by using the bispherical coordinate system.

Morse and Feshback (1953) give a detailed description of the bispherical coordinate system which is useful in solving boundary-value problems involving two spheres. The three coordinates of this system, μ, η, and λ are illustrated in Figure (3-3). Constant μ surfaces are spheres of radius a csch$|\mu|$ centered at z = a cothμ on the z-axis. The two poles on the z-axis at $\mu = \pm$ a and the central plane z = 0 is the surface $\mu = 0$. The surface $\eta = \eta_o$ is a fourth-order surface formed by rotating about the z-axis that part of the circle, in the x-z plane, of radius a csc η_o with center at z = 0, x = a cot η_o. Those for $\eta < 1/2\pi$ have "dimples" at each pole; those for $\eta > 1/2\pi$ have sharp points there. These bispherical coordinates are related to the Cartesian coordinates by

$$z = \frac{A \sin \mu}{\cosh \mu - \cos \eta} \tag{3-31}$$

$$x = \frac{A \sin \eta \cos \lambda}{\cosh \mu - \cos \eta} \tag{3-32}$$

$$y = \frac{A \sin \eta \sin \lambda}{\cosh \mu - \cos \eta} \tag{3-33}$$

Since two spheres can be represented by the surfaces $\mu = \mu_\ell$ and $\mu = -\mu_s$, it is necessary to relate μ_ℓ, μ_s, and A to the radii, a_ℓ, a_s, and to the separation of the spheres, r. Such a relationship is given by

$$\mu_\ell = \ell n(c_\ell + A) - \ell n\, A_\ell \tag{3-34}$$

$$\mu_s = \ell n(c_s + A) - \ell n\, A_s \tag{3-35}$$

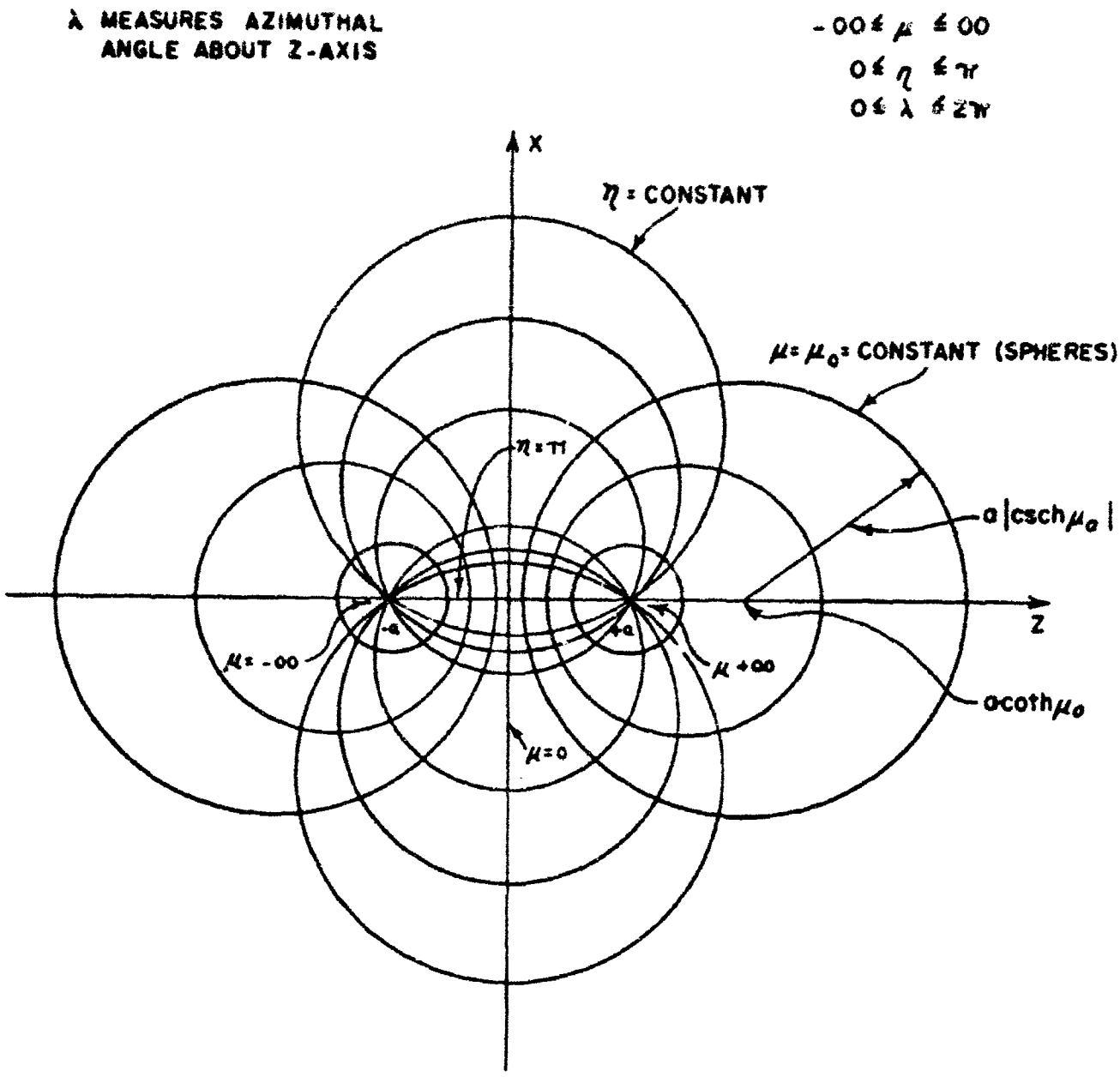

Figure 3-3 Illustration of the bispherical coordinate system.

where

$$A = (c_\ell^2 - a_\ell^2)^{1/2} = (c_s^2 - a_s^2)^{1/2} \tag{3-36}$$

$$c_\ell = (r^2 + a_\ell^2 - a_s^2)/2r \tag{3-37}$$

$$c_s = (r^2 + a_s^2 - a_\ell^2)/2r \tag{3-38}$$

The charge distributions on the spheres are not found directly, but by using properties of a Green's function as described by Jackson (1962), the surface charge density is related to the electric potential function by

$$\phi = \frac{1}{4\pi\epsilon}\left[\int_{\text{sphere}_\ell} \sigma_\ell \, G(\ell)\,d(\text{area}) + \int_{\text{sphere}_s} \sigma_s \, G(s)\,d(\text{area})\right] \tag{3-39}$$

where $G(\ell)$ and $G(s)$ are the Green's functions for spheres a_ℓ and a_s respectively. Now the problem has been changed to solving Laplace's equation for the electric potential function of two insulated conducting spheres, uncharged or carrying specified charges, in the presence of an external uniform electric field. The surface charge distribution is determined from this potential function which then allows the computation of the forces acting on the spheres.

Laplace's equation written in bispherical coordinates is given by

$$\nabla^2\phi = \frac{1}{h_\mu^2}\left[\frac{\partial}{\partial\mu}\left(h_\mu \frac{\partial\phi}{\partial\mu}\right) + \frac{1}{\sin\eta}\frac{\partial}{\partial\eta}\left(h_\eta \sin\eta \frac{\partial\phi}{\partial\eta}\right) + \frac{h_\lambda}{\sin^2\eta}\frac{\partial^2\phi}{\partial\lambda^2}\right] \tag{3-40}$$

where

$$h_\mu = h_\eta = \frac{A}{\cosh \mu - \cos \eta}$$

$$h_\lambda = \frac{A \sin \eta}{\cosh \mu - \cos \eta} \tag{3-41}$$

The appropriate form for the solution of the Laplace equation for two conducting spheres in a uniform electric field, $\bar{E}$, is given by

$$\phi = -E\, z \cos\omega - E\, x \sin\omega + E(\cosh\mu - \cos\eta)^{1/2}$$

$$\left\langle \cos\omega \sum_{n=0}^{\infty} \left\{ A_n \exp\left[(n+\tfrac{1}{2})\mu \right] + B_n \exp\left[-(n+\tfrac{1}{2})\mu \right] \right\} P_n(\cos\eta) \right. \tag{3-42}$$

$$\left. + \cos\lambda \sin\omega \sum_{n=1}^{\infty} \left\{ G_n \exp\left[(n+\tfrac{1}{2})\mu \right] + H_n \exp\left[-(n+\tfrac{1}{2})\mu \right] \right\} P_n^1(\cos\eta) \right\rangle$$

where ω is the angle the field makes with the line of centers of the spheres.

Knowing the form of Ø, the following expansions are assumed:

$$\sigma_\ell(\eta,\lambda) = \epsilon\, E(\cosh\mu_\ell - \cos\eta)^{3/2} \left[\cos\omega \sum_{n=0}^{\infty} Y_n P_n(\cos\eta) + \cos\lambda \sin\omega \sum_{n=1}^{\infty} W_n P_n^1(\cos\eta) \right] \tag{3-43}$$

$$\sigma_s(\eta,\lambda) = \epsilon\, E(\cosh\mu_s - \cos\eta)^{3/2} \left[\cos\omega \sum_{n=0}^{\infty} Y_n P_n(\cos\eta) + \cos\lambda \sin\omega \sum_{n=1}^{\infty} Z_n P_n^1(\cos\eta) \right] \tag{3-44}$$

By using Eq. (3-40) the coefficients of equations (3-43) and (3-44) can be related to the coefficients of the potential function Eq. (3-42) as follows:

$$X_n = A_n\left(\frac{2n+1}{A}\right)\ \exp[\,(n+1/2)\mu_\ell\,]$$

$$Y_n = B_n\left(\frac{2n+1}{A}\right)\ \exp[\,(n+1/2)\mu_s\,]$$

$$W_n = G_n\left(\frac{2n+1}{A}\right)\ \exp[\,(n+1/2)\mu_\ell\,] \qquad (3\text{-}45)$$

$$Z_n = H_n\left(\frac{2n+1}{A}\right)\ \exp[\,(n+1/2)\mu_s\,]$$

The task now is to evaluate the coefficients in the expansion for $\emptyset$. Solutions for the electric field in the z-direction and in the x-direction can be treated separately and superposed to obtain the solution for the field in an arbitrary direction.

The influence of the electric field applied in the z-direction is found in several steps. First, the boundary value problem of two grounded spheres in a uniform electric field oriented along the z-axis is solved. The total induced charges on these two grounded spheres are determined along with the coefficients of induction for this two-sphere system. This will relate the charges on the spheres to their corresponding potentials. Now a second boundary value problem of two insulated spheres which are held at arbitrary potentials but with no applied electric field must be solved. By assuming a charge for each sphere which will cancel the induced charge for the grounded sphere case (plus any net charge assumed for each sphere) and by using the coefficients of induction, the potentials for the case of two insulated spheres can be determined such that the superposition of the two potential functions will leave a zero net charge on each sphere. The resulting potential function will be that of two uncharged spheres in a uniform electric field directed along the z-axis

The solution for the influence of the electric field in the x-direction is relatively easy to obtain. Since no charge is induced on the spheres when they are grounded, only the boundary value problem of two grounded spheres in a uniform electric field oriented along the x-axis need be solved.

Now the sum of the contribution due to the z-and x-components of the field will give the complete potential function for the arbitrarily oriented electric field.

The coefficients of the surface charge densities are now determined and the net force on each sphere found by integrating the surface electrical stresses, $\sigma_\ell{}^2/2\epsilon$ and $\sigma_s{}^2/2\epsilon$, over each sphere. The z- and x-components of the force acting on the small sphere are given by

$$F_z = \frac{1}{2\epsilon} \int_{\substack{\text{sphere}\\(s)}} \sigma_s{}^2 \cos\theta \; d(\text{area}) \tag{3-46}$$

$$F_x = \frac{1}{2\epsilon} \int_{\substack{\text{sphere}\\(s)}} \sigma_s{}^2 \sin\theta \; d(\text{area}) \tag{3-47}$$

The components of the force acting on small sphere are

$$F_{ze} = \frac{K}{2} \sum_{n=0}^{\infty} \exp[(2n+1)\mu_s] S_n \left\{ (2n+1) S_n - (n+1)[\exp(2\mu_s)+1] S_{n+1} \right\}$$
$$+ K E^2 \sin^2\omega \sum_{n=0}^{\infty} \exp[(2n+1)\mu_s] n(n+1) T_n \left\{ (2n+1) T_n - (n+2)[\exp(2\mu_s)+1] T_{n+1} \right\} \tag{3-48}$$

$$F_{xe} = \frac{K}{2} E \sin\omega [\exp(2\mu_s)-1] \sum_{n=0}^{\infty} (n+1) \exp[(2n+1)\mu_s]$$
$$\left\{ n S_{n+1} T_n - (n+2) S_n T_{n+1} \right\} \tag{3-49}$$

where

$$S_n = \frac{E\cos\omega(2n+1)\left\{\exp[(2n+1)\mu_\ell]+1\right\} - (\phi_s/A)\exp[(2n+1)\mu_\ell] + (\phi_\ell/A)}{\exp[(2n+1)\mu_o - 1]} \tag{3-50}$$

$$T_n = \frac{\exp[(2n+1)\mu_\ell] - 1}{\exp[(2n+1)\mu_s] - 1} \tag{3-51}$$

The potentials of each sphere due to both the induced charges Q_ℓ and Q_s and the net charges, q_ℓ and q_s, are

$$\phi_\ell = P_{\ell\ell}(q_\ell - K\ E\ \cos\omega\ Q_\ell) + P_{\ell s}(q_s - K\ E\ \cos\omega\ Q_s) \tag{3-52}$$

$$\phi_s = P_{s\ell}(q_\ell - K\ E\ \cos\omega\ Q_\ell) + P_{ss}(q_s - K\ E\ \cos\omega\ Q_s) \tag{3-53}$$

The coefficients of induction are

$$P_{\ell\ell} = C_{ss}/(C_{\ell\ell}C_{ss} - C_{\ell s}^2) \tag{3-54}$$

$$P_{\ell s} = P_{s\ell} = C_{\ell s}/(C_{\ell\ell}C_{ss} - C_{\ell s}^2) \tag{3-55}$$

$$P_{ss} = C_{\ell\ell}/(C_{\ell\ell}C_{ss} - C_{\ell s}^2) \tag{3-56}$$

where the coefficients of capacitance are

$$C_{\ell\ell} = \frac{K}{A}\sum_{n=0}^{\infty} \frac{\exp[(2n+1)\mu_s]}{\exp[(2n+1)\mu_o] - 1} \tag{3-57}$$

$$C_{\ell s} = C_{s\ell} = \frac{K}{A}\sum_{n=0}^{\infty} \frac{1}{\exp[(2n+1)\mu_o] - 1} \tag{3-58}$$

$$C_{ss} = \frac{K}{A}\sum_{n=0}^{\infty} \frac{\exp[(2n+1)\mu_\ell]}{\exp[(2n+1)\mu_o] - 1} \tag{3-59}$$

The induced charge is

$$Q_\ell = K \sum_{n=0}^{\infty} (2n+1) \frac{\exp[(2n+1)\mu_s] + 1}{\exp[(2n+1)\mu_o] - 1} \tag{3-60}$$

$$Q_s = -K \sum_{n=0}^{\infty} (2n+1) \frac{\exp[(2n+1)\mu_\ell] + 1}{\exp[(2n+1)\mu_o] - 1} \tag{3-61}$$

where

$$K = 8\pi \epsilon a^2$$

and

$$\mu_o = \mu_\ell + \mu_s$$

3.4 Equations of Motion

Now the various forces acting of the droplet can be determined. Since the negative x-axis is selected as the direction of vertical fall, the gravitational force, $m_s g$, acts on the droplet in the negative x-direction as shown in Fig. 3-4.

The interaction of the viscous fluid, which flows around the drop, and the droplet can be expressed by the use of the well known Stokes equation for the drag of a sphere

$$\bar{F}_h = -6\pi \nu a_s D_s(\bar{v}_s - \bar{u}) \tag{3-62}$$

where ν is the viscosity of fluid, $\bar{u}$ is the velocity of the viscous fluid around the drop, $\bar{v}_s$ is the velocity of the droplet relative to the drop and D_s is the drag coefficient which has a value of unity for drops which are in the Stokes range.

The equations of motion including electrical forces are

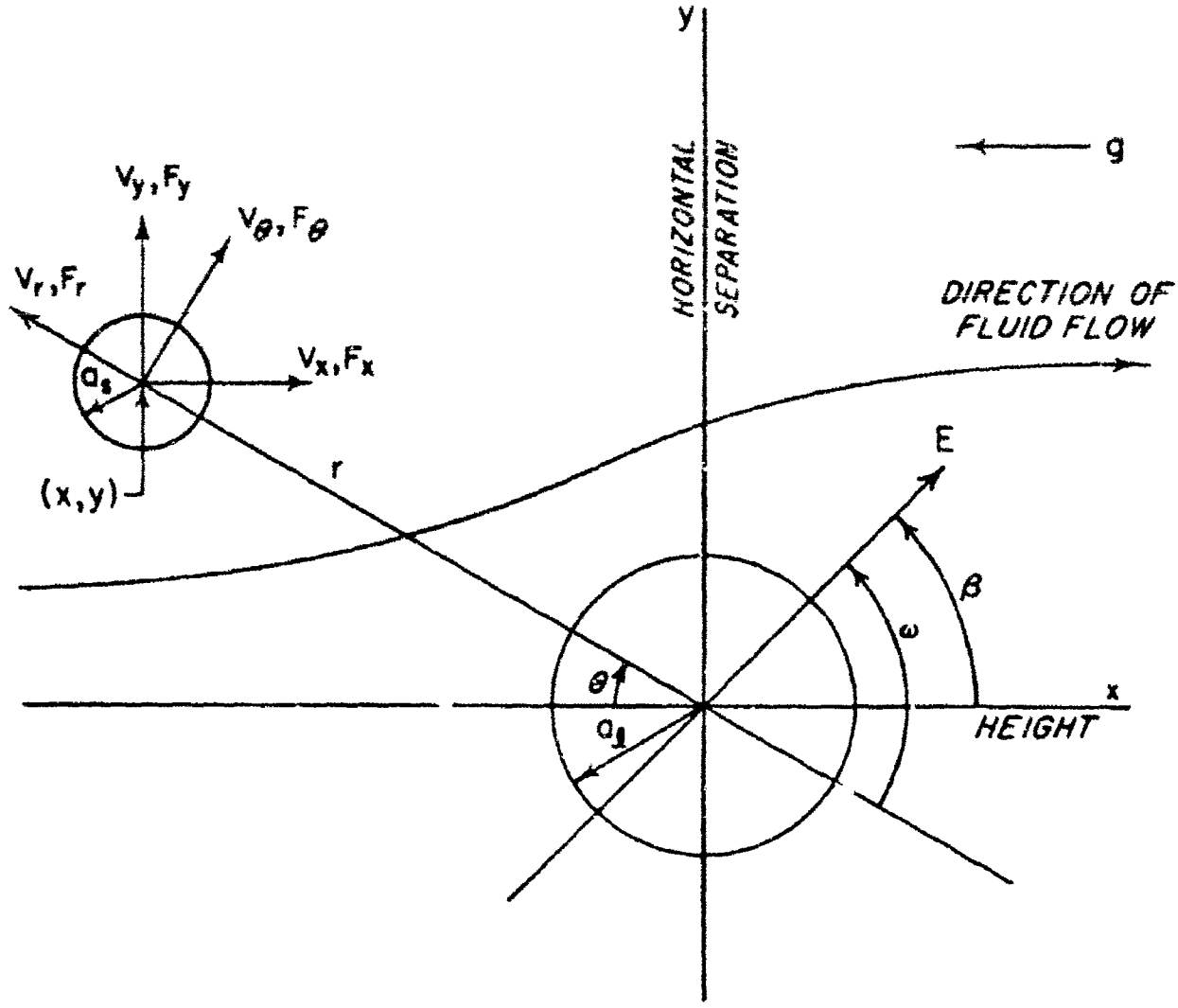

Figure 3-4 Motion of a droplet in an electric field, E, relative to a fixed drop.

$$m_s \frac{dv_{xs}}{dt} = -6\pi \nu a_s D_s (v_{xs} - u_x) - m_s g + F_{xe} \tag{3-63}$$

$$m_s \frac{dv_{ys}}{dt} = -6\pi \nu a_s D_s (v_{ys} - u_y) + F_{ye} \tag{3-64}$$

$$\frac{dx_s}{dt} = v_{xs} \tag{3-65}$$

$$\frac{dy_s}{dt} = v_{ys} \tag{3-66}$$

These equations of motion were solved on the IBM 7094 digital computer at the University of Illinois. A numerical integrating routine first described by Nordsieck (1962) was used. The routine incorporated automatic starting, automatic selection, and revision of the integration step. To start the integration, only the initial conditions and a logical elementary interval are necessary. At small distances from the drop, the interval is automatically shortened to obtain an accurate solution. When a smaller integration step is used that is necessary, excessive time is spent by the computer in developing a more accurate solution than is needed. Thus the routine gives a solution of a given accuracy in the least amount of time.

The initial velocities of the drop and droplet were determined by computing the terminal velocity of each when gravity acts on the mass and an electric field acts on any net charge. Since the center of the drop is assumed as the origin of a fixed coordinate system the initial velocity of the droplet is the difference between the terminal velocity of the two drops. The initial separation was 100 drop radii. At this separation, there is very little interaction between the disturbed fluid

around the drop and the droplet or between the net charges which may reside on either drop. The initial horizontal separation was one drop radius.

CHAPTER IV

EFFECTS OF ELECTROSTATIC FORCES ON THE COLLISION EFFICIENCY OF A PAIR OF DROPS

4.1 Without Electrostatic Forces

There are many possible combinations of droplet sizes, net charges, and applied electric fields. Therefore, it has been necessary to limit the investigation to a few cases which appear to be interesting and useful for future work.

When two uncharged drops fall in a field free space, only gravity and the drag force of the viscous medium influence their trajectories and, consequently, the collision efficiency. Figure (4-1) shows how this collision efficiency varies for drops of 25 to 70 microns paired with droplets of 5, 7.5, 10, 12.5, 15, and 20 microns. The collision efficiency goes to zero as the size of the droplet approaches the size of the drop since the relative velocity between the pair approaches zero. In general, for a droplet of a given size the collision efficiency increases as the size of the drop increases since it is more difficult to move the droplets with greater mass around the drop with only a hydrodynamic flow of the air.

4.2 With an Applied Electric Field

The collision efficiencies for both horizontal and vertical electric fields are shown in Figures 4-2, 4-3, and 4-4. The increase in the collision efficiency due to an applied electric field is a result of an induced nonuniform charge distribution on the surface of the two drops. The interaction of the two charge distributions can either be attractive or repulsive depending on the orientation of the applied field and the relative position of the drops. If only the dipole interaction is

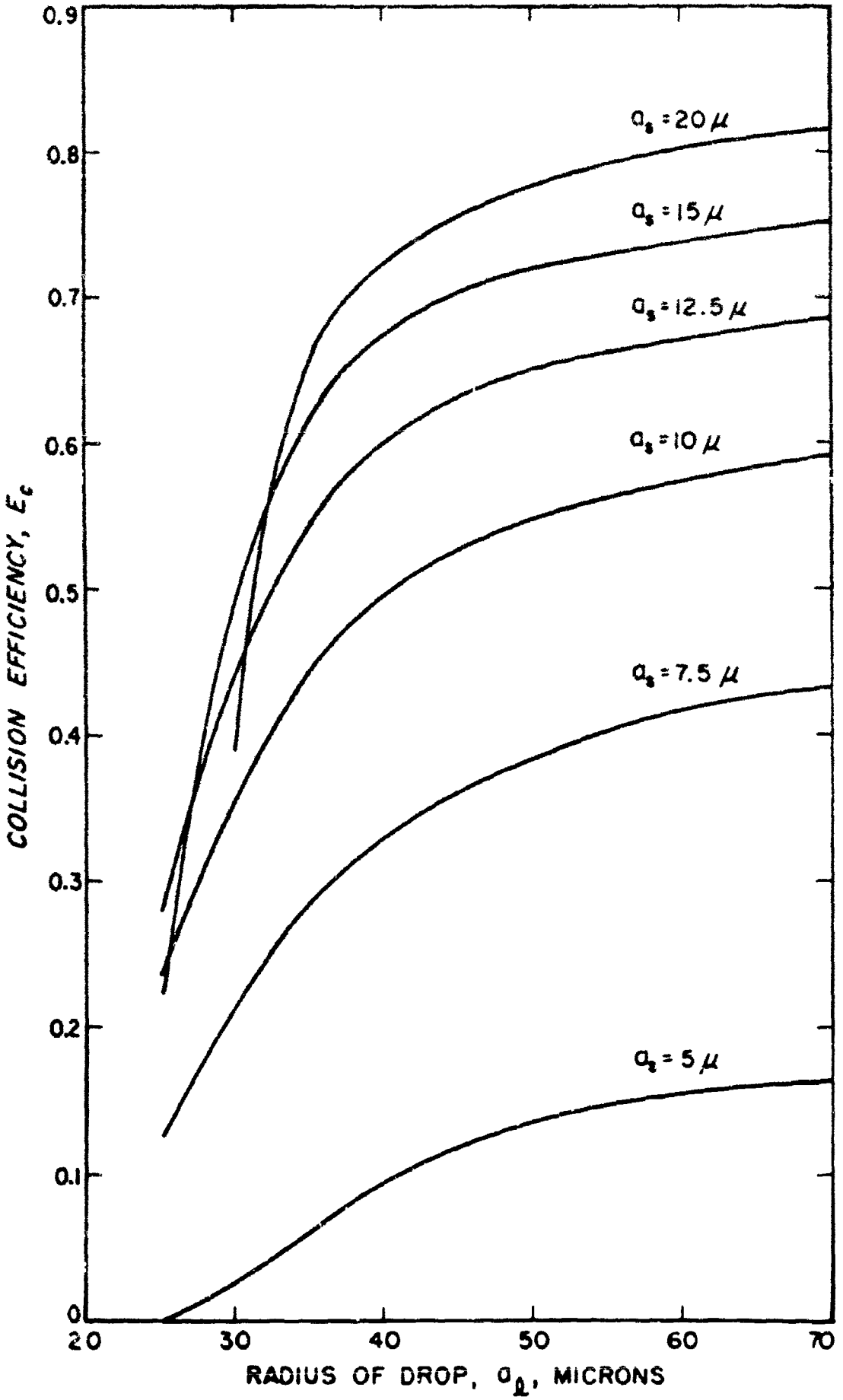

Figure 4-1 Collision efficiency curves when no electrostatic force is present.

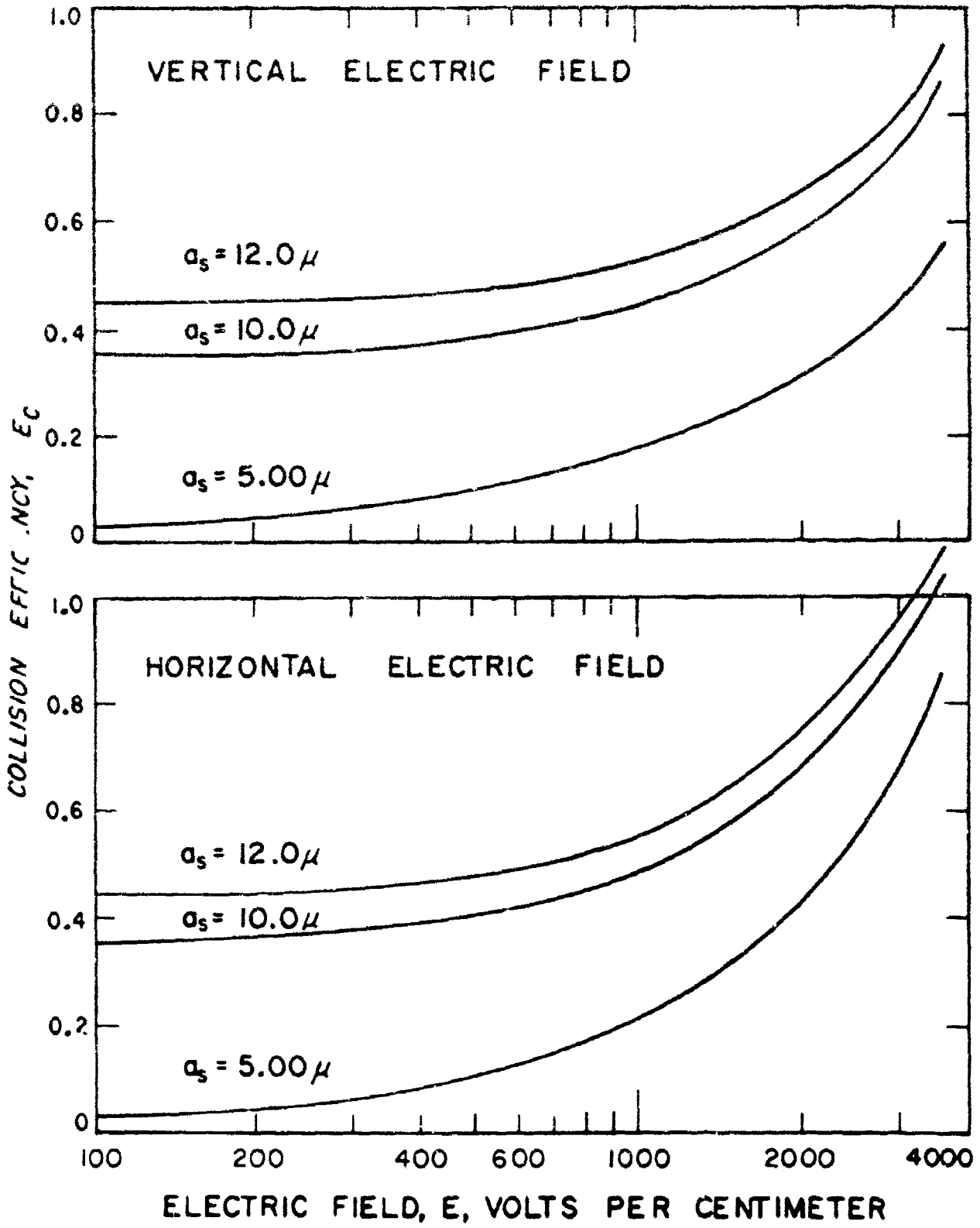

Figure 4-2 Collision efficiency curves for a 30 micron drop with a 5, 10, and 12 micron droplet.

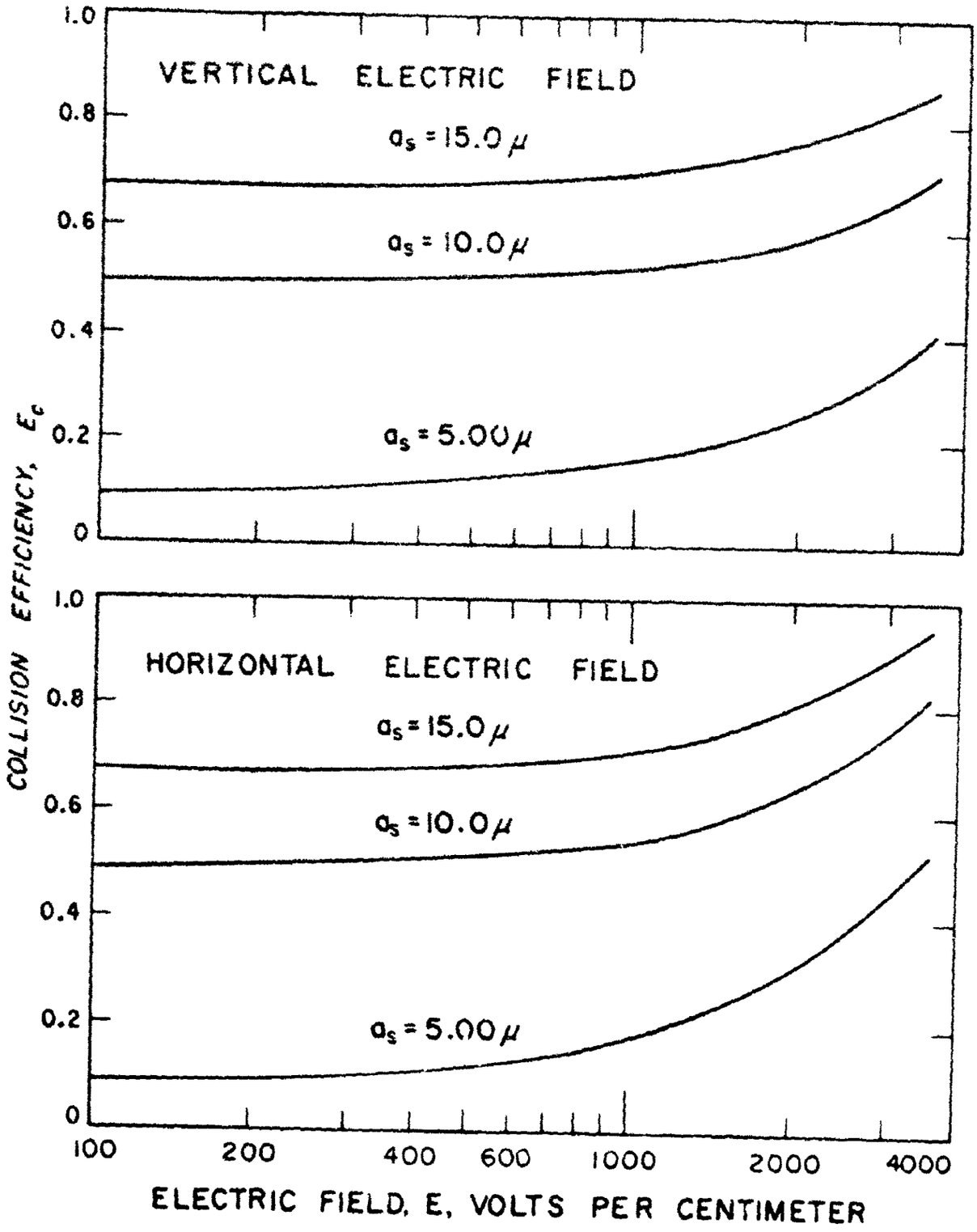

Figure 4-3 Collision efficiency curves for a 40 micron drop with a 5, 10, and 15 micron droplet.

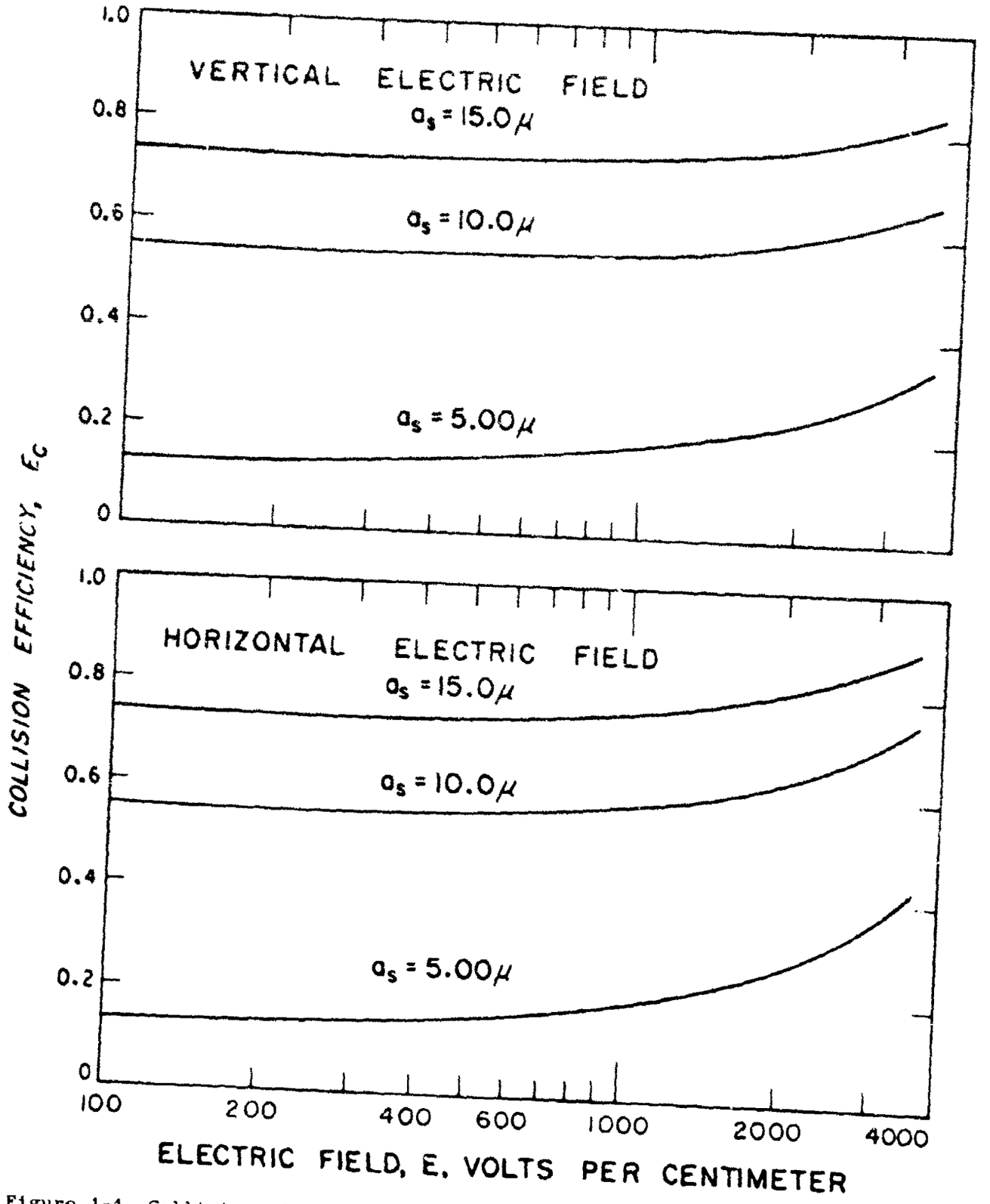

Figure 1-4 Collision efficiency curves for a 50 micron drop with a 5, 10, and 15 micron droplet.

considered, the regions of attraction and repulsion can be determined as illustrated by Lindblad and Semonin (1963).

The trajectories for the 30 micron drop and 5 micron droplet are shown in Figure 4-5. The effect of a region of repulsion about the y-axis is illustrated for the case of vertically applied electric fields. The initial trajectory of the droplet is toward the drop but it changes its direction of travel after entering this region of repulsion. The horizontally applied electric fields have a region of attraction about the y-axis and result in pulling the droplets into the back side of the drop for certain initial conditions.

It is observed from Figures 4-2, 4-3, and 4-4 that the horizontally applied electric fields produce the largest increase in collision efficiencies and it is greatest for the 30 and 5 micron pair of drops. A horizontal electric field of 3600 volts per centimeter increases the collision efficiency of a 30 and 5 micron pair by a factor of 34.5 compared to 5.6 for the 40 and 5 micron pair and 5.0 for the 50 and 5 micron pair. Thus, the collision efficiency curves flatten as the collector drop increases in size. This is due to the large difference between the relative velocities of the drop and droplet which does not allow a sufficient time for the electrical force to attract the pair together.

The effect of the orientation of the applied electric field can be seen in Figures 4-6 and 4-7 which show the change in the collision efficiency for various pairs of drops as a function of the angle β between the electric field, E, and the x-axis. The angle β is measured positively in the counter-clockwise direction. The largest collision

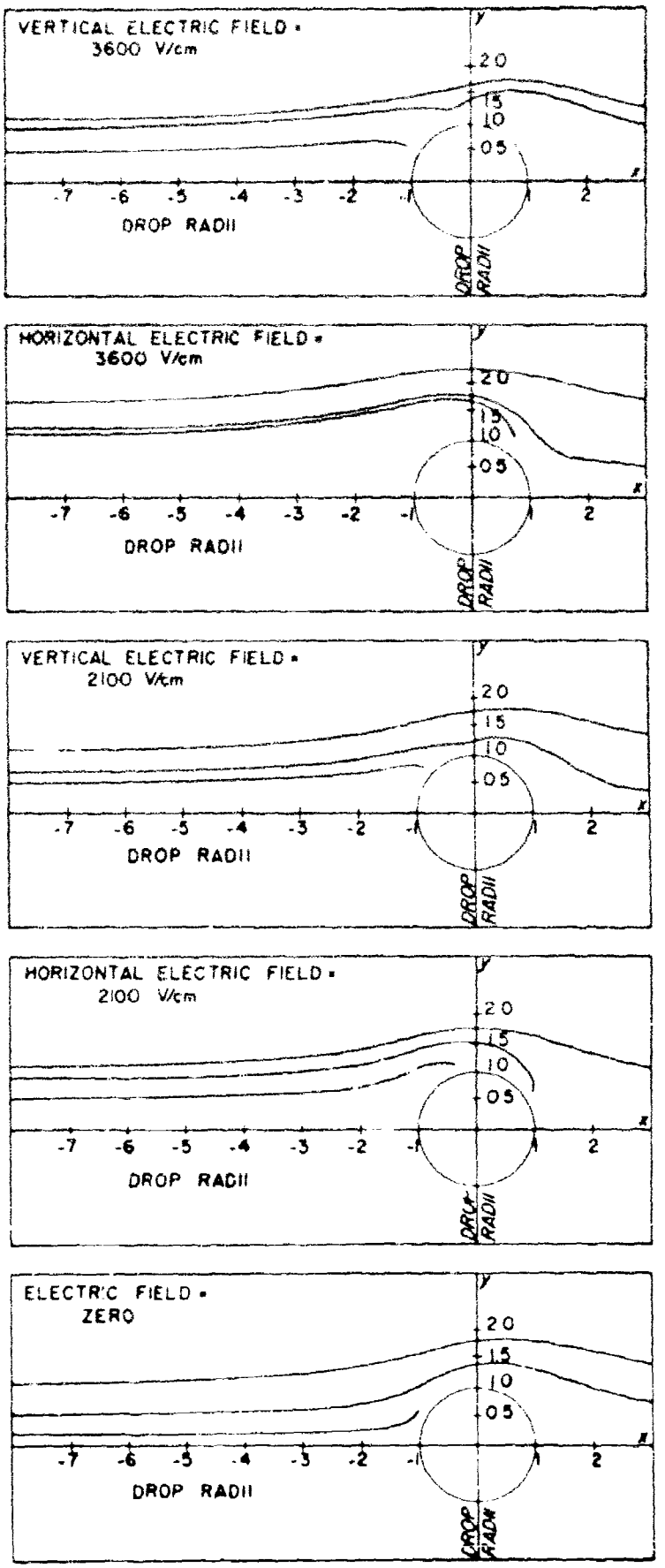

Figure 4-5 Trajectories for a 30 micron drop and a 5 micron droplet.

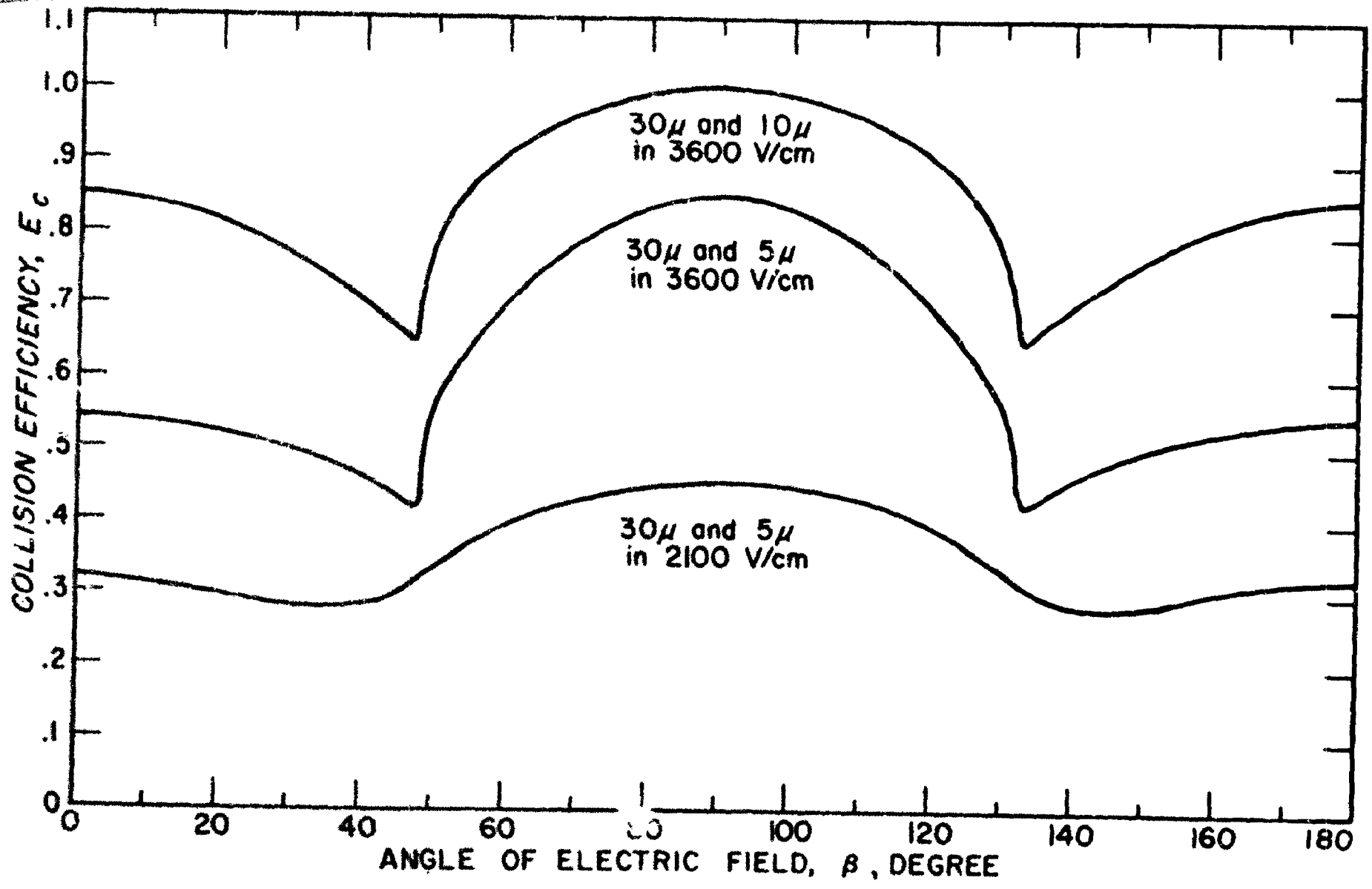

Figure 4-6 Change in collision efficiency of drop pairs for various orientations of electric field.

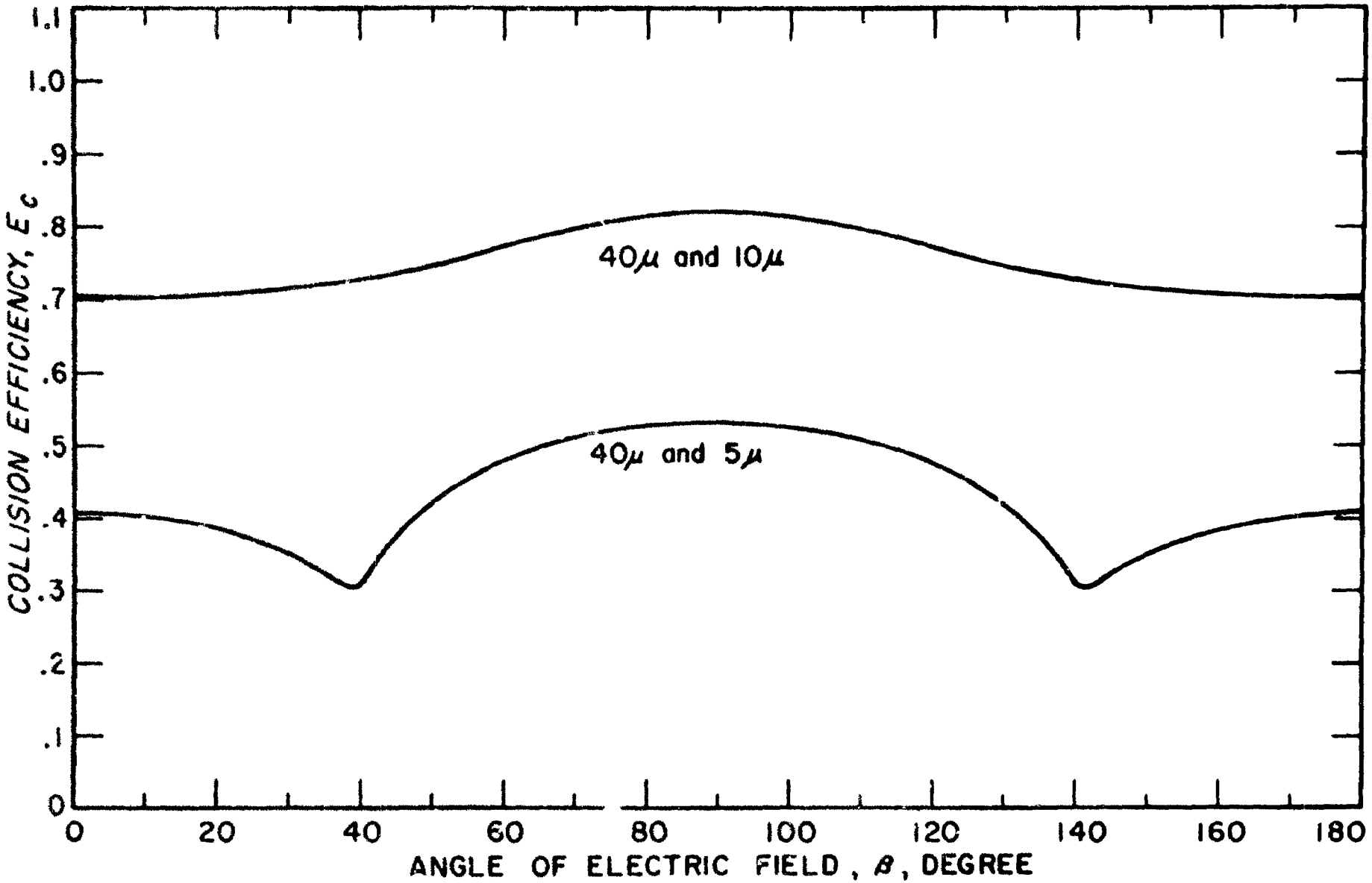

Figure 4-7 Change in collision efficiency of drop pairs for various orientations of electric fields at 3600 volts per centimeter.

efficiencies occur approximately in the range $50^{\circ} < \beta < 130^{\circ}$ and the lowest collision efficiency for β approximately equal to 42° and 138°. The maximum collision efficiency occurs for β equal to 90° (a horizontally applied electric field).

4.3 With a Net Electric Charge

The charge on the drop was arbitrarily selected to always be positive since the only critical conditions were the charge magnitudes and whether or not the two droplets had alike or opposite charges. Also, since there was an infinite number of possible combinations of charges to be considered on the two droplets, it was necessary to set a ratio of charge between the pairs of droplets. Gunn (1949) obtained some measurements of the charge on cloud droplets which indicated that the net charge varied approximately as the square of the radii of the droplets. Therefore, for this work the ratio of the charge on a pair of droplets was taken as the ratio of the surface area of the two droplets.

With these two conditions on the charges, the collision efficiencies of drops of 30, 40, and 50 microns paired with droplets of 5 and 10 microns are shown in Figures 4-8, 4-9, 4-10, and 4-11. As would be expected for charges of the same sign, which usually result in a repulsive electrostatic force between the droplets, the collision efficiency does not change appreciably until the charge on the droplet is greater than 1×10^{-17} coulombs, but decreases to zero for a charge between 1 and 5×10^{-16} coulombs. The collision efficiency of the 10 micron droplet is almost constant until it has a charge greater than 1×10^{-16} coulombs, then it decreases to zero for a charge between 2 and 5×10^{-15} coulombs.

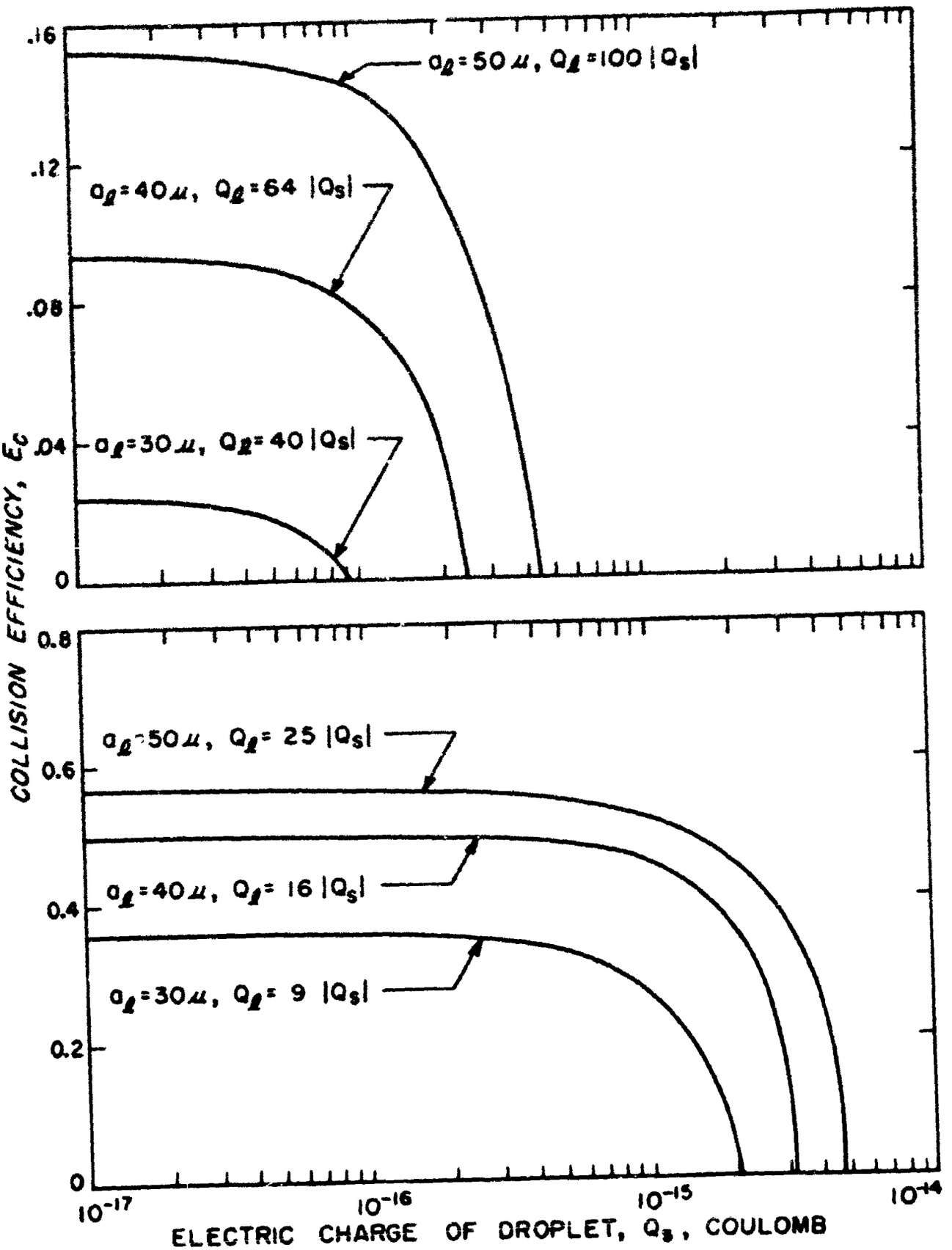

Figure 4-8 and 4-9 Collision efficiency curves for a 5 (above) and 10 (below) micron droplet with a 30, 40, and 50 micron drop.

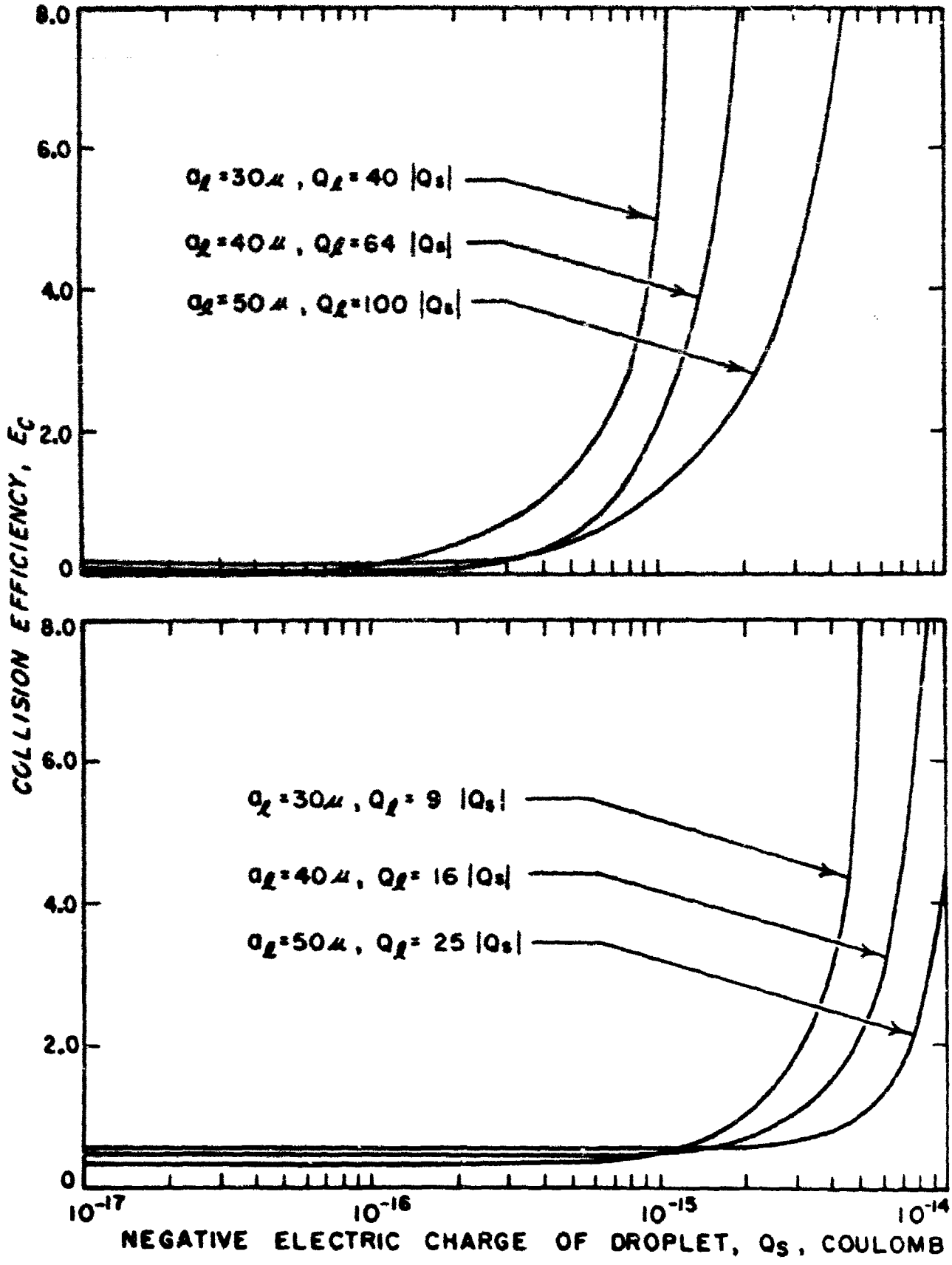

Figure 4-10 and 4-11 Collision efficiency curves for a 5 (above) and 10 (below) micron droplet with a 30, 40, and 50 micron drop.

For charges of the opposite sign on the droplets, the collision efficiency increases as the magnitudes of the charges are increased since the electrostatic force is attractive. There is no appreciable change in the collision efficiency of the 5 micron droplet until it has a magnitude of charge greater than 10^{-16} coulombs, then it increases very rapidly. But for the 10 micron droplet, the collision efficiency remains almost constant until its charge exceeds 1×10^{-15} coulombs, then its collision efficiency increases very sharpely.

4.4 With Both an Applied Electric Field and an Electric Charge.

As in the case of the drops in a region of an applied field, the sign of charge on the drop was selected to always be positive and the ratio of the charge for a pair of drops was selected as proportional to the ratio of the areas of the two drops. Since only fields of either 0° or 180° orientations are reported here, it is easy to show that all combinations can be determined with this selection of the sign of charge on the drop. For example, if both drops had negative charge with the applied field at 0°, then this would be the same condition as when both drops had positive charge but the same applied field had an orientation of 180°. Therefore only four separate combinations of field orientation and the sign of the charge on the droplet need be considered for only vertically applied fields.

Figures 4-12, 4-13, 4-14, and 4-15 show the family of curves for the collision efficiencies for a 30 and 5 micron pair of drops. For the magnitudes of the charge on the droplet of the order of 10^{-18} coulombs, the collision efficiency is the same as for only an applied electric field. The same is true for the 40 and 5 micron pair shown in

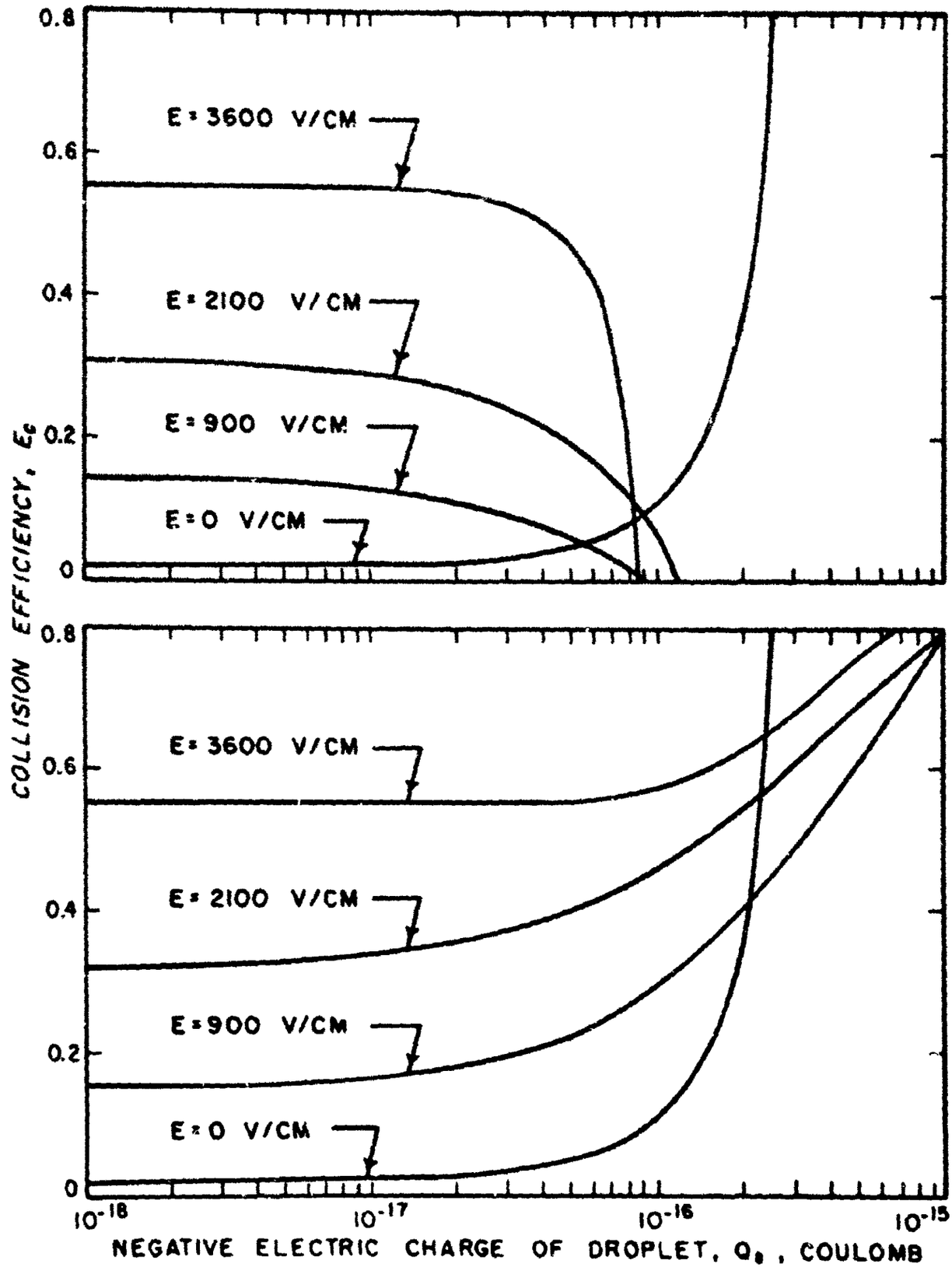

Figure 4-14 and 4-15 Collision efficiency curves for a 30 micron and 5 micron drop pair with an electric field directed upward (above) and downward (below). $Q_L = 40\,|Q_s|$.

Figures 4-16, 4-17, 4-18, and 4-19 and for the 50 and 5 micron pair shown in Figures 4-20, 4-21, 4-22, 4-23. The collision efficiencies are less for the 40 and 5 micron and the 50 and 5 micron pairs as expected from section 4.2.

For the case of positive charge on the droplet, the collision efficiency is found to increase with an increase in the electric field and with an increase in the electric charges as shown in Figures 4-12, 4-13, 4-16, 4-17, 4-20, and 4-21. As was noted in paragraph 4.3, with no applied field the collision efficiency goes to zero for a sufficiently large electric charge. In contrast, an applied electric field can prevent this decrease in the collision efficiency. This is an important result, since even in a cloud of positively charged droplets the collision efficiency can still be quite high if external electric fields are present.

With a negative charge on the droplet in a field-free region, the collision efficiency increases very rapidly with an increase in the charge as shown by the zero field curves in Figures 4-14, 4-15, 4-18, 4-19, 4-22, and 4-23. There is still an increase in the collision efficiency when the orientation of the applied field is at 180^{o} but the rate of increase is reduced. Since the relative velocity between the drop pair has been increased the time required for the droplet to pass the drop has been reduced resulting in less time for the attractive electrostatic force to pull the pair of drops together.

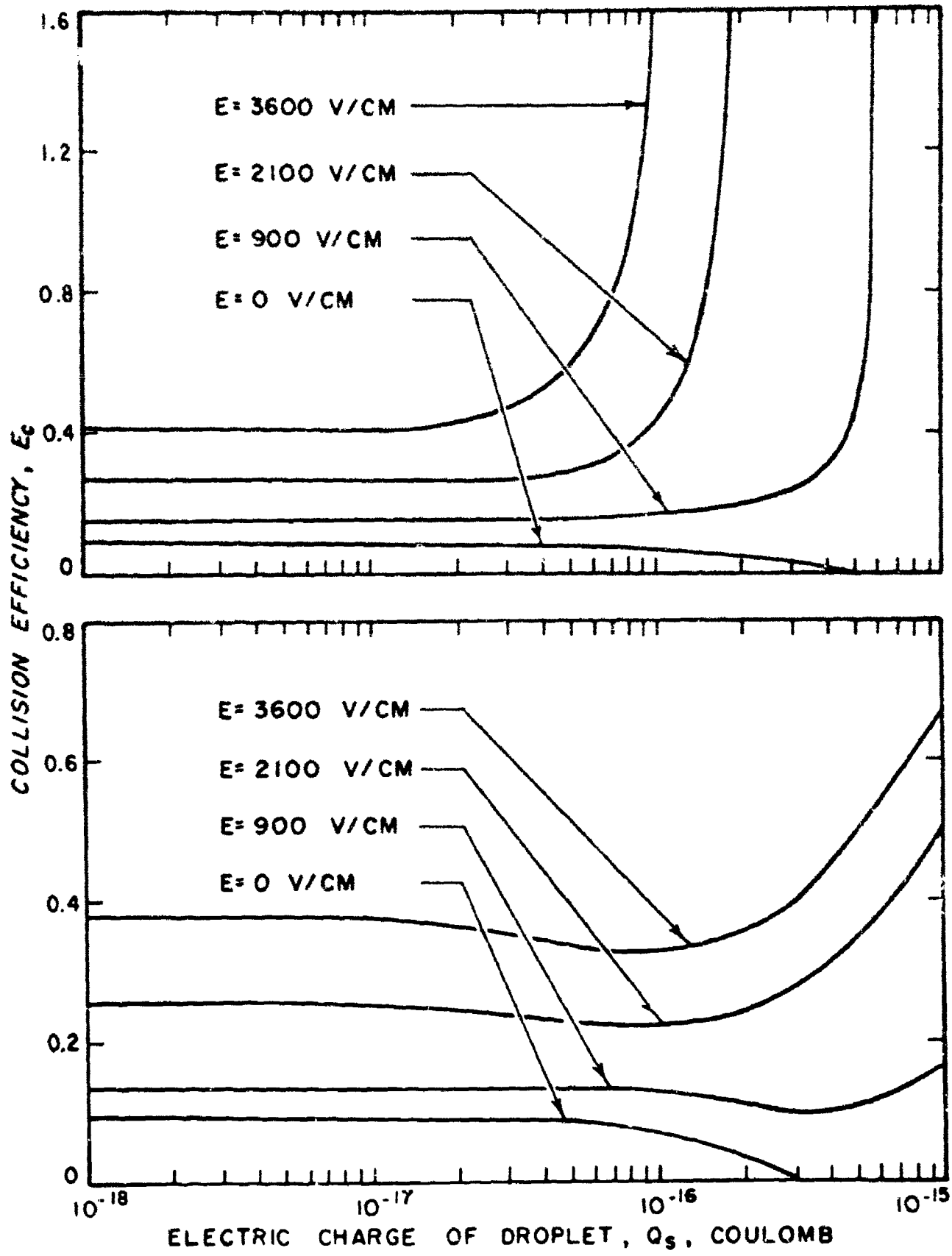

Figure 4-16 and 4-17 Collision efficiency curves for a 40 micron and 5 micron drop pair with an electric field directed upward (above) and downward (below). $Q_c = 64|Q_s|$.

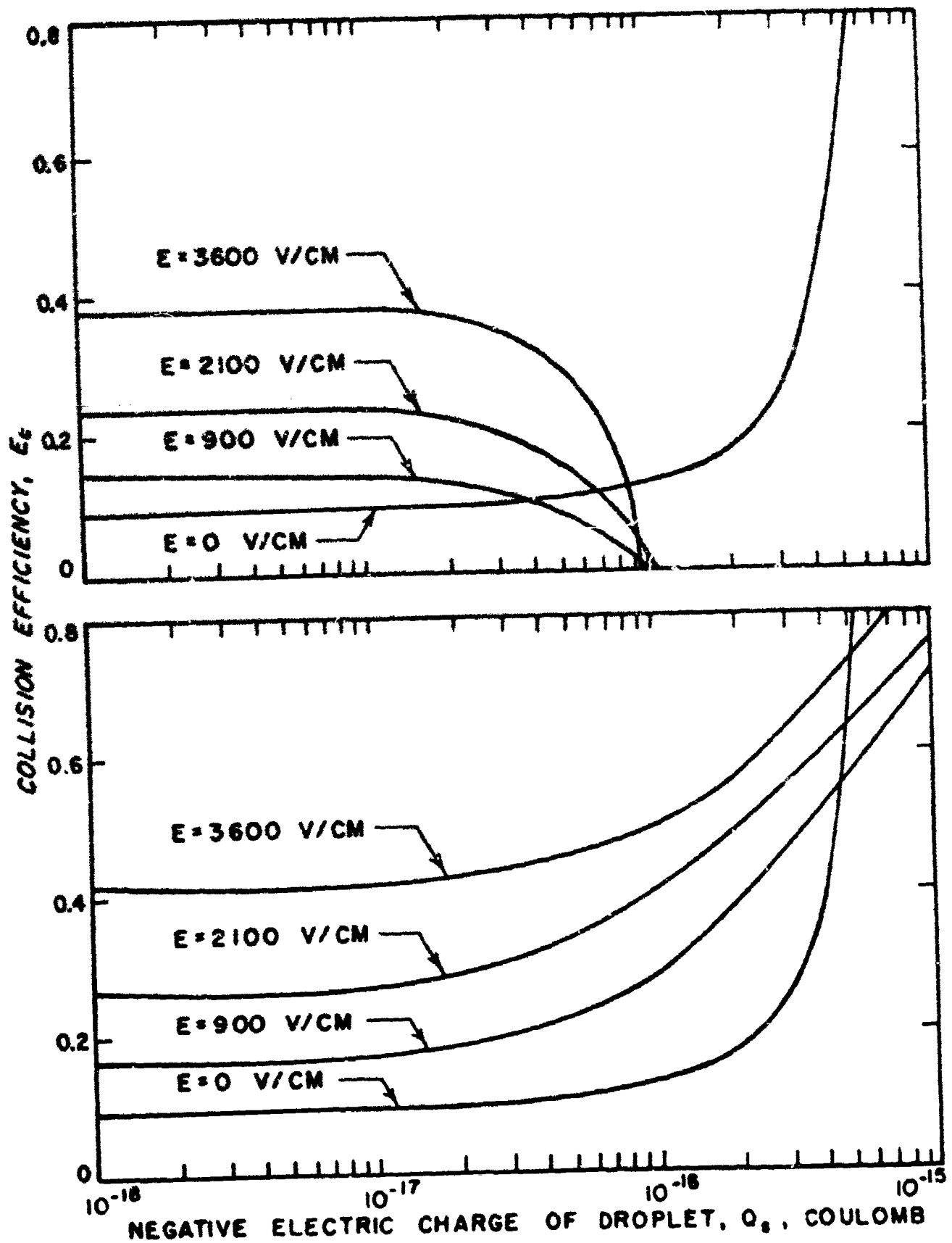

Figure 4-18 and 4-19 Collision efficiency curves for a 40 micron and 5 micron drop pair with an electric field directed upward (above) and downward (below). $Q_L = 64|Q_s|$.

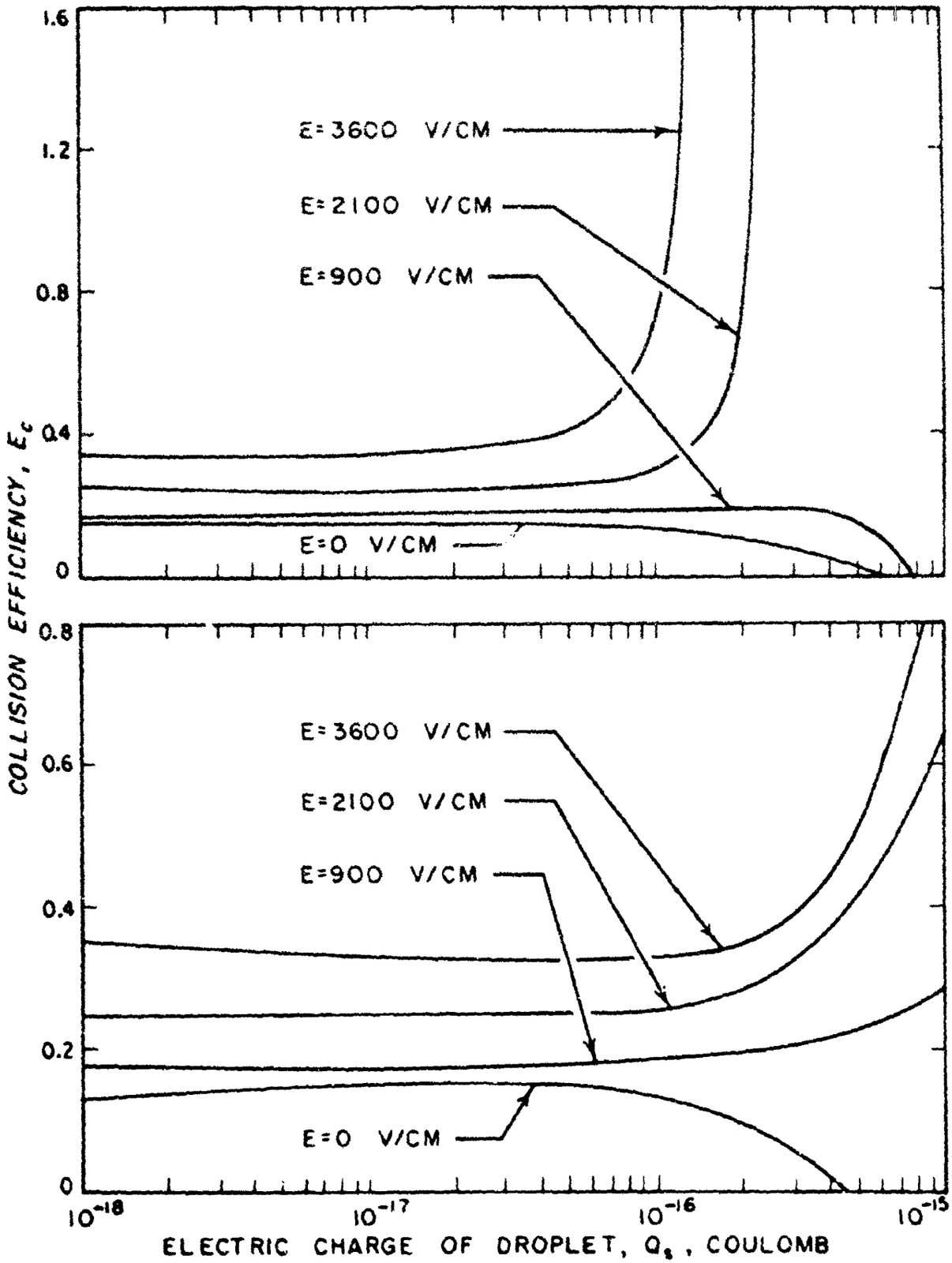

Figure 4-20 and 4-21 Collision efficiency curves for a 50 micron and 5 micron drop pair with an electric field directed upward (above) and downward (below). $Q_\ell = 100 \left|Q_s\right|$.

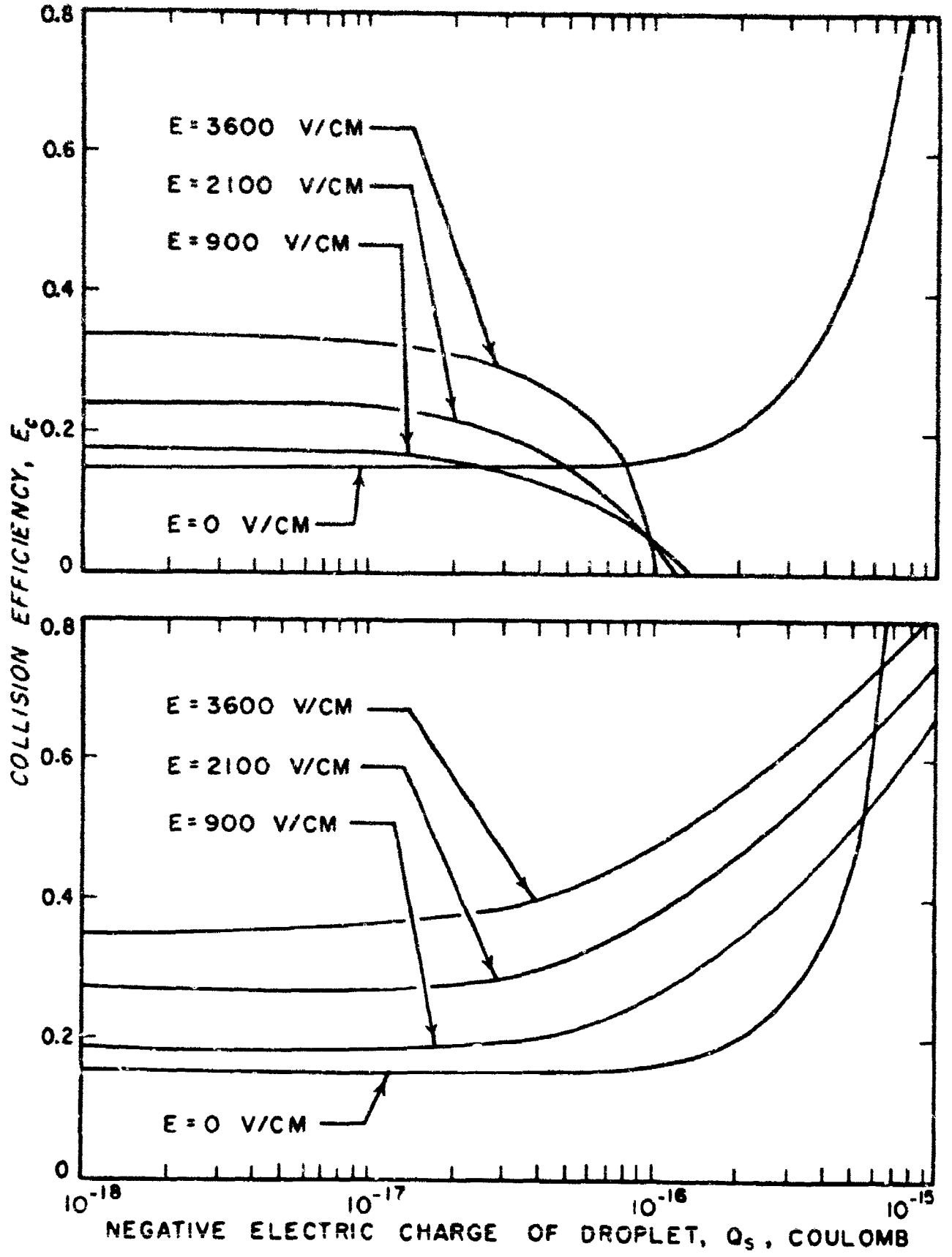

Figure 4-22 and 4-23 Collision efficiency curves for a 50 micron and 5 micron drop pair with an electric field directed upward (above) and downward (below). $Q_\ell = 100\ |Q_s|$

CHAPTER V

THEORETICAL ASPECTS OF THE COALESCENCE PROCESS

5.1 The Coalescence Process

The observation of the merging of two liquid surfaces immersed in a continuous media is made difficult by several factors. The concept of a boundary between a liquid and the continuous medium is complicated by the motion of molecules continually entering and leaving a rather nebulous transition region of the liquid. Random perturbations can exist in the transition region and can be caused by vibrations due to noise, non-uniform distribution of surface charge, impurities in the liquid or they can be periodic perturbations caused by vibrations of sound at a given frequency

To make the study of the coalescence of two liquid surfaces tractable, the surfaces are regarded as a distinct boundary. A pressure difference across the boundary of a liquid with a curved surface is caused by a phenomenon called surface ten. on. Surface tension has the property of trying to minimize the surface energy of the system. Therefore, it follows that for two liquid surfaces to coalescences, an interaction must develop such that the energy of a combined single surface is less than the energy of a system of two separate surfaces in proximity.

5.2 Trapped Gas Film Between the Colliding Surfaces

As the two liquid surfaces approach each other, the continuous medium in which they are immersed must be forced out of the way so the two surfaces can come close enough together to allow their coalescence. By observing the collision of two liquid surfaces, it is found that the surfaces deform into flat adjacent surfaces until coalescence occurs.

Many investigators (Gillespie and Rideal, 1956; Elton and Picknett, 1957; Charles and Mason, 1960; and Pincen, 1963) have considered various models of drops approaching a second liquid surface.

By using a cylindrical coordinate system, symmetry about the z-axis and the plane z = 0 exists. The flattened surfaces are located at $z = \pm h$ and the velocities of the surfaces are given by $V = -\frac{dh}{dt}$ as indicated in Figure 5-1. An incompressible fluid of viscosity, ν, is expelled radially from between the two surfaces at a velocity U(z, r). It will be assumed that the flow is laminar, radial, and that inertial effects are negligible. The distance from the plane z = 0 to the drop surfaces is given by ξ. The radial velocity may be written as

$$u(z,r) = (\xi^2 - z^2)\psi(r) \tag{5-1}$$

where $\psi(r)$ is a function of r and it is to be determined. Equation (5-1) implies a parabolic velocity profile with respect to z without slip at the adjacent surfaces, i.e., U(z, r) = 0 at $z = \pm \xi$. The volume flow of the expelled fluid per unit time, Q, is

$$Q = \int_{-\xi}^{\xi} 2\pi r\, u(z,r)dz \tag{5-2}$$

By substituting (5-1) into (5-2), we obtain

$$Q = 2\pi r\, \psi(r) \int_{-\xi}^{\xi} (\xi^2 - z^2)dz \tag{5-3}$$

Integrating (5-3) yields

$$Q = \frac{8\pi r\, \psi(r)\xi^3}{3} \tag{5-4}$$

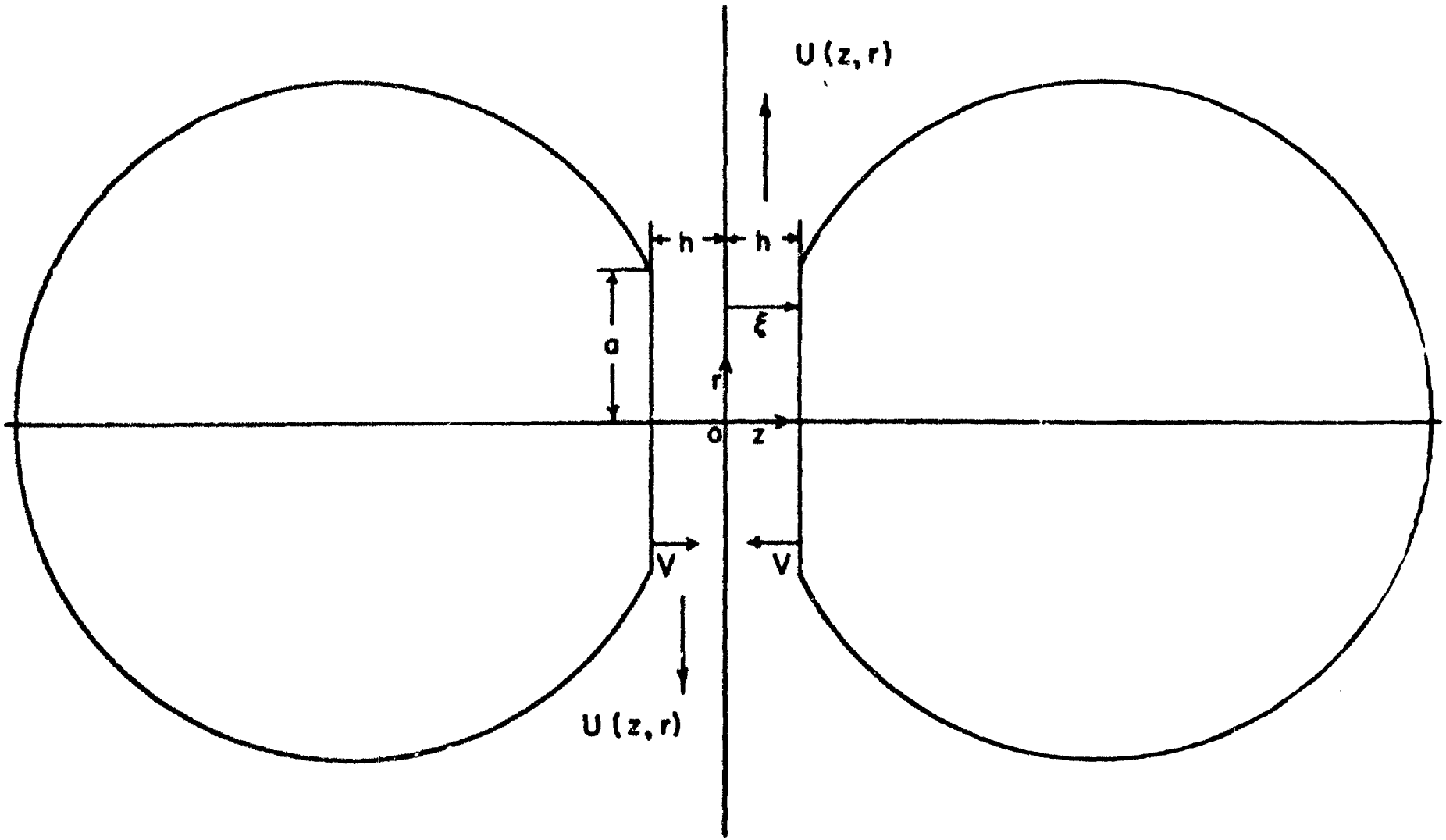

Figure 5-1 Illustration of the deformation of the adjacent surfaces of the colliding drops.

Equating the change in the volume flow per unit time to the volume of the gas displaced by the approaching surfaces per unit time between r and (r + dr), leads to

$$dQ = d\left(\frac{8\pi r\psi(r)\xi^3}{3}\right) = 2\cdot 2\pi rVdr \tag{5-5}$$

Integrating (5-5) and solving for $\psi(r)$ yields

$$\psi(r) = \frac{3Vr}{4\xi^3} \tag{5-6}$$

By putting (5-6) into (5-1), we obtain

$$u(z,r) = \frac{3Vr(\xi^2 - z^2)}{4\xi^3} \tag{5-7}$$

By equating the mechanical work per unit time expended in moving the two surfaces together at a velocity V, to the energy per unit time dissipated by the viscosity of the expelled fluid, we obtain from first principles

$$2FV = \int \nu\left(\frac{\partial u}{\partial z}\right)^2 d(\text{Volume}) = \int_o^a \int_{-\xi}^{\xi} \nu\left(\frac{\partial u}{\partial z}\right)^2 2\pi r dr dz \tag{5-8}$$

where F is the force acting on the surfaces. Differentiating (5-7) with respect to z gives

$$\frac{\partial u}{\partial z} = \frac{-3Vrz}{2\xi^3} \tag{5-9}$$

By substituting (5-9) into (5-8) and integrating, it follows that

$$FV = \frac{3\pi V^2 \nu}{2} \int_o^a \frac{r^3}{\xi^3}\, dr \tag{5-10}$$

since V is independent of ξ and r. Solving for V yields

$$V = -\frac{dh}{dt} = \frac{2F}{3\pi\nu \int_o^a \frac{r^3}{\xi^3}\, dr} \tag{5-11}$$

For this investigation, it is assumed that ξ is equal to h and is independent of r for $0 \leq r \leq a$ which gives

$$\int_o^a \frac{r^3}{\xi^3}\, dr = \frac{a^4}{4h^3} \tag{5-12}$$

Substituting (5-12) into (5-11) gives

$$\frac{dh}{dt} = \frac{-8Fh^3}{3\pi\nu a^4} \tag{5-13}$$

Equation (5-10) gives the velocity at which each surface is moving. This velocity is a function of the physical parameters of the system as well as the force, F, acting to move the surfaces together. An interesting case is produced if it is assumed that F is a constant, F_o, and that the radius of the deformation, a, is a constant.

Equation (5-13) can be rewritten as

$$\int_o^{t_1} dt = \frac{-3\pi\nu a^4}{8F_o} \int_{h_o}^{h_1} \frac{dh}{h^3} \tag{5-14}$$

which when integrated yields

$$t_1 = \frac{3\pi\nu a^4}{16F_o}\left(\frac{1}{h_1^2} - \frac{1}{h_o^2}\right) \qquad (5\text{-}15)$$

where t_1 is a measure of the time required for the surfaces to move from h_o to h_1. For this case, the time of approach is directly proportional to the radius of deformation but is inversely proportional to the force pushing the surfaces together. Equation (5-15) is the same result obtained by Reynolds (1886) for two parallel plates moving together in a viscous medium.

5.3 Effects of an Electric Potential Difference

Since the deformation of the drops is assumed to be flat, the electrostatic force between these flat surfaces can be found by assuming that the surfaces represent a circular parallel plate capacitor. Harnwell (1949) calculated such a force and determined it to be

$$F_e = \frac{\pi a^2 \varepsilon \phi_o^2}{8h^2} \qquad (5\text{-}16)$$

where ϕ_o is the electric potential difference between the surfaces and ε is the permittivity of the gas trapped between the surfaces.

In addition to an electrostatic force, another force is acting to move the surfaces together resulting from the initial momentum of the liquid. For convenience, let the additional force be given by a constant force per unit area, P_o. Since the net force on the flat surface is

proportional to the square of its radius, the force can be expressed as $\pi a^2 P_o$. Therefore, the total force bringing the liquid surfaces together is given by

$$F = \frac{\pi a^2 \varepsilon \phi_o^2}{8h^2} + \pi a^2 P_o \qquad (5\text{-}17)$$

It is also observed that the deformation of the approaching liquid surfaces is not constant but varies as a function of time. The experimental results given in Section 6.5 indicate that the radius of deformation grows independently of the potential difference and can be expressed as

$$a = 3.2 \times 10^{-4} t^{3/8} \qquad (5\text{-}18)$$

Since the deformation of the drop is independent of the potential difference, the neglecting of the interaction of the curved portion of the drop surfaces is justified.

By substituting (5-17), and (5-18) into (5-13) and rearranging the terms, we obtain

$$\int_o^t \frac{dt}{t^{3/4}} = -3.84 \times 10^{-8} \nu \int_{h_o}^{h_1} \frac{dh}{h^3 \left[\frac{\varepsilon \phi_o^2}{8h^2} + P_o\right]} \qquad (5\text{-}19)$$

Integrating (5-19) yields

$$4t_1^{1/4} = \frac{1.536 \times 10^{-7} \nu}{\varepsilon \phi_o^2} \left[\ln\left(\frac{h_o}{h_1}\right)^2 + \ln\left(\frac{\varepsilon \phi_o^2 + 8F_o h_1^2}{\varepsilon \phi_o^2 + 8F_o h_o^2}\right)\right] \qquad (5\text{-}20)$$

Solving for t_1 gives

$$t_1 = \left(\frac{3.84\times10^{-8}\nu}{\epsilon\phi_o^2}\right)^4 \left[\ell n\left(\frac{h_o}{h_1}\right)^2 + \ell n\left(\frac{\epsilon\phi_o^2 + 8F_o h_1^2}{\epsilon\phi_o^2 + 8F_o h_o^2}\right)\right]^4 \qquad (5\text{-}21)$$

where t_1 is the time, starting with the deformation of the surfaces, required for the surface separation to change from $2h_o$ to $2h_1$.

5.4 Stability of the Liquid Surfaces

Since the stability of the two approaching surfaces can be indicated by the time interval between the onset of the deformation and their coalescence, t_1 in (5-21) is a measure of this stability if h_1 is the position of the surfaces at coalescence. Coalescence itself is probably a random process since the surfaces are not well defined and perturbations on the surfaces lead to a probability of coalescence for any separation. However, equation (5-21) does indicate the general influence of the various parameters on the stability of this system.

Equation (5-21) indicates that the stability increases as the fourth power of the viscosity of the gas trapped between the surfaces. This type of dependence appears reasonable, since gases of higher viscosity should be more difficult to squeeze from between the two surfaces. However, the viscosity of a gas is not dependent on the pressure of the gas until very low pressures are reached; therefore, for a moderate pressure the stability of the system will be independent of this pressure. Viscosity is dependent on temperature however; therefore, the stability should be a function of the temperature.

If the electrostatic force between the surfaces is small compared to the constant force, P_o, the limit of equation (5-21) as $\phi_o \to 0$ becomes

$$t_1 = \left(\frac{2.4\times10^{-8}\nu}{P_o}\right)^4 \left(\frac{1}{h_1^2} - \frac{1}{h_o^2}\right)^4 \qquad (5\text{-}22)$$

Under this condition, the stability of the system varies as the inverse of the fourth power of the constant force, P_o, compared to only its first power in (5-15), the difference being that the equation (5-15) did not include any change in the deformation as the surfaces move together.

The last case to consider is that in which the electrostatic force is much larger than the constant force. The limit of equation (5-21) as $\phi_o \to \infty$ becomes

$$t_1 = \left(\frac{7.68\times10^{-8}\nu}{\epsilon\phi_o^2}\right)^4 \left[\ell n\left(\frac{h_o}{h_1}\right)\right]^4 \qquad (5\text{-}23)$$

It appears that the stability is inversely proportional to the eighth power of the potential difference, ϕ_o. However, the electrostatic force is such that any perturbations on the surfaces will enhance this force and amplify the perturbations. The growth of the perturbations will influence the probability of coalescence at any given separation. The implication is that h_1 should also be a function of ϕ_o. Therefore, t_1 is not necessarily inversely proportional to the eighth power of ϕ_o. The proportionality will depend on the variation of h_1 with ϕ_o. As an example, if h_1 varies as

$$\frac{h_1}{h_o} = K \exp(-\phi_o) \tag{5-24}$$

It follows that

$$\left[\ell n\left(\frac{h_o}{h_1}\right)\right]^4 = \left[-\phi_o^2 + \ell n\ K\right]^4 \tag{5-25}$$

Substituting (5-25) into (5-23) yields

$$t_1 = \left(\frac{7.68\times10^{-8}\nu}{\epsilon}\right)^4 \left(1 - \frac{\ell n\ K}{\phi_o^2}\right)^4 \tag{5-26}$$

and for large ϕ_o

$$t_1 = \left(\frac{7.68\times10^{-8}\nu}{\epsilon}\right)^4 \tag{5-27}$$

Of course, in this case t_1 is independent of ϕ_o which does not appear to be correct. Therefore, it is left to experimentation to determine the correct form of t_1 as is done in Section 6.2. By using the model of two drops with flat surfaces, some speculation can be made about the variation of h_1 with respect to the applied potential which is helpful since this dependence is not easily measured.

CHAPTER VI

EXPERIMENTAL OBSERVATIONS OF THE COALESCENCE PROCESS

6.1 Experimental Technique

No satisfactory method has been found to allow careful study of two single coalescing drops freely falling in air. Therefore, it has been necessary to constrain the two drops in order to conduct an investigation. In this study, drops were formed at the tips of two number-18 hypodermic needles which were etched so the tip would be flat. One needle was mounted rigidly inside a sealed, electrically shielded chamber. The second needle was mounted on pivots in such a way that the tip would swing very close to the tip of the stationary needle, permitting a collision between the drop pair. The velocity at which the drops collided was varied by changing the length of the arc through which the pendulum swung. The pressure of the air inside the chamber was varied by means of a vacuum pump. The temperature and relative humidity were measured with an electric hygrometer indicator.

A 16 mm Fastax camera was used to take high speed photographs of the profile view of the two colliding drops. Since the one drop was held stationary, the optical system for photography was greatly simplified. Two dc carbon arc lamps were used to illuminate the drops. One lamp was placed slightly to the right and above the camera itself. This lamp furnished the front lighting giving a better three-dimensional appearance to the photographs. The second lamp was placed behind the drops directly in line with the camera lens. A mylar diffusion screen was placed approximately 0.5 centimeters behind the drops to reduce highlights. With this arrangement, photographs at a speed of 14,000 frames

per sec. were taken of the profile view of the collision and coalescence of the two drops. The sequence of events for taking these photographs was predetermined by timing clocks. The camera was started first to allow it to reach a high film velocity before the pendulum was released from a solenoid operated clamp.

The potential between the two drops was varied by electrically insulating the two needles and applying variable voltages between them. A Keithley 600 A Electrometer was used to measure this potential difference. A precision 10 ohm resistor was placed in series with this circuit, as shown in Figure 6-1. The current in the circuit was monitored by measuring the voltage across this resistor with one channel of a dual beam Tektronix oscilloscope, type 551. The second channel monitored the potential applied between the two needles, and a Tektronix oscilloscope camera model C-12 was used to record these quantities. The oscilloscope was adjusted so the trace was triggered by the initiation of the current. Since the circuit was normally open, only with the coalescence of the two drops did any charge flow.

Two neon lamps were mounted in the Fastax camera in such a way that their light was recorded along the extreme edges of the 16 millimeter film. One lamp was used to record 1000 cycles per second timing pulses which were of equal on and off duration. This provided a means to measure the time between different events photographed on the film. The second neon lamp was used to record the time of the initial flow of current in the electrical circuit. The lamp was turned on by a thyratron tube triggered by the initial current. A time delay of less than 20 microseconds

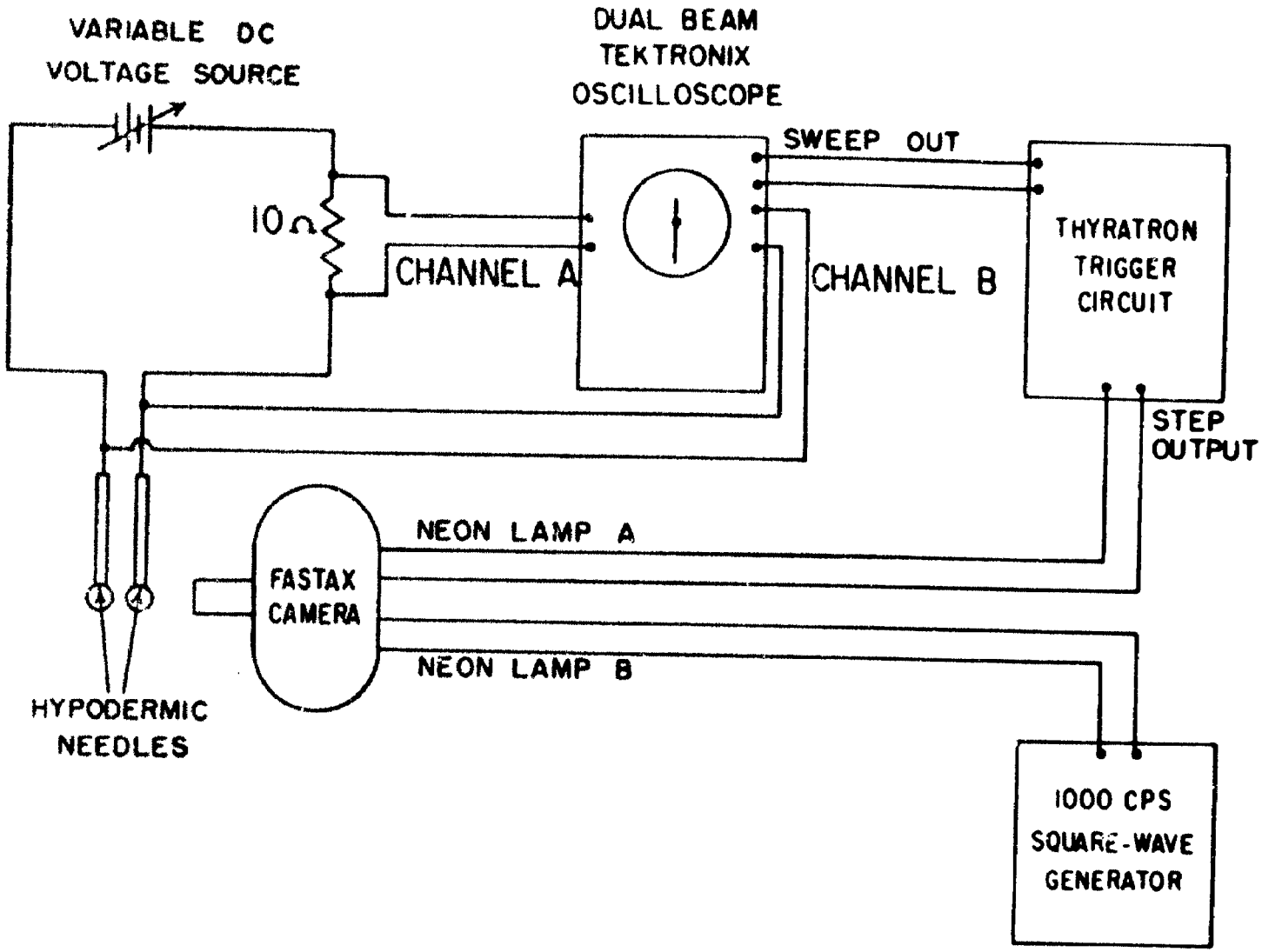

Figure 6-1 Block diagram of the experimental apparatus for measuring the current between colliding water drops.

was measured for air triggering circuit. This procedure provided a means to measure the time interval between the initial current and coalescence recorded on the film.

Measurements from the film were taken by the use of an analog-to-digital converter. Scaling of distances was accomplished by accurately measuring the diameter of the tip of a hypodermic needle and comparing this with its measurement from the film. The collision velocity was determined by measuring the approach of the two drop surfaces as a function of the 1000 cycles per second timing marks along the edge of the film. After the collision of the two drops, but before their coalescence, the rate of deformation of the adjacent surfaces was determined by measuring the height of the flattened region. At coalescence a transition region between the drops was formed which has the appearance of a lens. Photographs of both the flattening and the lens are shown in Figure 6-2. The rate of growth of both the height and width of this lens was measured.

The initial appearance of this lens was taken as the beginning of the coalescence process. The time between the visual contact of the drop surfaces until appearance of the lens is defined as the coalescence time. The time between the initial flow of charge and the initial appearance of the lens is defined as the current time. The intervals of time measured were easily determined within 2 frames of the film giving an accuracy of $\pm$ 150 microseconds.

To insure adequate current for reliable measurements, distilled water with a small amount of hydrochloric acid was used. This solution had a pH = 1.9 and a conductivity $\sigma = 6 \times 10^{-3}$ mhos/centimeter. Both drops had a radius of approximately 2 millimeters. The voltage between the drops was

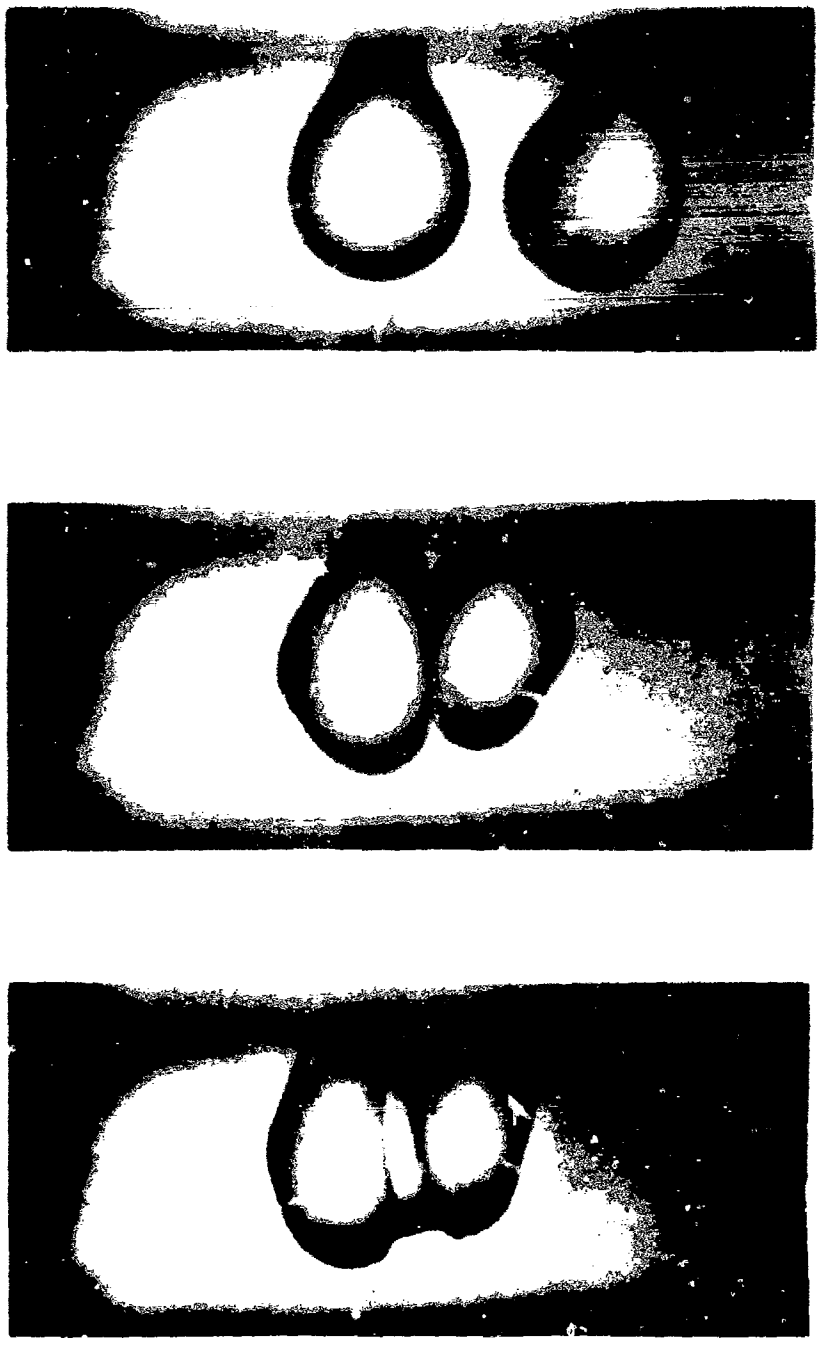

Figure 6-2 Photographs showing the profile of two water drops before collision, after collision, and after coalescence.

varied between 0 to 10 volts d-c. Temperature and relative humidity were approximately 25°C and 50 percent respectively. A typical set of photographs of the collision and coalescence are shown in Figure 6-3.

6.2 Effects of Electrostatic Forces on the Coalescence Process

A plot of the reciprocal of the coalescence time for two collision velocities as a function of the applied voltage is shown in Fig. 6-4. The curves drawn are found by the method of least squares as discussed in Wylie (1951). For potential less than 1 volt the spread in the data increased and became somewhat random. This range of voltage was not investigated and the curves are merely projected to 0 voltages. For the range of 0-0.5 volts, a collision followed by a separation of the two drops is easily obtained since the drops separate before the minimum coalescence time. Photographs of this separation are shown in Fig. 6-5.

The relationship between the applied voltage and the coalescence time is determined from the experimental data by applying the method of least squares. First, the following relationship is assumed

$$t = A\,\phi_o^b \tag{6-1}$$

By taking the logarithm of (6-1), we obtain

$$\log(t) = \log(A) + b\,\log(\phi_o) \tag{6-2}$$

Now, by using the logarithms of t and ϕ_o both log(A) and b are determined by the method of least squares. It is found that b = - 1.0235 which indicates that an inverse relationship should exist. This result agrees with that of Berg (1963).

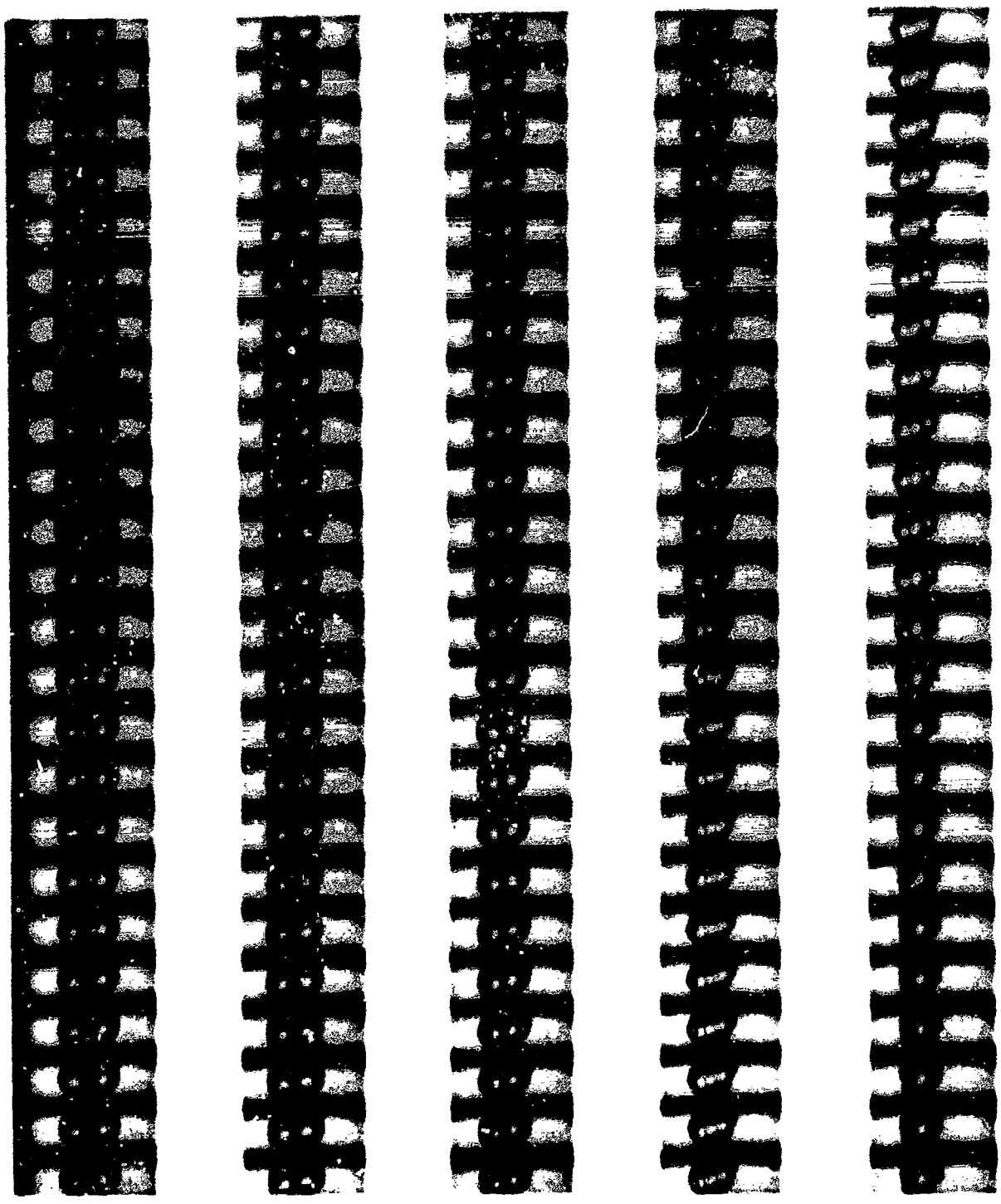

Figure 6-3 A sequence of photographs taken at 14,000 frames per second of colliding and coalescing water drops with a potential difference of 1 volt.

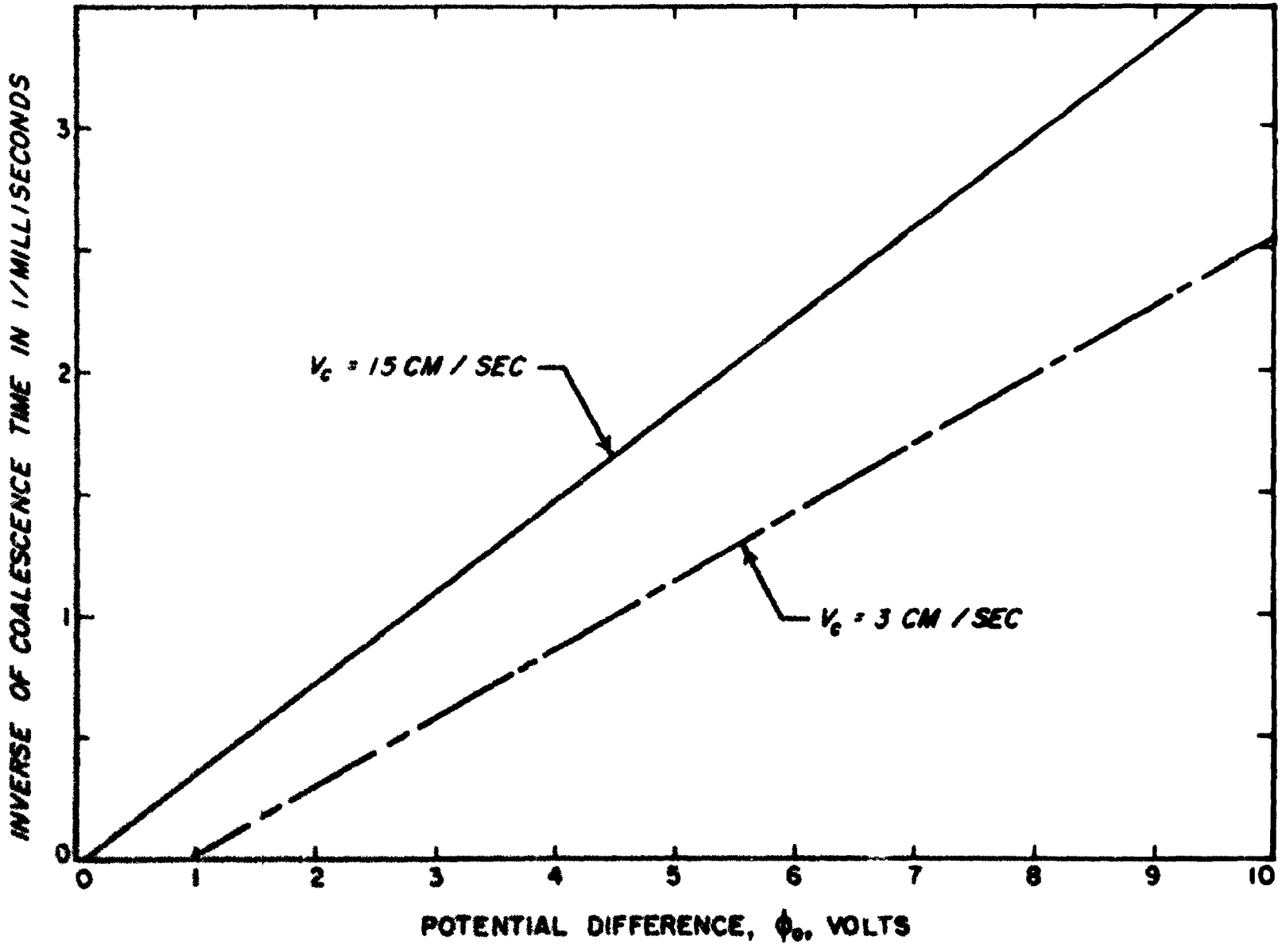

Figure 6-4 A plot of the inverse of coalescence time as a function of the potential difference between drops.

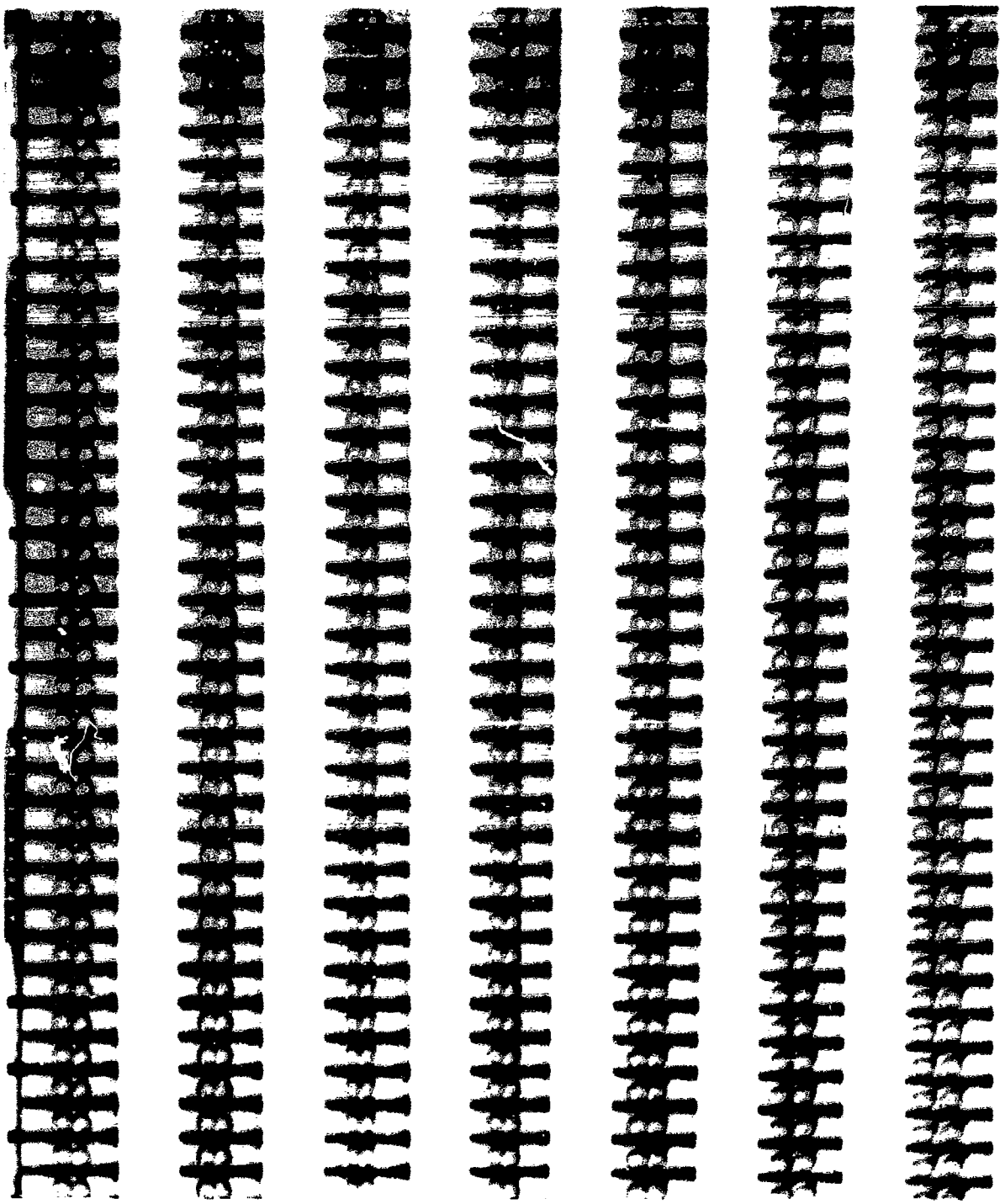

Figure 6-5 A sequence of photographs taken at 14,000 frames per second of colliding and separating water drops with no potential difference.

Figure 6-4 does indicate that the coalescence time is inversely proportional to the applied voltage, but the slopes of the curves are slightly different for different collision velocities. Therefore, the coalescence time decreases as the voltage is increased. For a collision velocity of 14 centimeters per second, the coalescence time is 0.266 milliseconds when the potential difference is 10 volts as compared to 2.0 milliseconds when the potential difference is 1 volt.

For the model of two drops approaching each other with a flat deformation, t_1 is found to have the following limit for large ϕ_o

$$t_1 = \left(\frac{7.68\times10^{-8}\nu}{\epsilon\phi_o^2}\right)^4 \left[\ell n\left(\frac{h_o}{h_1}\right)\right]^4 \qquad (5\text{-}23)$$

But as was suggested in section (5-4), h_1 may also be a function of ϕ_o which means that equation (5-23) is not complete. Since experimentally it is found that t_1 is inversely proportional to ϕ_o, then it follows from (5-23) that

$$\frac{1}{\phi_o^7}\left[\ell n\left(\frac{h_o}{h_1}\right)\right]^4 = k^4(\text{constant}) \qquad (6\text{-}3)$$

for large ϕ_o. Therefore,

$$\frac{h_1}{h_o} = \exp(-k\phi_o^{7/4}) \qquad (6\text{-}4)$$

From (5-23). t_1 can now be written as

$$t_1 = \left(\frac{7.68\times10^{-8}\nu}{\epsilon}\right)^4 \frac{k^4}{\phi_o} \qquad (6\text{-}5)$$

compared to

$$t_l = \frac{2.88\times10^{-6}}{\phi_o} \qquad (6\text{-}6)$$

determined from experimentation. Therefore, solving for k by equating (6-5) and (6-6) yields

$$k = \frac{1.07\times10^{6}\epsilon}{\nu}$$

For air $k = .26$

6.3 Effects of Pressure on the Coalescence Process

The coalescence times for air pressures of 190, 380, and 760 millimeters of mercury inside the sealed chamber containing the colliding drops are given in Fig. 6-6. The temperature, relative humidity, and collision velocity are maintained at 20°C, 50 per cent, and 14 centimeters per second, respectively. The relationships between the coalescence time and the applied potential for these different pressures are determined by the method of least squares. The correlation coefficient, as described by Parratt (1961), for the data at the various pressures is 0.822 for 190 millimeters of mercury, 0.956 for 380 millimeters of mercury, and 0.953 for 760 millimeters of mercury. However, when the data for the three different pressures is considered together, a correlation coefficient of 0.962 is determined which indicates a good correlation of all the data independent of any influence of pressure for the 2 millimeter drops examined.

This result agrees with the conclusion of Section 5.4. The model used indicates that the only dependence of the coalescence time on air is that it is proportional to the fourth power of the viscosity of the air. However, the viscosity of gases does not vary with moderate changes in pressure; therefore, the coalescence time is also independent of pressure.

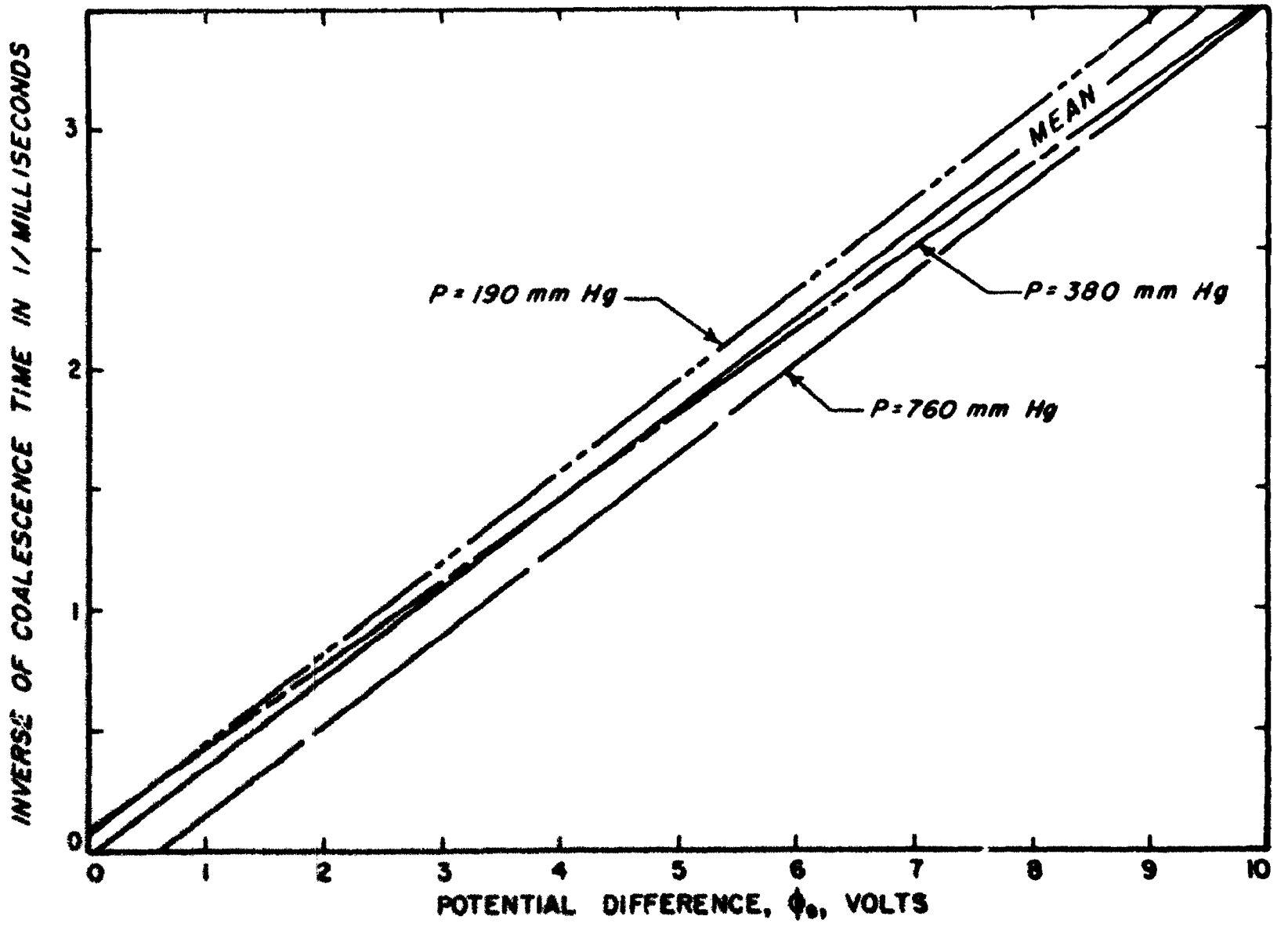

Figure 6-8 A plot of the inverse of coalescence time as a function of the potential difference between drops for various air pressures, P.

6.4 Charge Flow Before Coalescence

A plot of the current time is given in Fig. 6-7. Since the current is found to start before the apparent coalescence determined by the profile view of the drops on the film, this current indicates the possibility that charge is transferred between the drops before their coalescence. Although the voltage applied between the surfaces is less than 10 volts for a very small separation between the surfaces, the local electric field can exceed the value that is normally required to initiate ionization of the air. However, the electrons can not obtain enough kinetic energy in this short distance to produce ionization of the air molecules since the ionization potential of oxygen is 13.5 volts, nitrogen is 14.5 volts and carbon dioxide is 14.4 volts. These ionization potentials are greater than the 10 volts applied between the drops; therefore, a discharge between the surfaces by ionization of the air is not likely. However, just before coalescence small perturbations of liquid on the surfaces may be pulled off due to the high electrostatic forces present and they would carry a net charge. The charge carried by this transfer of mass could account for the indicated current before coalescence. Since no current is observed for the case when the drops collide and separate, this charge flow would contribute to the initiation of the coalescence precess.

6.5 Rate of Growth of the Deformation

The rate at which the deformation of the colliding surfaces develop is given by a plot in Fig 6-8 of the height of the flattened area as a function of the time after the initial deformation. It is observed that

after contact.

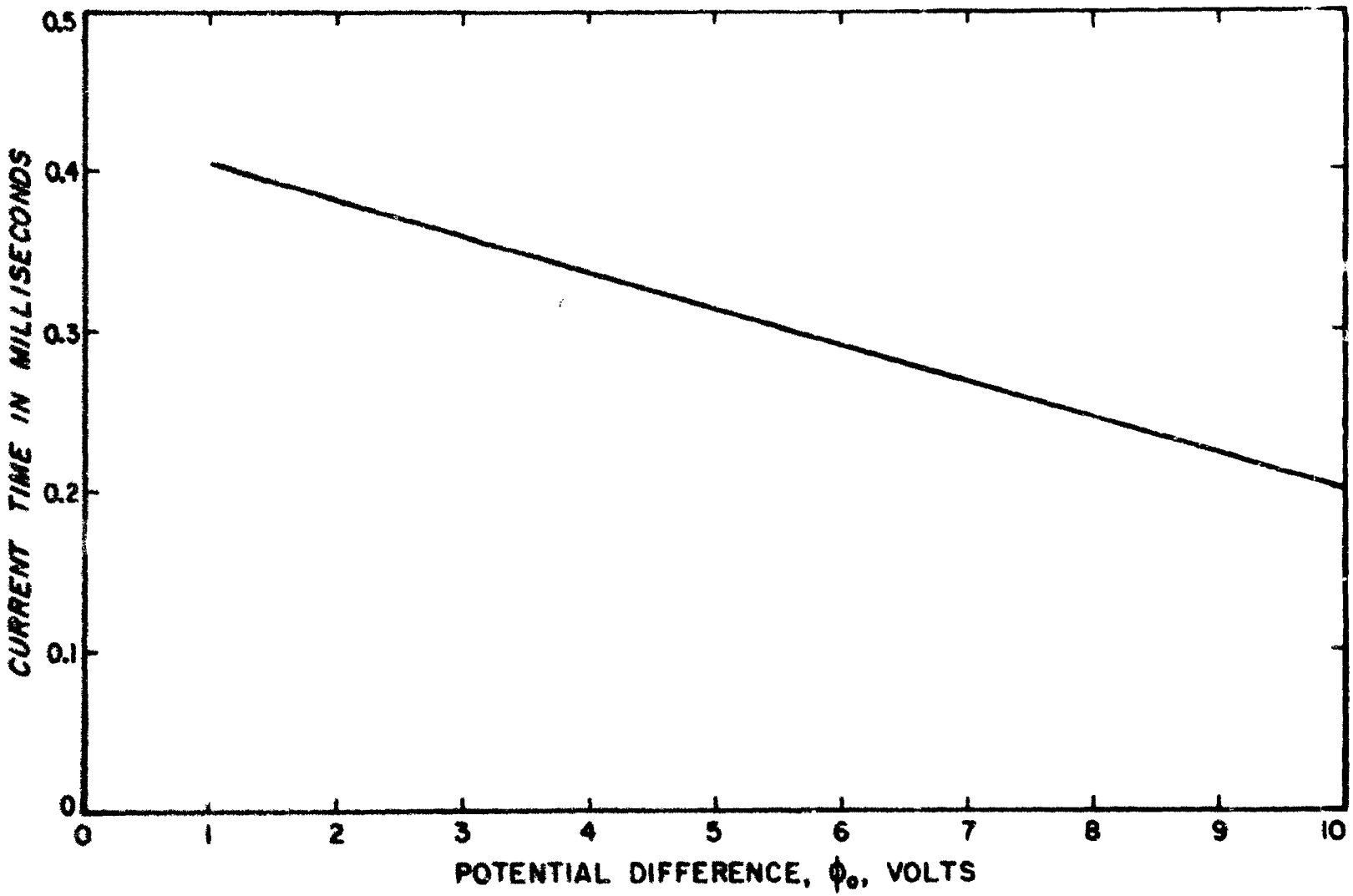

Figure 6-7 A plot of the current time as a function of the potential difference between drops.

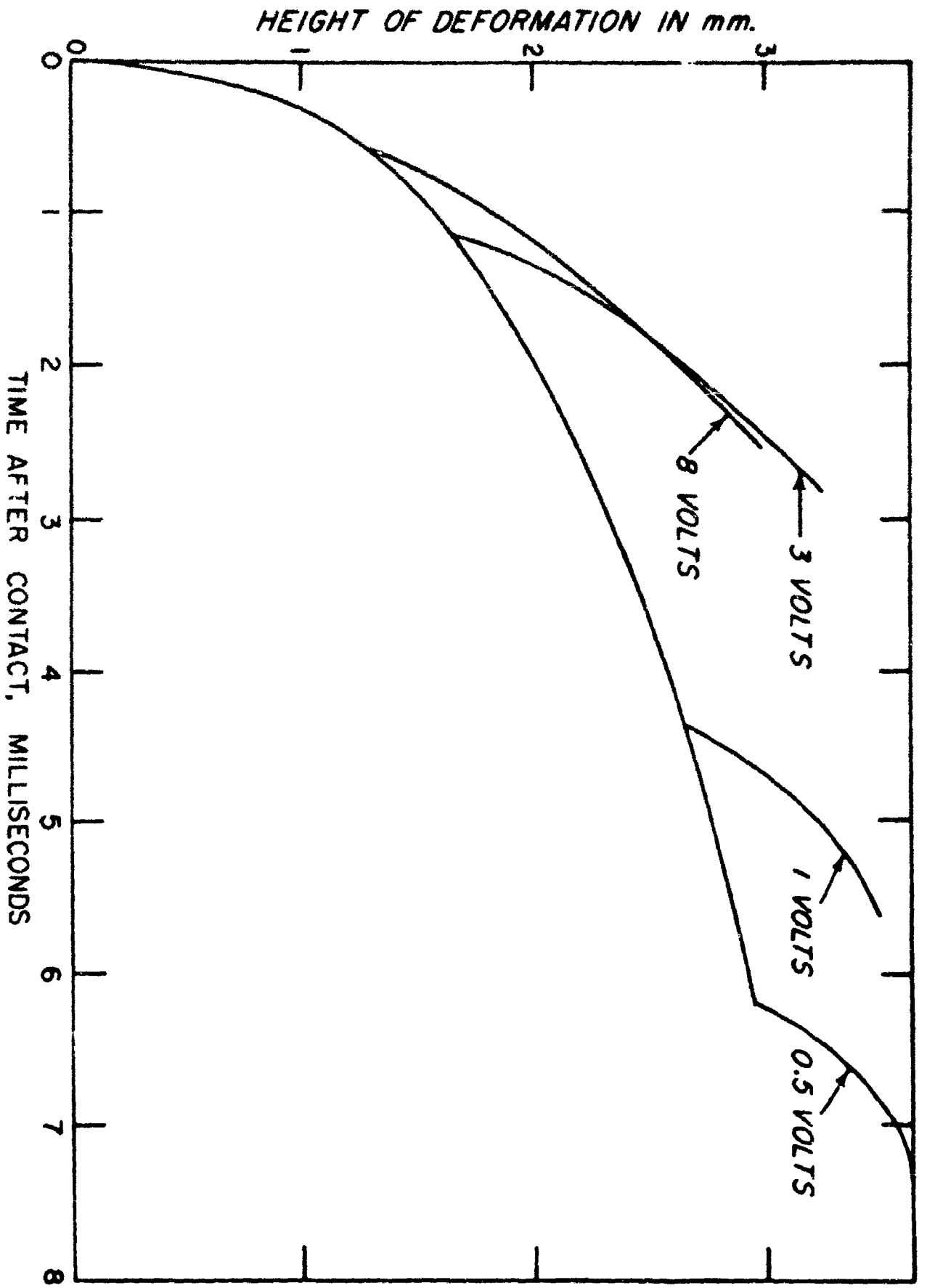
HEIGHT OF DEFORMATION IN mm.
0
1
2
3
TIME AFTER CONTACT, MILLISECONDS
0
1
2
3
4
5
6
7
8
8 VOLTS
3 VOLTS
1 VOLTS
0.5 VOLTS

the rate of growth of the deformation is common to all of the different applied voltages until a lens is formed at the time of coalescence. The relationship for the height of the deformation, 2a, is again determined from the experimental data by using the method of least squares and the logrithms of a and t. This relationship is found to be

$$2a = 6.4 \times 10^{-4} t^{3/8} \qquad (6\text{-}7)$$

The drops do not deviate from their original spherical shape until the flattening of the adjacent surfaces begins. However, the height of the flattened area at coalescence does decrease with an increase in the potential difference since the coalescence time decreases.

The growth of the lens height after coalescence is more rapid than the rate of increase of the height of the flattened area before coalescence. Also, the growth rate of the lens height is greater for smaller voltages than for larger voltages.

The rate of growth of the lens width is shown in Fig. 6-9. This rate of growth increases in a linear manner although the rate is less for larger voltages than for smaller ones.

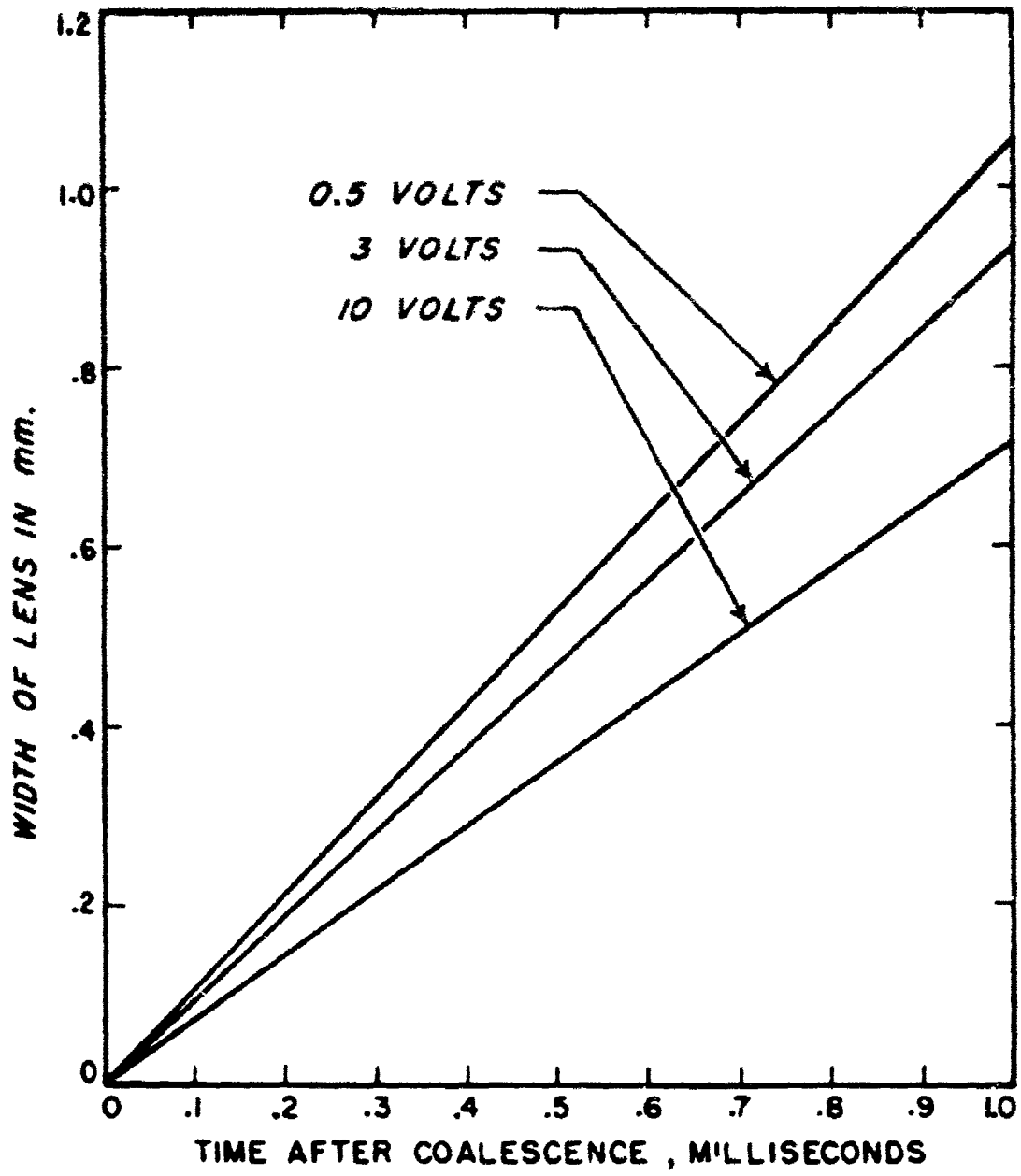

Figure 6-9 A plot of the lense width as a function of time after coalescence.

CHAPTER VII

SUMMARY

7.1 Collision Efficiency of Drop Pairs

7.1a No Electrostatic Force

For the mathematical model of a pair of drops described in Chapter III, it is found that for uncharged drops ranging in size from 5 to 70 microns falling in a field free space the collision efficiency increases as the size of the drop increases for a fixed droplet size as illustrated in Figure 4-1. For a 5 micron droplet, the collision efficiency is zero when paired with a 25 micron drop or less but it increases to 0.1638 when paired with a 70 micron drop. The collision efficiency also increases as the size of the droplet increases for a fixed drop size. For a 50 micron drop, the collision efficiency is 0.1338 when paired with a 5 micron droplet but increases to 0.7676 when paired with a 20 micron droplet. This is an increase in the collision efficiency by a factor of 5.74 and indicates that the collision efficiency of a drop falling in a cloud of droplets will increase as drop grows in size. Therefore, even though the collision efficiency of drops in the initial stages of warm clouds is small, it increases as the size of the drops in the cloud grows.

7.1b Electric Field Present

For a given pair of uncharged drops, their collision efficiency increases with an applied electric field as shown in Figures 4-2, 4-3, and 4-4. It is found that horizontally oriented electric fields produce a greater increase in collision efficiencies than do vertically

oriented fields. For a 5 micron droplet paired with a 30 micron drop, a 3600 volt per centimeter field oriented vertically increases the collision efficiency by a factor of 22.1 compared to an increase of 34.5 for the same field oriented horizontally.

For a given drop size the increase in collision efficiency is less for larger droplet sizes. With a horizontally applied field of 3600 volts per centimeter the collision efficiency for a 30 micron drop paired with a 5 micron droplet increases by a factor of 34.5 compared with 29.0 when paired with a 10 micron droplet.

For a given field strength, it is found that if the field is oriented either at 42° or 138° from the vertical, the collision efficiency for a drop pair is a minimum where as the maximum collision efficiency occurs for the horizontally applied field. When the drop size is constant, the difference between the maximum and minimum collision efficiencies decreases as the droplet size increases. This is illustrated in Figures 4-6 and 4-7.

7.1c Charged Drops

The collision efficiency of pairs of charged drops in a field free region decreases for charges of the same sign and increases for charges of opposite sign. No noticeable effect is observed on the collision efficiency when the charge on the droplet is less than 10^{-17} coulombs but its effect becomes very evident for an increase of one order of magnitude of charge as is shown in Figures 4-8, 4-9, 4-10, and 4-11.

For charges of the same sign, the collision efficiency goes to zero for charge on the droplet greater than 10^{-16} coulombs while for charges of the opposite sign, the collision efficiency exceeds 8.0 when the charge on the droplet is greater than 10^{-15} coulombs. This is an expected result, since the electrostatic force for sufficient charges would be attractive or repulsive depending upon the signs of the charges involved. Therefore, for a cloud of charged drops with alike signs, the collision efficiency of the drops would be small compared to a cloud composed of charged drops with both signs.

7.1d Charged Drops in an Electric Field

Only vertically oriented electric fields are reported here, but the collision efficiency of pairs of drops with changes of the same sign can be increased to values above one. For the charges of opposite signs the collision efficiency can be decreased to zero as the magnitude of charges is increased. These results are illustrated in the Figures 4-12 through 4-23 and are the reverse of the results of Section 7.1c where the drops were charged but no applied field was present. It is indicated that clouds of drops with charges of the same sign can have high collision efficiencies when correctly applied electric fields are present. This is an important result since in clouds composed of charged drops, regions exist where one sign of charge predominates and the collision efficiency of the drops is small unless an electric field is present. Then the collision efficiency of these drops can be increased to values greater than one.

7.2 Coalescence of Drop Pairs

7.2a Effects of an Electric Potertial Difference

The coalescence time for 2 millimeter drops is found to vary as the inverse of their potential difference, ϕ_o, as given in Fig. 6-5. For the model of two drops with flat deformations, the ratio of the separation of the surfaces at coalescence, $2h_1$, to the separation at the start of the deformation, $2h_o$, is given by

$$\frac{h_1}{h_o} = \exp(-k\ \phi_o^{7/4}) \qquad (6\text{-}4)$$

where k is a constant. This dependence arises from the influence of the electrostatic force on the growth of perturbation on the surfaces of the liquid which changes the probability of coalescences at any given separation.

7.2b Effects of Collision Velocity

For a decrease in the collision velocity of the approaching drops, the coalescence time will increase as shown in Figure 6-5. Since the initial momentum of the liquid drops is greater for higher collision velocities. Considering the model of two drops with flat deformations, the coalescence time is found to be inversely proportional to the fourth power of the inertia force when no electrostatic force is present. This inertial force is very important to the coalescence process, since it is necessary for the coalescence of uncharged drops.

7.2c Effects of Air Pressure

The coalescence time of two drops 2 millimeters in radius is found to be independent of the pressure of the air in the continuous medium as illustrated in Fig. 6-7. This is in agreement with the results from using the model of two drops with flat deformation since the calculated

coalescence time depends only on the viscosity of the air which is independent of pressure. This is a useful verification of the result from the model since this justifies neglecting any small variation in pressure, of the continuous medium when considering coalescence.

7.2d Charge Flow Before Coalescence

The current in the external network of the two drops suspended on hypodermic needles is found to start a fraction of a millisecond before any visible coalescence occurs as shown in Figure 6-8. However, the potential difference between the surfaces is less than 10 volts which is too low to cause the air to ionize even if the electric field between the surfaces exceeds the normal ionization value. Since oxygen, which has the lowest ionization potential of any air constituent, has an ionization potential of 12.5 volts, the electrons can not obtain enough energy to ionize the air. Therefore, it appears that perhaps small amounts of charged liquid are removed from the surfaces immediately before their coalescence carrying charge across the air gap. This phenomenon could be the result of perturbations on the liquid surfaces and would be the initiation of the coalescence process, since no current was ever observed for any case where the droplets separated.

7.2e Rate of Growth of Deformation

The initial rate of deformation of the colliding surfaces is found to be independent of the potential applied between the drops. The radius, a, of the flatten deformation is found to vary as

$$a = 3.2 \times 10^{-4} t^{3/8} \qquad (6\text{-}6$$

This result is helpful since it is useful in deriving a working model for two colliding drops and it implies that the electrostatic force outside the deformed region can be neglected since it does not aid in the growth of the deformation.

After coalescence, the height of the deformation increases at a greater rate than before and the width of the lens grows linearly with time. If this linear relationship holds from the beginning of coalescence, then it can be used to accurately determine the time of coalescence. The time of coalescence found by this method is in good agreement, with the visible evidence of coalescence from a profile view of the colliding drops.

7.3 Recommendations for Further Research

To date, neither the theoretical models nor the laboratory experiments have been completely adequate in studying the interaction of drops in proximity. Further work based on preliminary results already obtained is essential in explaining the complete behavior of aggregations of drops. Therefore, from the results reported in the previous chapters, further research recommended is as follows:

1) The collision efficiencies reported in Chapter IV should be used to compute the growth rate of drops falling through a cloud of droplets.

2) Laboratory experiments should be designed and implimented to obtain more accurate measurements of the hydrodynamics and the collision efficiencies of micron size drops moving in a viscous medium.

3) The theoretical model for the motion of two drops which collide and coalesce should be extended to include additional parameters and other possible configurations of the deformation of the adjacent surfaces.

Two additional parameters to be included should be the effect of relative humidity of the surrounding medium and the influence of the evaporation of liquid from the surfaces of the drops. One possible configuration of the deformation should be such that a gas bubble is trapped between the adjacent surfaces reversing the curvature of the drop surfaces.

5) The measurements of coalescence times and the rate of growth of deformation of millimeter size drops should be extended to include a wider range of collision velocities, different humidities, different temperatures, and different liquids.

6) Laboratory experiments should be designed and implimented to obtain measurements on the coalescence of micron size drops. This study should include the effects of electric field, charge, collision velocity, relative humidity, temperature, and viscosity of the medium for a wide range of micron size drops.

References

1. Berg, T. G. O., G. C. Fernish, and T. A. Gaukler, 1963: "The Mechanism of Coalescence of Liquid Drops," Journ. of the Atmospheric Sciences, Vol. 20, p. 153.

2. Best, A. C., 1951: "The Size of Cloud Droplets in Layer-type Clouds," Quart. Journ. Roy. Meteorol. Soc., Vol. 77, p. 241.

3. Buckholz, H., 1957: Electrische and Magnetische Potentialfelder, Springer-Verlag, Berlin.

4. Charles, G. E., and S. G. Mason, 1960: "The Mechanism of Partial Coalescence of Liquid Drops at Liquid/Liquid Interfaces," Journ. of Colloid Sci., Vol. 15, p. 105.

5. Cockbain, E. G., and T. S. McRoberts 1953: "The Stability of Elementary Emulsion Drops and Emulsions," Journ. Colloid Sci., Vol. 8, p. 440.

6. Dady, G., 1947: "Contributions to the Study of Precipitation," Academic Des Sciences, Vol. 22, p. 1349.

7. Das P. K., 1950: "The Growth of Cloud Droplets by Coalescence," Indian J. Met. Geophys., Vol. 1, p. 137.

8. Davies, C. N., 1945: "Definitive Equations for the Fluid Resistance of Spheres," Proc. Roy. Soc., Vol. 57, p. 18.

9. Davis, M. H., 1962: "The Forces Between Conducting Spheres in a Uniform Electric Field," Rand Corp. Memorandum RM-3307-1PR.

10. Derjaguin, B., and M. Kussakov, 1938: "Anomalous Properties of Thin Polymolecular Films. V," Acta Physicochim, Vol. 10, p. 25.

11. Elton, G. A. H., 1948: "The Flow of Liquids Between Surfaces in Close Proximity," Proc. Roy. Soc. A, Vol. 194, p. 259.

12. Elton, G. A. H., and R. G. Picknett, 1957: "The Coalescence of Aqueous Droplets with an Oil/Water Interface," Proc. 2nd International Congress of Surface Activity, Vol. I, p. 288, Butterworths, London.

13. Fiendeisen, W., 1932: "Messungen der Größe und Anzahl der Nebeltropfen zum Studium der Koagulation inhomogenen Nebels," Beitr. Geophys., Vol. 35, p. 295.

14. Fiendeisen, W., 1939: "Das Verdampfen der Wolken-und Regentropfen," Met. Z., Vol. 55, p. 121.

15. Freir, G., 1960: "The Coalescence of Water Drops in an Electric Field," Journ. of Geophys. Research, Vol. 65, No. 12, p. 3979.

16. Gillespie, T., and E. K. Rideal, 1955: "The Coalescence of Drops at an Oil-Water Interface," Trans. Faraday Soc., Vol. 52, p. 173.

17. Goldstein, S., 1929: "The Steady Flow of Viscous Fluid Past a Fixed Spherical Obstacle at Small Reynolds Numbers", Proc. Roy. Soc. A, Vol. 123, p. 225.

18. Groothuis, H., and F. J. Zuiderweg, 1960: "Influence of Mass Transfer on Coalescence of Drops," Chem. Eng. Sci., Vol. 12, p. 288.

19. Gunn, R., 1949: "The Free Electrical Charge on Thunderstorm Rain and its Relation to Droplet Size," J. of Geophys. Research, Vol. 54, No. 1, p. 57.

20. Gunn, K., and W. Hitschfeld, 1951: "Laboratory Investigation of the Coalescence Between Large and Small Water-Drops," J. of Meteorol., Vol. 8, p. 7.

21. Harnwell, G. P., 1949: Principles of Electricity and Electromagnetism, McGraw-Hill Book Company, Inc., New York, p. 53.

22. Hazelhurst, T. H., and H. A. Neville, 1937: "Liquid Drops on Liquid Surfaces," Journ. Phys. Chem., Vol. 41, p. 1205.

23. Hocking, L. M., 1959: "Three-dimensional Viscous Flow Problems Solved by the Stokes and Oseen approximation," Ph.D. Thesis, 100 pp. University of London.

24. Hocking, L. M., 1959: "The Collision Efficiency of Small Drops," Quart. J. Roy. Meteorol. Soc., Vol. 85, p. 44.

25. Jackson, J. D., 1962: Classical Electrodynamics, John Wiley and Sons, Inc., New York, p. 18.

26. Jenson, V. G., 1959: "Viscous Flow Round a Sphere at Low Reynolds Numbers," Proc. Roy. Soc. London, A, Vol. 249, p. 346.

27. Kaplun, S., and P. A. Lagerstrom, 1957: "Asymptotic Expansions of Navier-Stokes Solutions for Small Reynolds Numbers," Jour. of Math and Mech., Vol. 6, No. 5, p. 585.

28. Kawaguti, M., 1948: "An Approximate Solution to the Viscous Flow at Low Speeds (II) The Flow Past a Sphere," Rep. Inst. Sci., Tokyo, Vol. 2, p. 66.

29. Kawaguti, M., 1950: "Numerical Solution for the Viscous Flow Past a Sphere," Rep. Inst. Sci., Tokyo, Vol. 4, p. 154.

30. Kinzer, G. D., and W. E. Cobb, 1958: "Laboratory Measurements and Analysis of the Growth and Collection Efficiency of Cloud Droplets," Journ. of Meteorol., Vol. 15, p. 138.

31. Lagerstrom, P. A., [illegible] J. D. Cole, 1955: "Examples Illustrating Expansion Procedures for the [illegible]vier-Stokes Equations," Journ. Rational Mech. Analysis, Vol. 4, p. 817.

32. Langmuir, I., and K. B. Blodgett, 1944-1946, "Mathematical Investigation of Water Droplet Trajectories," G. E. Research Lab., Report No. RL-225.

33. Langmuir, I., 1948: "The Production of Rain by a Chain Reaction in Cumulus Clouds at Temperatures Above Freezing," Journ. of Meteor., Vol. 5, No. 5, p. 175.

34. Lindblad, N. R., and R. G. Semonin, 1963: "Collision Efficiency of Cloud Droplets in Electric Fields," J. of Geophys. Research, Vol. 68, No. 4, p. 1051.

35. Lindblad, N. R., and R. G. Semonin, 1963b: "Reply," J. of Geophys. Research, Vol. 68, No. 15, p. 4633.

36. Linton, M., and K. L. Sutherland, 1956: "The Coalescence of Liquid Drops," Journ. Colloid Sci., Vol. 11, p. 391.

37. Ludlam, F. H., 1951: "The Production of Showers by the Coalescence of Cloud Droplets," Q. J. R. Met. Soc., Vol. 77, p. 52.

38. Moore, C. B., and B. Vonnegut, 1960: "Estimates of Raindrop Collection Efficiencies in Electrified Clouds," Physics. of Precipitation, Geophys. Monograph 5, p. 291.

39. Morse, P. M., and H. Feshbach, Methods of Theoretical Physics, McGraw-Hill Book Company, Inc., New York, p. [illegible] and 1299.

40. Nielson, L. E., R. Wall, and G. Adams, 1958: "Coalescence of Liquid Drops at Oil-Water Interfaces," Journ. of Colloid Sci., Vol. 13, p. 441.

41. Nordsieck, A. T., 1962: "On Numerical Integration of Ordinary Differential Equations," Math. Computation, Vol. 16, p. 22.

42. Oseen, C. W., 1910: "Uber die Stokessche Formel und uber eine verwandte Aufgabe in der Hydrodynamik," Ark. Mat. Astr. Fys., Vol. 6, No. 29, p. 175.

43. Parratt, L. G., 1961: Probability and Experimental Errors in Science, John Wiley and Sons, Inc., New York, p. 147.

44. Pearcey, T., and G. W. [illegible] 1957: "A Theoretical Estimate of the Collection Efficiencies of Small Droplets," Q. J. R. Met. Soc., Vol. 83, No. 355, p. 77.

45. Pearcey, T., and G. Mungall, 1955: "Calculation of Viscous Flow Around Spheres at Low Reynolds Numbers," Phil. Mag. (7), Vol. 46, p. 783.

46. Prokhorov, P. S., 1954, "The Effects of Humidity Deficit on Coagulation Processes and the Coalescence of Liquid Drops," Discussions, Faraday Soc., Vol. 18, p. 41.

47. Proudman, I., and J. R. A. Pearson, 1957: "Expansions at Small Reynolds Numbers for the Flow Past a Sphere and a Circular Cylinder," Journ. of Fluid Mech., Vol. 2, p. 237.

48. Ranz, W. E., 1951: "The Impaction of Aerosol Particles on Cylindrical and Spherical Collectors," Contract No. AT(30-3)-28, U.S.A.E.C.

49. Rayleigh, J. W. S., 1945: The Theory of Sound, Vol. II, Dover Publications, New York, p. 369.

50. Reynolds, O., 1881: "On Drops Floating on the Surface of Water," Chem. News, Vol. 44, p. 211.

51. Reynolds, O., 1886: "On the Theory of Lubrication and its Application to Mr. Beauchamp Tower's Experiments, including an Experimental Determination of Viscosity of Olive Oil," Phil. Trans. Vol., 177, p. 157.

52. Sartor, D., 1954, "A Laboratory Investigation of Collision Efficiencies Coalescence and Electrical Charging of Simulated Cloud Droplets," J. Meteor., Vol. 11, p. 91.

53. Sartor, J. D., 1960: "Some Electrostatic Cloud-Droplet Collision Efficiencies," J. of Geophys. Research, Vol. 65, No. 7, p. 1953.

54. Schotland, R. M., 1957: "The Collision Efficiency of Cloud Drops of Equal Size," J. of Meteorol., Vol. 14, No. 5, p. 381.

55. Schotland, R. M., and E. J. Kaplin, 1956: "The Collision Efficiency of Cloud Droplets," N. Y. Univ. Sci. Rept. 1, Dept. of Meteorology and Oceanography, New York University.

56. Sell, W., 1931: "Dust Precipitation on Simple Bodies and in Air Filters," Forsch. Gibiete Ingenieurw., 2, Forschungsheft, 347.

57. Shafrir, U., and M. Neiburger, 1963: "Collision Efficiencies of Two Spheres Falling in a Viscous Medium," J. of Geophys. Research, Vol. 68, No. 13, p. 4141.

58. Smythe, W. R., 1950: Static and Dynamic Electricity, Ch. 5, McGraw-Hill Book Co., Inc., New York.

59. Stokes, G. G., 1851: "On the Effect of the Interval Friction of Fluids on the Motion of Pendulums," Transactions, Cambridge Phil. Soc., Vol. IX, Pt. II. p. 8.

60. Swinbank, W. C., 1947: "Collisions of Cloud Droplets," Nature, Vol. 159, No. 4051, p. 849.

61. Telford, J. W., N. S. Thorndike, and E. G. Bowen, 1955: "The Coalescence Between Small Water Drops," Quart. J. Roy. Meteor. Soc., Vol. 81, p. 241.

62. Tomotika, S., and T. Aoi, 1950: "The Steady Flow of Viscous Fluid Past a Sphere and Circular Cylinder at Small Reynolds Numbers," Quart. Journ. Mech. and Applied Math., Vol. III, Pt. 2, p. 140.

63. Weickmann, H. K., and H. J. Aufm Kampe, 1953: "Physical Properties of Cumulus Clouds," J. Met., Vol. 7, p. 404.

64. Whitehead, A. N., 1889: "Second Approximations to Viscous Fluid Motion," Quart. J. Math, Vol. 23, p. 143.

65. Wylie, C. R., Jr., 1951: Advanced Engineering Mathematics, McGraw-Hill Book Company, Inc., New York, p. 527.